The Pennsylvania State University

The Graduate School

Energy and Mineral Engineering

THERMAL RESPONSE MODELING AND THERMODYNAMIC ANALYSIS OF

HORIZONTAL WELLBORE FLUIDS

A Thesis in

Energy and Mineral Engineering

by

Ting Dong

Submitted in Partial Fulfillment
of the Requirements
for the Degree of

Master of Science

August 2014

The thesis of Ting Dong was reviewed and approved[*] by the following:

Luis F. Ayala H.
Associate Professor of Petroleum and Natural Gas Engineering
Associate Head of John and Willie Leone Family Department of Energy and
Mineral Engineering for Graduate Education
Thesis Advisor

M. Thaddeus Ityokumbul
Associate Professor of Mineral Processing and Geo-Environmental Engineering
Undergraduate Program Chair of Environmental Systems Engineering

Antonio Nieto
Associate Professor of Mining Engineering;
Thomas V. Falkie Faculty Fellow

***Signatures are on file in the Graduate School

ABSTRACT

Wellbore models are required for integrated reservoir management studies as well as the optimization of production operations. Distributed Temperature Sensing (DTS) is a smart well technology deployed for permanent downhole monitoring. Temperature is measured via fiber optic sensors installed along horizontal wellbores. Correct interpretation of DTS surveys has thus become of utmost importance and analytical models for analysis of temperature distribution behavior are critical. This study conducted a comprehensive thermodynamic analysis to interpret thermal response of horizontal wellbore fluids. A generalized wellbore thermal response model (η_s-driven model) is derived starting from 1-D conservative mass, momentum and energy balance equations. Steady-state velocity, pressure and temperature profiles are presented along with its single-phase and two-phase solution procedures. Steady-state applications are conducted and discussed. In steady state, both single-phase and two-phase flows are considered in both openhole and perforated wellbore conditions. Both the homogeneous and drift-flux models are implemented in two-phase flow, together with the comparison of results between the two models. Results show that for single-phase flow, oil and water are heated, while gas is cooled along the horizontal wellbore; thermal behavior of wellbore fluid is driven by wellbore inclination, flowrate, roughness, radius and completion type. When two-phase flow appears, a temperature derivation compared with single-phase case can be detected from temperature profiles. The effects of each thermal factor on overall thermal response are also discussed in the study for both horizontal and inclined wellbores. Rather than only utilizing the common accepted tool value of Joule Thomson Coefficient to predict heating or cooling effect in wellbore, this study show cases on the importance of Isentropic Thermal Coefficient, which always contributes to cooling.

CONTENTS

LIST OF TABLES

LIST OF FIGURES

NOMENCLATURE

A : Cross Sectional Area of Wellbore, L^2, ft^2

C_o : Profile Parameter, [-]

C_h : Fluid Heat Transfer Coefficient, m/t^3-T, BTU/ ft^2·hr·F

C_L : Liquid Heat Transfer Coefficient, m/t^3-T, BTU/ ft^2·hr·F

C_P : Isobaric Heat Capacity, L^2/t^2-T, BTU/lbm·R

C_v : Isochoric Heat Capacity, L^2/t^2-T, BTU/lbm·R

d : Wellbore Diameter, L, ft

e : Internal Energy per Unit Mass, L^2/t^2, BTU/lbm

F : Force per Unit Volume, m/L^2-t^2, lbf/ft^3

F_s : Shape Factor, [-]

F_P : Flow Pattern Factor, [-]

G_p : Formation Pressure Gradient, m/L^2-t^2, psi/ft

G_T : Formation Temperature Gradient, T/L, F/ft

f : Friction Factor, [-]

g : Acceleration factor, L/t^2, 32.174 ft/s^2; Apparent Mass Flux, m/L^2-t, lbm/ft^2·s

g_c : Unit Conversion Factor, 32.174 lbm·ft/lbf·s^2

h : Fluid Specific Enthalpy at Wellbore Conditions , L^2/t^2, BTU/lbm

h^* : Fluid Specific Enthalpy at Reservoir Conditions, L^2/t^2, BTU/lbm

i : phase, [-]

J_0 : Pressure Unit Conversion, 144 lbf/ft^2·psia

J_1 : Energy Unit Conversion, 778.16 lbf· ft /BTU

J_2 : Energy Unit Conversion, 5.4 psia $\cdot$ ft^3/BTU

K : Conductivity, m/t^2-T, BTU/hr$\cdot$ft$\cdot$F

k : Heat Capacity Ratio, [-]

L : Length of Wellbore, L, ft

M : Mass Rate, M/t, lbm/s

Pr : Prandtl Number

p : Pressure, m/L-t^2, psia

Q : Conductive heat flux, m/t^3, BTU/ ft^2$\cdot$hr

q : Flowrate, L^3/t, ft^3/s

Re : Reynolds Number, [-]

r : Wellbore Radius, L, ft

s : Fluid Specific Entropy, L^2/t^2-T, BTU/lbm$\cdot$F

T : Temperature, T, R

T* : Reservoir Temperature, T, R

t : Time, t, s

U : Overall Heat Transfer Coefficient, m/t^3-T, BTU/ ft^2$\cdot$hr$\cdot$F

u : Velocity, L/t, ft/s

u* : Inflow Fluid Velocity, L/t, ft/s

W : Mass Rate, m/t, lbm/s

X : Apparent Volume Fraction, [-]

x : Quality, [-]

y : Holdup, [-]; Gas Void Fraction,[-]

GREEK:

α : Coefficient of Thermal Expansion, 1/T, 1/F

ε : Roughness, L, ft

θ : Inclination Angle, degree

τ : Interfacial Tension, m/t^2, dyne/cm

Γ : Radial Mass Influx, m/L^3-t, $lbm/ft^3 \cdot s$

η_s : Isentropic Thermal Coefficient, $T/(m/L-t^2)$, F/psi

η_h : Joule Thomson Coefficient, $T/(m/L-t^2)$, F/psi

Υ : Isothermal Compressibility, $1/(m/L-t^2)$, 1/psi

γ : Pipe Open Ratio, [-]

ρ : Density, m/L^3, lbm/ft^3

SUBSCRIPT

B   : Bulk

c   : Continuous

D   : Drift

d   : Dispersion

f   : Friction

G   : Gas

g   : Gravity

h   : Enthalpy

ke   : Kinetic Energy

L   : Liquid

ht   : Heat Transfer

j : Segment Number

m : Mixture

me : Mass Exchange

O : Oil

p : Pressure

pe : Potential Energy

ref : Reference

so : Superficial Velocity of Oil

sg : Superficial Velocity of Gas

T : Temperature

t : Total

tp : Two Phase

W : Water; wall

w : Friction

g : Gravity

ACKNOWLEDGEMENTS

It is with immense appreciation that I acknowledge my advisor, Dr. Luis F. Ayala, for the support, guidance, patience and encouragement he gave me during my research on this subject. This thesis would have remained a dream without the opportunity he gave me to study and work under his supervision. It also gives me great pleasure in acknowledging Dr. Ityokumbul and Dr. Nieto as being my committee members.

I owe my deepest gratitude to my parents, Hongjun Dong and Xinping Wang. Their endless love to me can always be my beacon towards the rest of my life. Without their support I could not be who I am today.

I wish to thank all my friends at Penn State, for their kind help and support in my life. Their heartfelt help allowed me to overcome the challenges and difficulties of my two- year study here

CHAPTER 1

INTRODUCTION

As horizontal wells progressively become the most commonly used well architecture in the oil and gas industry (due to their ability to provide enhanced productivity compared to vertical wells), the availability of modern interpretation tools like Distributed Temperature Sensing (DTS) has become ubiquitous. DTS technology enables the monitoring of wellbore temperature profiles in real time. As the use of DTS technology becomes more widespread, understanding the thermal response of fluid due to its withdrawal from the reservoir also becomes crucial. A number of studies have attempted to describe how DTS surveys should be interpreted and have provided thermal models for analysis. Thermal models developed for well applications typically rely on a number of modifications applied to equations used in pipe flow modeling. One of the earliest attempts to model wellbore thermal responses was presented by Ramey (1962) who presented an approximate solution for vertical wellbore fluid temperature as a function of depth and time. The solution incorporated an overall heat transfer coefficient between reservoir and wellbore single-phase fluid. Assumptions in Ramey's solutions are: (1) that fluid is incompressible and ideal, (2) heat transfer in wellbore is in steady state, and (3) effects of kinetic energy and friction are ignored. Alves et al. (1992) significantly expanded the application and developed a steady-state unified model applicable for wellbore tubing and pipeline flow under single- or two-phase flow conditions. Hassan and Kabir (1994) have also developed a steady-state two-phase flow temperature prediction model. Their method incorporated thermal diffusivity equation and considered both conductive and convective heat transfer for the wellbore/formation system. A thermal parameter was introduced that combined Joule-Thompson and kinetic energy effects. The parameter was calculated by either empirical expression or mechanistic approach.

Wide use of the horizontal well with DTS technology requires a thermal model to interpret DTS temperature data in monitoring and controlling the reservoir production. Yoshioka et al. (2005a) first proposed a horizontal wellbore flowrate, pressure and temperature prediction model using mass, momentum and energy equations. The Joule-Thomson effect of wellbore fluid (heating of oil and cooling of gas) is emphasized. Trajectories and watery entry effects are included in a sensitivity study. Yoshioka et al. (2005b) later developed a single-phase fluid reservoir thermal model coupled with a horizontal wellbore model at steady state. In the reservoir model, oil, water and gas arrive at wellbore at different temperatures because oil and water are heated, while gas is cooled from the boundary of the reservoir to the wellbore because of the Joule-Thomson effect. Based on Yoshioka's work, while keeping the wellbore model in steady state, Li and Zhu (2009) improved the reservoir model to a 3-D multiphase transient flow form to make it more applicable for interpreting DTS data. Their attempt partially matched the thermal response of DTS data and production history. Pourashary et al. (2008) developed a compositional fully-coupled mechanistic multi-phase flow wellbore/reservoir simulator for a horizontal well, in conjunction with vertical wellbores. The model assumes that the wellbore system reaches steady-state at the end of each reservoir simulation time. Pressure and temperature profiles, component mass-flow rate and hold up can be generated from the model. Radespiel (2010) developed a robust numerical model for the prediction of wellbore thermal responses in horizontal wellbores. He presented analytical approximations for the interpretation of wellbore thermal responses in horizontal wells in terms of wellbore velocity gradients and mass radial influx. Yoshida and Zhu (2013) presented a temperature prediction model in a stimulated well. Reservoir thermal and wellbore flow models are coupled with transverse fractures. The temperature model can be used to interpret fracture geometry and fracture diagnostic technology.

Two-phase flow frequently appears during wellbore production. A Two-phase flow wellbore model is needed to simulate the physical process and interpret the behavior of two-phase flow in wellbores. Zuber and Findlay (1965) proposed a general drift-flux method to predict average volumetric concentration in vertical two-phase flow systems. Velocity and concentration profiles are generated by considering the effects of the relative velocity between two phases and nonuniform flow. Franca and Lahey (1992) applied drift-flux techniques in horizontal air/water two-phase flows. Their model is able to predict and correct experiment data in various flow regimes. Hasan et al. (1999) applied drift-flux approach and developed a simplified model for oil-water flow in vertical and deviated wellbore. After investigating three flow patterns, a single expression for calculating drift-flux velocity was developed. Shi et al. (2005) proposed a drift-flux model of water/gas and oil/water two-phase flow in wellbores ranging from vertical to near-horizontal. The model used experiment data from large diameter pipe to determine drift-flux parameters. Hapanowicz (2008) tested the accuracy of available drift-flux models in evaluating the slip between water and oil phases in a horizontal pipe. A flow pattern determination method was proposed for implementing the drift-flux model. Based on previous work, Choi et al. (2012) developed a drift-flux closure relationship to estimate phase holdup in gas-liquid pipe flow. The correlation gave good prediction of phase holdup over a wide range of flow patterns and wellbore inclination conditions. Hasan and Kabir (1988b) presented a mechanistic model for multiphase flow in vertical wells. The model is able to predict flow pattern, void fraction and pressure drop of vertical wellbore fluid. They also presented a similar mechanistic model that can be applied in deviated wells (Hasan and Kabir, 1988a). Petalas and Aziz (1998) proposed a mechanistic model for multiphase flow in pipe. New empirical correlations were developed for liquid-gas flow in different flow patterns, along with solution procedures. Ouyang and Aziz (2000) published a

homogeneous model for gas-liquid flow in horizontal wells. In their pressure gradient equation, accelerational pressure gradient caused by wall influx/outflux and fluid expansion is considered. Yoshioka et al. (2005a,b) proposed homogeneous model for oil-water flow and drift-flux model for oil-gas flow in his wellbore temperature prediction models.

Problem Statement & Objectives

The thermal models in most of these studies so far attribute different fluid thermal behaviors to the Joule-Thomson effect. However, there is little thermodynamic analysis discussing how each thermal factor determines the wellbore fluid's overall thermal behaviors. Because the wellbore condition is proved to be never isenthalpic nor isentropic in our studies, a thermal response wellbore model with detailed thermodynamic analysis is needed to explain the specific reasons and factors that control the thermal behaviors of each fluid. By understanding the thermodynamic process in horizontal wellbores and how it is related to wellbore fluid thermal behavior, the DTS surveys can be better interpreted in monitoring the thermal production of reservoirs.

The primary objective of this study is to analyze the thermodynamic process and thermal response in a horizontal wellbore system. Starting from 1-D conservative mass, momentum and energy balance equations, we derive enthalpy, entropy gradient equations of wellbore fluid along with a velocity, pressure and temperature prediction model. Comparison of our model with the industry standard thermal model is conducted to illustrate the different thermal response behavior generated with different assumptions. Unlike emphasizing the Joule-Thomson effect, our η_s-driven model highlights the importance of Isentropic Coefficient as a newly-introduced thermal factor in determining thermal behavior of wellbore fluid. Completion type in our wellbore system can either be openhole or perforated.

We begin with the single-phase flow model development, then expand our single-phase fluid model into a two-phase fluid model, including a homogenous model and a drift-flux model. In a case study for single-phase fluid, oil, gas and water are considered. Peng-Robinson equation of state is applied in calculating fluid thermal properties (Zakaria, 2012). Different thermal responses of fluid are observed, and the reasons for the difference are illustrated. A sensitivity study also contains the thermal response of wellbore fluid in response to changes in wellbore inclination, flowrate, roughness, radius and completion type. In addition, for the two-phase fluid case study, oil-water and oil-gas flow are selected. Our model can be applied in interpreting water entry and gas blending effects while in production.

CHAPTER 2

THERMODYNAMIC PROCESS IN HORIZONTAL WELLBORE SYSTEM

2.1 Governing Equations in Wellbores for Single-phase Flow
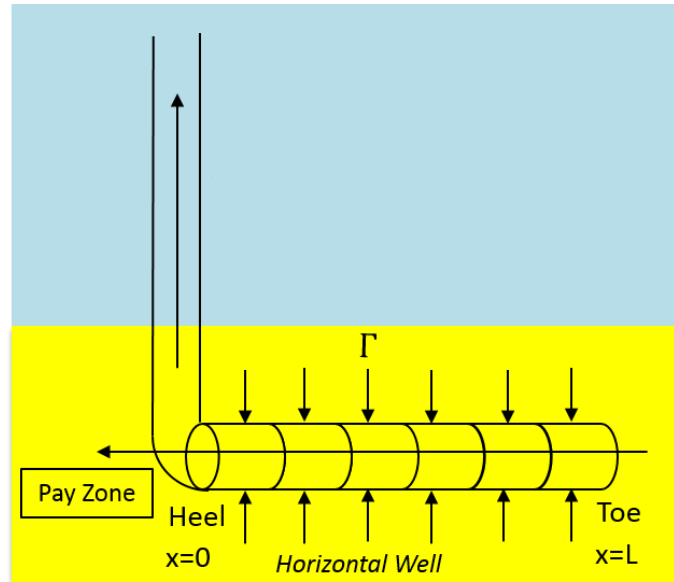
Fig.2.1 Schematic of a Horizontal Wellbore
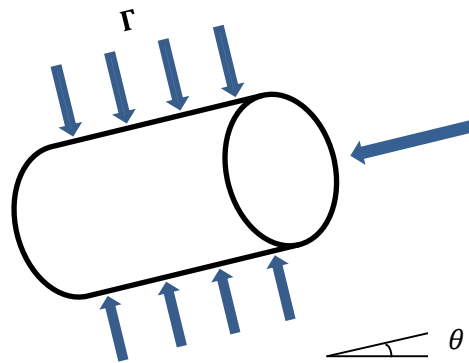
Fig.2.2 Differential Volume Element of a Wellbore

Figure 2.1 shows a discretized wellbore where location x=0 corresponds to the 'heel' and x=L corresponds to the 'Toe'. Figure 2.2 shows a differential volume element of a wellbore. During production, flow in two directions goes into the wellbore--axial flow (towards the wellbore) and radial flow (perpendicular to wellbore). Because of the pressure difference between the reservoir and the wellbore, reservoir flow continuously goes in to wellbore. Fluid in the wellbore first goes

in an axial direction from toe to heel (refer to Figure 2.1); then it is transported from the reservoir to the surface via tubing.

The physical process which happens in the horizontal wellbore during production can be studied by deriving three conservative equations—mass, momentum and energy balance equations. In this section, we derive the one-dimensional governing equations for a wellbore system of a single-phase flow. A thermal response model with steady-state considerations is developed.

2.1.1 Mass Balance

A mass conservation equation is developed with the following relationship:

$$\left\{\begin{array}{c} \text{rate of} \\ \text{increase} \\ \text{of mass} \end{array}\right\} = \left\{\begin{array}{c} \text{rate of} \\ \text{mass} \\ \text{in} \end{array}\right\} - \left\{\begin{array}{c} \text{rate of} \\ \text{mass} \\ \text{out} \end{array}\right\} \tag{2.1}$$

Translating the physical statement into a mathematical expression, we have:

$$\pi r^2 \Delta x \frac{\partial \rho}{\partial t} = -\pi r^2 [(\rho u)_x - (\rho u)_{x+\Delta x}] + \pi r^2 \Delta x \Gamma \tag{2.2}$$

where ρ denotes density, u is wellbore fluid velocity, Δx is the length of one segment of wellbore, and radial mass influx is denoted as $\Gamma(\frac{lbm}{ft^3 s})$. Dividing by $\pi r^2 \Delta x$, taking the limit as Δx goes to zero, the conservation mass equation (2.2) becomes,

$$\frac{\partial \rho}{\partial t} + \frac{\partial \rho u}{\partial x} = \Gamma \tag{2.3a}$$

Expanding equation (2.3a), we have the non-conservative form of the mass balance equation,

$$\frac{\partial \rho}{\partial t} + \rho \frac{\partial u}{\partial x} + u \frac{\partial \rho}{\partial x} = \Gamma \tag{2.3b}$$

2.1.2 Momentum Balance

To derive a momentum balance equation, the momentum conservation statement is written as follows:

$$
\left\{\begin{array}{c} \text{rate of} \\ \text{increase} \\ \text{of momentum} \end{array}\right\} = \left\{\begin{array}{c} \text{rate of} \\ \text{momentum} \\ \text{in} \end{array}\right\} - \left\{\begin{array}{c} \text{rate of} \\ \text{momentum} \\ \text{out} \end{array}\right\} + \left\{\begin{array}{c} \text{external} \\ \text{force on} \\ \text{the fluid} \end{array}\right\} \tag{2.4}
$$

The momentum balance equation can be written as:

$$
\pi r^2 \Delta x \frac{\partial \rho u}{\partial t} = -\pi r^2 [(\rho u^2)_x - (\rho u^2)_{x+\Delta x}] - \pi r^2 [(p)_x - (p)_{x+\Delta x}] + \pi r^2 \Delta x (F_w + F_g) \tag{2.5}
$$

Dividing by $\pi r^2 \Delta x$ and with Δx going to zero, equation (2.5) becomes:

$$
\frac{\partial \rho u}{\partial t} + \frac{\partial \rho u^2}{\partial x} + \frac{\partial p}{\partial x} = F_w + F_g \tag{2.6a}
$$

By expanding equation (2.6a) into a non-conservative form of the momentum balance equation, one can have:

$$
\frac{\partial u}{\partial t} + u \frac{\partial u}{\partial x} + \frac{1}{\rho} \frac{\partial p}{\partial x} = \frac{1}{\rho}(F_w + F_g) - \frac{u}{\rho}\left[\frac{\partial \rho}{\partial t} + \frac{\partial \rho u}{\partial x}\right] \tag{2.6b}
$$

where F_w is friction force and F_g is force of gravity. Because we set the direction heel to toe (refer to Figure 2.1) as a positive direction, F_w and F_g have positive values, given as follows:

$$
F_w = \frac{f_M \rho u^2}{2 d g_c} \tag{2.7}
$$

$$
F_g = \frac{\rho g \sin\theta}{g_c} \tag{2.8}
$$

where f_M is the Moody friction factor, which is a function of Reynolds number Re and wellbore

roughness ε. θ is the wellbore inclination angle (refer to Figure 2.1). Expression of the Reynolds

number is:

$$Re = \frac{\rho u d}{\mu} \tag{2.9}$$

If the Reynolds number is less than 2100, the flow is said to be laminar. Friction factor can be

calculated as:

$$f_M = \frac{64}{Re} \tag{2.10}$$

When the Reynolds number is higher than 2100, Chen's (Chen, 1979) correlation is chosen as

follows,

$$f_M = \left\{ -2.0 \log_{10} \left[\frac{\left(\frac{\varepsilon}{d}\right)}{3.7065} - \frac{5.0452}{Re} \log_{10} \left(\frac{\left(\frac{\varepsilon}{d}\right)^{1.1098}}{2.8257} + \frac{5.8506}{Re^{0.8981}} \right) \right] \right\}^{-2} \tag{2.11}$$

2.1.3 Energy Balance

An energy balance can be expressed as follows:

$$\left\{ \begin{array}{c} \text{rate of kinetic} \\ \text{and internal} \\ \text{energy increase} \end{array} \right\} = \left\{ \begin{array}{c} \text{rate of} \\ \text{total energy} \\ \text{in} \end{array} \right\} - \left\{ \begin{array}{c} \text{rate of} \\ \text{total energy} \\ \text{out} \end{array} \right\} + \left\{ \begin{array}{c} \text{rate of work} \\ \text{done on system} \\ \text{by external forces} \end{array} \right\} \tag{2.12}$$

In our wellbore system, we consider convective energy, including kinetic energy and internal

energy, plus conductive energy through heat conduction via a perforated wellbore surface. The

rate of kinetic and internal energy increase is:

$$\begin{Bmatrix} \text{rate of kinetic} \\ \text{and internal} \\ \text{energy increase} \end{Bmatrix} = \pi r^2 \Delta x \frac{\partial}{\partial t}\left(\frac{1}{2}\rho u^2 + \rho e\right) \tag{2.13}$$

The rate of total energy in is:

$$\begin{Bmatrix} \text{rate of} \\ \text{total energy} \\ \text{in} \end{Bmatrix} = \begin{Bmatrix} \text{rate of kinetic} \\ \text{and internal} \\ \text{energy addition by} \\ \text{convection} \end{Bmatrix} + \begin{Bmatrix} \text{rate of heat} \\ \text{addition by} \\ \text{conduction} \end{Bmatrix} \tag{2.14}$$

The rate of total energy in by convection is:

$$\begin{Bmatrix} \text{rate of total} \\ \text{energy in by} \\ \text{convection} \end{Bmatrix} = -\left\{ \pi r^2 \left[\left(\frac{1}{2}\rho u^2 + \rho h\right)u\right]_x - \pi r^2 \left[\left(\frac{1}{2}\rho u^2 + \rho h\right)u\right]_{x+\Delta x} \right\}$$

$$+ \pi r^2 \Delta x \Gamma \left(h^* + \frac{u^{*2}}{2}\right) \tag{2.15}$$

where $\Gamma h^*, \Gamma u^{*2}/2$ are incoming/outgoing energy due to mass exchange and kinetic energy change.

The rate of heat addition by conduction is:

$$\begin{Bmatrix} \text{rate of heat} \\ \text{addition by} \\ \text{conduction} \end{Bmatrix} = (1-\gamma)2\pi r \Delta x U(T^* - T) \tag{2.16}$$

where γ is wellbore open ratio, defined as:

$$\gamma = \frac{\text{Open area of pipe}}{\text{Surface area of pipe}}$$

T^* represents reservoir inflow fluid temperature. U is the overall heat transfer coefficient. The calculation of overall heat transfer coefficient is discussed in Appendix A.

Rate of work done on the system by external forces is:

$$\left\{ \begin{array}{c} \text{rate of work} \\ \text{done on system} \\ \text{by external forces} \end{array} \right\} = \pi r^2 \Delta x u F_g \tag{2.17}$$

The equation (2.12) therefore becomes:

$$\pi r^2 \Delta x \frac{\partial}{\partial t}\left(\frac{1}{2}\rho u^2 + \rho e\right) = \left\{\pi r^2\left[\left(\frac{1}{2}\rho u^2 + \rho h\right)u\right]_x - \pi r^2\left[\left(\frac{1}{2}\rho u^2 + \rho h\right)u\right]_{x+\Delta x}\right\}$$

$$+\pi r^2 \Delta x \Gamma\left(h^* + \frac{u^{*2}}{2}\right) + (1-\gamma)2\pi r \Delta x U(T^* - T) + \pi r^2 \Delta x u F_g$$

$$\tag{2.18}$$

Dividing the equation by $\pi r^2 \Delta x$ and letting Δx go to zero, equation (2.18) becomes:

$$\frac{\partial}{\partial t}\left(\rho\left(e + \frac{u^2}{2}\right)\right) + \frac{\partial}{\partial x}\left(\rho u\left(h + \frac{u^2}{2}\right)\right) = \Gamma\left(h^* + \frac{u^{*2}}{2}\right) + \frac{2(1-\gamma)}{r}U(T^* - T) + u F_g$$

$$\tag{2.19a}$$

The definition of enthalpy of a real fluid can be described as:

$$h = e + \frac{p}{\rho} \tag{2.20}$$

Converting the conservation energy equation into a non-conservative form, we have:

$$\frac{\partial e}{\partial t} + u\frac{\partial e}{\partial x} + u\left[\frac{\partial u}{\partial t} + u\frac{\partial u}{\partial x}\right] + \frac{1}{\rho}\frac{\partial u p}{\partial x} = \frac{\Gamma}{\rho}\left(h^* + \frac{u^{*2}}{2}\right) - \frac{1}{\rho}\left(e + \frac{u^2}{2}\right)\left[\frac{\partial \rho}{\partial t} + \frac{\partial \rho u}{\partial x}\right]$$

$$+ u F_g + \frac{2(1-\gamma)}{r}U(T^* - T)$$

$$\tag{2.19b}$$

2.1.4 Internal Energy, Entropy and Enthalpy Equations

Material derivatives D/Dt can be used to describe the time rate of change of the property of fluid following the path taken by the fluid (Bird et al. 2007; Wilkes, 2006). Therefore, in terms of material derivative, substitute relations in equation (2.3b) and (2.6b) into (2.19b), internal energy change is given as:

$$\frac{De}{Dt} = \frac{\partial e}{\partial t} + u\frac{\partial e}{\partial x} = \frac{\Gamma}{\rho}\left[(h^* - h) + \frac{p}{\rho} + \frac{(u^2 + u^{*2})}{2}\right] + \frac{2(1-\gamma)}{\rho r}U(T^* - T) - \frac{p}{\rho}\frac{\partial u}{\partial x} - \frac{u}{\rho}F_w$$

(2.21)

Equation (2.21) states that flow of a particle along a wellbore is not iso-energetic because $\Gamma \neq 0$, $F_w \neq 0$, and the velocity gradient is non-zero ($\frac{\partial u}{\partial x} \neq 0$) for any injector or producer.

One can rewrite the internal energy evolution equation in terms of evolution of entropy by applying the thermodynamic identity $Tds = de - \frac{p}{\rho^2}d\rho$ to obtain:

$$\frac{Ds}{Dt} = \frac{\Gamma}{\rho T}\left[(h^* - h) + \frac{(u^2 + u^{*2})}{2}\right] + \frac{2(1-\gamma)}{T\rho r}U(T^* - T) - \frac{u}{\rho T}F_w \qquad (2.22)$$

Equation (2.22) shows that the requirement for the flow of any particle along a wellbore to follow an isentropic path is for $\Gamma=0$ (no fluid leaving or entering the wellbore radially) and for friction between the wellbore fluid and the wellbore to be negligible. Therefore, the wellbore flow is not fully isentropic. Alternatively, by enforcing the thermodynamic relation $\frac{Dh}{Dt} = T\frac{Ds}{Dt} + \frac{1}{\rho}\frac{D\rho}{Dt}$, equation (2.22) can be expressed in terms of enthalpy as follows:

$$\frac{Dh}{Dt} = \frac{1}{\rho}\frac{Dp}{Dt} + \frac{\Gamma}{\rho}\left[(h^* - h) + \frac{(u^2 + u^{*2})}{2}\right] + \frac{2(1-\gamma)}{\rho r}U(T^* - T) - \frac{u}{\rho}F_w \qquad (2.23a)$$

Substituting the value of $1/\rho F_w$ from momentum balance equation in its non-conservative form in (equation (2.6b)), and equation (2.23a) becomes:

$$\frac{Dh}{Dt} = \frac{1}{\rho}\frac{\partial p}{\partial t} + \frac{\Gamma}{\rho}\left[(h^* - h) + \frac{(u^{*2} - u^2)}{2}\right] + \frac{2(1-\gamma)}{\rho r}U(T^* - T) - u\frac{Du}{Dt} + \frac{u}{\rho}F_g \quad (2.23b)$$

Equations (2.23a) and (2.23b) show that wellbore flow is not fully isenthalpic because of the non-zero values of mass exchange ($\Gamma \neq 0$), friction, and velocity and pressure gradients.

2.2 Single-Phase Wellbore Flow Model

2.2.1 η_s-driven Model

We start from the enthalpy equation in order to develop temperature equation. Enthalpy is a function of temperature and pressure and can be described as follows:

$$dh = \left(\frac{\partial h}{\partial T}\right)_p dT + \left(\frac{\partial h}{\partial p}\right)_T dp \quad (2.24)$$

where,

$$\left(\frac{\partial h}{\partial T}\right)_p = C_p \quad (2.25a)$$

$$\left(\frac{\partial h}{\partial p}\right)_T = \frac{1}{\rho} - T\left(\frac{\partial V}{\partial T}\right)_p = \frac{1}{\rho} - \frac{\alpha T}{\rho} \quad (2.25b)$$

Then Joule-Thomson Coefficient is defined and calculated as,

$$\eta_h = \left(\frac{\partial T}{\partial P}\right)_h = \frac{\alpha T - 1}{\rho C_p} \quad (2.26)$$

where α is the thermal expansion coefficient.

Then equation (2.24) becomes,

$$dh = C_p dT + \eta_h C_p dp \tag{2.27}$$

On the other hand, for any entropy change, the dependency of temperature and pressure drop can be expressed as:

$$ds = \left(\frac{\partial s}{\partial T}\right)_p dT + \left(\frac{\partial s}{\partial p}\right)_T dp \tag{2.28}$$

The thermodynamic identity $TdS = de - \frac{p}{\rho^2} d\rho$ is substituted into equation (2.27) and by dividing it by dT, one can obtain the expression of $\left(\frac{\partial s}{\partial T}\right)_p$:

$$\left(\frac{\partial s}{\partial T}\right)_p = \frac{C_p}{T} \tag{2.29}$$

In addition, the following thermodynamic identity is implemented:

$$\left(\frac{\partial s}{\partial p}\right)_T = -\left(\frac{\partial v}{\partial T}\right)_p = -\frac{\alpha}{\rho} \tag{2.30}$$

Substituting equation (2.29) and (2.30) into equation (2.28), the change of temperature due to pressure change at constant entropy can be written as follows:

$$\eta_s = \left(\frac{\partial T}{\partial p}\right)_s = \eta_h + \frac{1}{\rho C_p} = \frac{\alpha T}{\rho C_p} = \frac{Y}{\alpha}\frac{k-1}{k} \tag{2.31}$$

where η_s is the isentropic thermal coefficient.

Substituting equation (2.27) into equation (2.23a), one can obtain the thermodynamic transient model as follows:

$$\frac{DT}{Dt} = \frac{\Gamma}{\rho C_p}\left[(h^* - h) + \frac{(u^2 + u^{*2})}{2}\right] + \frac{2(1-\gamma)}{r\rho C_p}U(T^* - T) - \frac{u}{\rho C_p}F_w + \eta_s\frac{Dp}{Dt} \quad (2.32)$$

Note that the first three terms in equation (2.32) are the similar three terms at the right-hand side of the entropy equation (2.22). Hence, the terms prevent the wellbore process from being fully isentropic. This thermal model shows that the wellbore thermal response may also be reasoned in terms of deviations from the isentropic model without regards to the fluid's JTC (Joule-Thomson Coefficient) value. It is also customary to evaluate wellbore models for steady-state conditions, where the influence of time-dependent accumulation terms is neglected on the premise that the rate of mass accumulation inside the wellbore is normally much smaller than its change along the wellbore. For such conditions, Equation (2.32) reduces into the following steady-state thermal model:

$$(2.33a)$$

$$\frac{dT}{dx} = \frac{\Gamma}{\rho u C_p}\left[(h^* - h) + \frac{(u^2 + u^{*2})}{2}\right] + \frac{2(1-\gamma)}{r\rho u C_p}U(T^* - T) - \frac{1}{\rho C_p}F_w + \eta_s\frac{dp}{dx}$$

or,

$$\left(\frac{dT}{dx}\right)_t = \left(\frac{dT}{dx}\right)_{ex} + \left(\frac{dT}{dx}\right)_f + \left(\frac{dT}{dx}\right)_{\eta_s} \quad (2.33b)$$

where:

$\left(\frac{dT}{dx}\right)_{ex} = \frac{\Gamma}{\rho u C_p}\left[(h^* - h) + \frac{(u^2 + u^{*2})}{2}\right] + \frac{2(1-\gamma)}{r\rho u C_p}U(T^* - T)$ *temperature change due to energy exchange;*

$\left(\frac{dT}{dx}\right)_f = -\frac{1}{\rho C_p}F_w = -\frac{1}{C_p}f_M\frac{u^2}{2d}$ *temperature change due to frictional effects;*

$\left(\frac{dT}{dx}\right)_{\eta_s} = \eta_s\frac{dp}{dx}$ *temperature change due to isentropic expansion effects.*

Equation (2.33) may be readily implemented to predict temperature profiles along a producing wellbore. It should be further noted that the model is fully applicable to inclined wellbores, even

in the absence of an explicit elevation term in the thermal model. The elevation term was fully considered by the outlined derivation, and its effect is ultimately captured by the resulting pressure gradient.

2.2.2 η_h-driven Model

Yoshioka et al. (2005a) emphasized the importance of the Joule-Thomson coefficient (JTC) in determining the thermal behavior of horizontal wellbores. In order to assess the effect that JTC may have on wellbore thermal behavior, the η_s -driven wellbore thermal model in Equation (2.32) may be recast in terms of JTC by substituting the thermodynamic identity $\eta_s = \eta_h + 1/\rho C_p$ and the momentum equation (2.6b) to yield:

$$\frac{DT}{Dt} = \frac{1}{\rho C_p}\frac{dp}{dt} + \frac{\Gamma}{\rho C_p}\left[(h^* - h) + \frac{(u^{*2} - u^2)}{2}\right] + \frac{2(1-\gamma)}{r\rho C_p}U(T^* - T) - \frac{u}{C_p}\frac{Du}{Dt} + \frac{u}{\rho C_p}F_g + \eta_h\frac{Dp}{Dt}$$

(2.34)

For steady-state conditions, Equation (23) becomes:

$$\frac{dT}{dx} = \frac{\Gamma}{\rho u C_p}\left[(h^* - h) + \frac{(u^{*2} - u^2)}{2}\right] + \frac{2(1-\gamma)}{r\rho u C_p}U(T^* - T) - \frac{u}{C_p}\frac{du}{dx} + \frac{1}{\rho C_p}F_g + \eta_h\frac{dp}{dx} \quad (2.35a)$$

or,

$$\left(\frac{dT}{dx}\right)_t = \left(\frac{dT}{dx}\right)_{ex} + \left(\frac{dT}{dx}\right)_{ke} + \left(\frac{dT}{dx}\right)_{pe} + \left(\frac{dT}{dx}\right)_{\eta_h} \tag{2.35b}$$

where:

$\left(\frac{dT}{dx}\right)_{ex} = \frac{\Gamma}{\rho u C_p}\left[(h^* - h) + \frac{(u^{*2}-u^2)}{2}\right] + \frac{2(1-\gamma)}{r\rho u C_p}U(T^* - T)$ *temperature change due to energy exchange;*

$\left(\frac{dT}{dx}\right)_{ke} = -\frac{u}{\rho C_p}\frac{du}{dx}$ *temperature change due to kinetic energy effects;*

$\left(\frac{dT}{dx}\right)_{pe} = \frac{1}{\rho C_p}F_g$ *temperature change due to potential energy effects;*

$\left(\frac{dT}{dx}\right)_{\eta_h} = \eta_h\frac{dp}{dx}$ *temperature change due to JTC effects.*

When compared against Equation (2.35a), Yoshioka's model embraced two additional assumptions: (1) Kinetic energy effects can be neglected when solving for wellbore temperature responses; (2) Enthalpic jump $(h^* - h)$ between reservoir and wellbore conditions can be decoupled from pressure (the pressure difference between the reservoir and the wellbore can be neglected). Thus, the single-phase thermal wellbore model proposed by Yoshioka, et al (2005a) is written for wellbores fully opened to reservoir flow as follows:

$$\frac{dT}{dx} = \frac{\Gamma}{\rho u}(T^* - T) + \frac{1}{\rho C_p}F_g + \eta_h \frac{dp}{dx} \tag{2.36}$$

where the approximation $h^* - h = C_p dT$ used in Yoshioka's model has been applied.

2.3 Two-Phase Wellbore Flow Model

Three types of models are commonly used by the petroleum industry to model the impact of multiphase fluid on wellbores—homogeneous, drift-flux and mechanistic. The fundamental assumption in the homogeneous model is that fluids in the system are perfectly mixed so that there is no slip between each phase, hence forming a homogeneous mixture (Hasan and Kabir, 2002). Treated as a single-phase fluid, the two-phase fluid is considered to have one velocity-mixture velocity, and the properties of the two-phase fluid can be represented by mixture properties. The homogeneous model with slip between phases is named the drift-flux model. To allow for the slip between phases, empirical parameters are needed to estimate the volume fraction of each phase. Generally, mechanistic models are the most accurate among these three models for their consideration of the detailed physics of each flow pattern. However, at some flow-pattern transitions, the mechanistic model can cause discontinuities of pressure drop or holdup, resulting in a convergence problem (Shi et al., 2005). In our study, both the homogeneous and drift-flux models are implemented in the wellbore thermal models.

2.3.1 Two-phase Flow Variables

2.3.1.1 Liquid Holdup and Gas Void Fraction

Liquid holdup (y_L) is the fraction of a two-phase flow volume element occupied by the respective liquid phase. Similarly, the gas void fraction (y_G) is the fraction of the volume element that is occupied by the gas phase (Shoham, 2006).

For oil-gas two-phase flow:

$$y_O + y_G = 1 \tag{2.37a}$$

and for the oil-water two-phase flow:

$$y_O + y_W = 1 \tag{2.37b}$$

We take the oil-gas two-phase flow as an example in our following discussion of two-phase flow variables and models.

2.3.1.2 Superficial Velocity

Superficial velocity describes the volumetric flow rate per unit area, which is the volumetric flux of the phase. Superficial velocity of oil and gas are:

$$u_{SO} = \frac{q_O}{A} \tag{2.38a}$$

$$u_{SG} = \frac{q_G}{A} \tag{2.38b}$$

where A is the cross-sectional area of the wellbore.

2.3.1.3 Mixture Velocity

The mixture velocity refers to the total volumetric flow rate of both phases per unit area. In oil and gas flow, mixture velocity is given as:

$$u_m = u_{SO} + u_{SG} \tag{2.39}$$

2.3.1.4 Actual Velocity

The actual velocity of a specific phase is its volumetric flowrate divided by the actual cross-sectional area occupied by the phase. The actual velocity of the oil and gas phases is:

$$u_O = \frac{q_O}{A_O} = \frac{u_{SO}}{y_O} \tag{2.40a}$$

$$u_G = \frac{q_G}{A_G} = \frac{u_{SG}}{y_G} \tag{2.40b}$$

2.3.2 Homogeneous Model

Because of the no-slip assumption of the homogeneous model, the volume fraction of each phase can be directly evaluated by the ratio of the flowrate of one phase to the total volumetric flowate. For homogeneous flow, liquid holdup can be estimated as:

$$y_O = \frac{q_O}{q_O + q_G} \tag{2.41}$$

Two-phase fluid is transported at same velocity, which is mixture velocity:

$$u_m = u_{SO} + u_{SG} \tag{2.42}$$

Secondly, the momentum balance equation at steady-state is considered as one system equation with mixture properties:

$$\frac{d(\rho_m u_m{}^2)}{dx} + \frac{dp}{dx} = \frac{f_m \rho_m u_m{}^2}{2d} + \rho_m g sin\theta \tag{2.43}$$

Mixture density ρ_m is expressed as:

$$\rho_m = y_O \rho_O + y_G \rho_G \tag{2.44}$$

where f_m is the mixture friction factor. In its calculation, the mixture Reynolds number can be calculated as:

$$Re_m = \frac{\rho_m u_m d}{\mu_m} \tag{2.45}$$

in which the mixture viscosity is given as:

$$\mu_m = y_O\mu_O + y_G\mu_G \tag{2.46}$$

Thirdly, the temperature equation at steady-state for each phase i becomes:

$$y_i\rho_i u_m C_{p_i}\frac{dT_i}{dx} = \Gamma_i\left[(h^*_i - h_i) + \frac{(u^2_m + u^{*2}_i)}{2}\right] + \frac{2(1-\gamma)}{r}Q_i - y_i u_m F_w + y_i\rho_i u_m C_{p_i}\eta_{s_i}\frac{dp_i}{dx}$$

$$\tag{2.47}$$

Summation of equations for the two-phase flow is shown as:

$$u_m\sum_i y_i\rho_i C_{p_i}\frac{dT_i}{dx} = \sum_i \Gamma_i\left[(h^*_i - h_i) + \frac{(u^2_m + u^{*2}_i)}{2}\right] + \frac{2(1-\gamma)}{r}\sum Q_i$$

$$-u_m F_w + u_m\sum_i y_i\rho_i C_{p_i}\eta_{s_i}\frac{dp_i}{dx} \tag{2.48}$$

Here, we assume that in each phase pressure and temperature are the same; then the equation becomes:

$$u_m\sum_i y_i\rho_i C_{p_i}\frac{dT}{dx} = \sum_i \Gamma_i\left[(h^*_i - h_i) + \frac{(u^2_m + u^{*2}_i)}{2}\right] + \frac{2(1-\gamma)}{r}U(T^* - T)$$

$$-u_m F_w + u_m\sum_i y_i\rho_i C_{p_i}\eta_{s_i}\frac{dp}{dx} \tag{2.49}$$

The final form of the temperature equation becomes:

$$\frac{dT}{dx} = \frac{\sum_i \Gamma_i}{u_m\sum_i y_i\rho_i C_{p_i}}\left[(h^*_i - h_i) + \frac{(u^2_m + u^2_i)}{2}\right] + \frac{2(1-\gamma)}{ru_m\sum_i y_i\rho_i C_{p_i}}U(T^* - T)$$

$$-\frac{1}{\sum_i y_i\rho_i C_{p_i}}F_w + \frac{\sum_i y_i\rho_i C_{p_i}\eta_{s_i}}{\sum_i y_i\rho_i C_{p_i}}\frac{dp}{dx} \tag{2.50}$$

2.3.3 Drift-Flux Model

In the drift-flux model, slip between phases is considered. Because of the non-uniform velocity profiles, one phase of two-phase flow is transported at a higher velocity than the other phase. For the oil-gas two-phase flow, gas tends to have a higher velocity than oil; while for the water-oil flow, it depends on whether the flow pattern is O/W (oil phase dispersed in water phase) or W/O (water phase dispersed in oil phase). Dispersed phase has higher velocity than the continuous phase. Compared to the homogeneous model, the evaluation of holdup (in-situ volume fraction) of each phase comes from an empirical correlation based on experiment.

Two mechanisms are considered in the oil-gas two-phase flow drift-flux model—first, the non-uniform velocity and phase distribution profiles over the cross section of the wellbore. In the center of the pipe, gas tends to have the highest concentration, with the highest local mixture velocity, so the average gas velocity is higher than that of oil. Second, due to a buoyancy effect in vertical wells, gas has the tendency to rise vertically through oil (Shi et al. 2005).The drift-flux model for the oil-gas phase can be expressed as:

$$u_G = C_o u_m + u_D \tag{2.51}$$

where C_o is the profile parameter (distribution coefficient) that describes the velocity effect and concentration profiles. u_D is the drift-flux velocity, which represents the buoyancy effect. C_o varies between 1.0 and 1.2 and is estimated by Choi et al. (2012) in their proposed model as:

$$C_o = \frac{2}{1 + (Re_m/1000)^2} + \frac{1.2 - 0.2\sqrt{\rho_G/\rho_O}\,(1 - \exp(-18y_G))}{1 + (1000/Re_m)^2} \tag{2.52}$$

Choi (2012) also presented a modified model to calculate drift velocity, including the inclination effect:

$$u_D = A\cos\theta + B\left(\frac{g\tau_{O-G}|\Delta\rho|}{\rho_O{}^2}\right)^{0.25}\sin\theta \qquad (2.53)$$

$$A = 0.0246, B = 1.606$$

where $|\Delta\rho|$ is the absolute value of the density difference between the oil and gas phases, τ_{O-G} is

surface tension between the oil and gas phases.

With the gas velocity calculated by drift-flux model, the volume fractions of gas phase and liquid

phase can be evaluated as:

$$y_G = \frac{u_{SG}}{u_G} \qquad (2.54a)$$

$$y_O = \frac{u_{SO}}{u_O} = 1 - y_G \qquad (2.54b)$$

In water-oil flow, two types of flow system are considered— W/O and O/W. The determination

of flow pattern is based on the boundary line in generalized flow patterns mapped by

Hapanowicz, (2008) and written as:

$$g_O = 1.3525g_W{}^{0.812} \qquad (2.55)$$

where g_O , g_W are the apparent mass flux of oil and water expressed as:

$$g = \frac{\dot{m}}{A} \qquad (2.56)$$

where $\dot{m}$ is the mass flow rate written as:

$$\dot{m} = q \cdot \rho \qquad (2.57)$$

To determine the flow pattern of oil-water flow system, g_O and g_W are calculated respectively. If $g_O > 1.3525 g_W{}^{0.812}$, the flow pattern of the system is considered as W/O; Otherwise, the flow pattern of the system is considered as O/W.

The drift-flux model of the liquid-liquid flow system given by Hapanowicz (2008) is:

$$u_d = C_d u_m + u_D \tag{2.58}$$

where subscript d denotes dispersion phase.

Determination of the profile parameter C_d and drift velocity of the dispersion phase u_D are determined the relationship (Dix, 1971):

$$C_d = X_d \left[1 + \left(\frac{1}{X_d} - 1 \right)^{\left(\frac{\rho_d}{\rho_c} \right)^{0.1}} \right] \tag{2.59}$$

$$u_D = 2.9 \left(\frac{g \tau_{O-W} |\Delta \rho|}{\rho_c{}^2} \right)^{0.25} \tag{2.60}$$

Firoozabadi and Ramey's (1988) correlation is used in calculating the surface tension (τ_{O-W}) between the oil and water phases. X_d is the apparent volume fraction of the dispersion phase determined by the flowrate of the two-phase flow:

$$X_d = \frac{q_d}{q_d + q_c} \tag{2.61}$$

where subscript c denotes a continuous phase.

In our application of oil-water drift-flux model, we assume the flow pattern is W/O in order to have continuous pressure and temperature profiles. Oil and liquid holdup can be calculated as follows:

$$y_W = \frac{u_{SW}}{u_W} \tag{2.62}$$

$$y_O = \frac{u_{SO}}{u_O} = 1 - y_W \tag{2.63}$$

Assume that the system has one pressure in each segment, pressure equation for each phase i is:

$$\frac{d(y_i \rho_i u_i{}^2)}{dx} + y_i \frac{dp}{dx} = y_i F_{w_i} + y_i F_{g_i} \tag{2.64}$$

$$F_{w_i} = \frac{f_{M_i} \rho_i u_i{}^2}{2 d_e g_c} \tag{2.65}$$

where d_e is phase wetted equivalent diameter(Ayala, 2001).

Summation of pressure equation of each phase, we have:

$$\frac{d(\sum y_i \rho_i u_i{}^2)}{dx} + \frac{dp}{dx} = \sum y_i F_{w_i} + \sum y_i F_{g_i} \tag{2.66}$$

The temperature equation at steady-state for each phase i becomes:

$$y_i \rho_i u_i C_{p_i} \frac{dT_i}{dx} = \Gamma_i \left[(h^*{}_i - h_i) + \frac{(u^2{}_i + u^{*2}{}_i)}{2} \right] + \frac{2(1-\gamma)}{r} Q_i - y_i u_i F_{w_i} + y_i \rho_i u_i C_{p_i} \eta_{s_i} \frac{dp_i}{dx}$$

Summation of equations for the two-phase flow is shown as: $\tag{2.67}$

$$\sum_i y_i \rho_i u_i C_{p_i} \frac{dT_i}{dx} = \sum_i \Gamma_i \left[(h^*{}_i - h_i) + \frac{(u^2{}_i + u^{*2}{}_i)}{2} \right] + \frac{2(1-\gamma)}{r} \sum Q_i$$

$$- \sum_i y_i u_i F_{w_i} + \sum_i y_i \rho_i u_i C_{p_i} \eta_{s_i} \frac{dp_i}{dx} \tag{2.68}$$

Here, we assume that in each phase pressure and temperature are the same; then the equation becomes:

$$\sum_i y_i \rho_i u_i C_{p_i} \frac{dT}{dx} = \sum_i \Gamma_i \left[(h^*{}_i - h_i) + \frac{(u^2{}_i + u^{*2}{}_i)}{2} \right] + \frac{2(1-\gamma)}{r} U(T^* - T)$$

$$- \sum_i y_i u_i F_{w_i} + \sum_i y_i \rho_i u_i C_{p_i} \eta_{s_i} \frac{dp}{dx} \tag{2.69}$$

The final form of the temperature equation becomes:

$$\frac{dT}{dx} = \frac{\sum_i \Gamma_i}{\sum_i y_i \rho_i u_i C_{p_i}} \left[(h^*{}_i - h_i) + \frac{(u^2{}_i + u^{*2}{}_i)}{2} \right] + \frac{2(1-\gamma)}{r \sum_i y_i \rho_i u_i C_{p_i}} U(T^* - T)$$

$$- \frac{\sum_i y_i u_i}{\sum_i y_i \rho_i u_i C_{p_i}} F_{w_i} + \frac{\sum_i y_i \rho_i u_i C_{p_i} \eta_{s_i}}{\sum_i y_i \rho_i u_i C_{p_i}} \frac{dp}{dx} \tag{2.70}$$

CHAPTER 3

SOLUTION PROCEDURE

In this chapter, the solution procedure of the proposed model is discussed in both its single-phase

and two-phase flow form at steady-state conditions. Figure 3.1 shows a simplified schematic of a
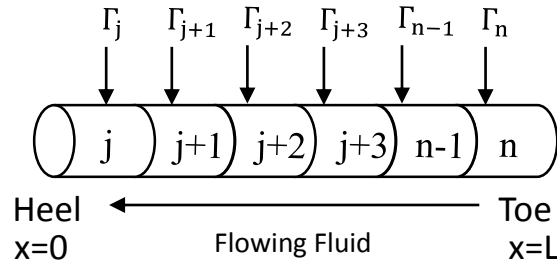
discretized wellbore.

Fig. 3.1 A Schematic of a Discretized Wellbore

3.1 Single-phase Flow

The steady-state mass equation (2.3a) can be written as follows:

$$\rho \frac{\partial u}{\partial x} + u \frac{\partial \rho}{\partial x} = \Gamma \tag{3.1}$$

The steady-state equation above can be converted to its forward finite difference form as follows:

$$\rho_j \frac{u_{j+1} - u_j}{\Delta x_j} + u_j \frac{\rho_{j+1} - \rho_j}{\Delta x_j} = \Gamma_j \tag{3.2}$$

Therefore, by making the velocity of the investigated segment as the objective, equation (3.2)

can be solved utilizing the following expression:

$$u_j = A_j u_{j+1} - B_j \tag{3.3}$$

$$A_j = \frac{\rho_j}{2\rho_j - \rho_{j+1}}$$

$$B_j = \frac{\Gamma_i \Delta x_i}{2\rho_j - \rho_{j+1}}$$

Because we set heel to toe as a positive direction (refer to Fig 2.1), while fluid flows from toe to

heel, the velocities that we solved have a negative value.

In a similar way, the momentum equation (2.6a) in its steady-state can be:

$$\frac{\partial \rho u^2}{\partial x g_c J_0} + \frac{\partial p}{\partial x} = \frac{F_w + F_g}{J_0} \tag{3.4}$$

Again, to solve the equation above, a finite difference form of the equation is expressed as:

$$\frac{p_{j+1} - p_j}{\Delta x_j} = -\left(\frac{\rho_{j+1} u_{j+1}^2 - \rho_j u_j^2}{\Delta x_j g_c J_0}\right) + \frac{F_{wj}}{J_0} + \frac{F_{gj}}{J_0} \tag{3.5}$$

Then, the pressure at each segment can be solved in the following expression:

$$p_j = p_{j+1} + C_j \tag{3.6}$$

where,

$$C_j = \Delta x_j \left[-\frac{F_{wj}}{J_o} - \frac{F_{gj}}{J_o}\right] + \left[\frac{(\rho_{j+1} u_{j+1}^2) - (\rho_j u_j^2)}{g_c J_0}\right]$$

Finally, the thermal response equation (2.33a) can be expressed as:

$$\frac{T_{j+1} - T_j}{\Delta x_j} = \frac{\Gamma_j}{\rho_j u_j C_{p_j}} \left[(h^*_j - h_j) + \frac{(u_j^2 + u_j^{*2})}{2 g_c J_1}\right] + \frac{2(1-\gamma)}{r \rho_j u_j C_{p_j}} U_j(T_j^* - T_j) - \frac{1}{\rho_j C_{p_j} J_2 J_0} F_{wj}$$

$$+ \frac{\alpha_j T_j}{\rho_j C_{p_j} J_2} \frac{p_{j+1} - p_j}{\Delta x_j} \tag{3.7}$$

Therefore,

$$T_j = \frac{T_{j+1} + \Delta x_j \left(-D_j - E_j T_j^* + F_j\right)}{1 + \Delta x_j \left(-E_j + G_j\right)} \tag{3.8}$$

$$D_j = \frac{\Gamma_j}{\rho_j u_j C_{p_j}} \left[(h^*_j - h_j) + \frac{(u_j^2 + u_j^{*2})}{2 g_c J_1}\right]$$

$$E_j = \frac{2(1-\gamma)}{r \rho_j u_j C_{p_j}} U_j$$

$$F_j = \frac{1}{\rho_j C_{p_j} J_2 J_0} F_{wj}$$

$$G_j = \frac{\alpha_j}{\rho_j C_{p_j} J_2} \frac{p_{j+1} - p_j}{\Delta x_j}$$

J_0, J_1, J_2 are unit conversion constants and are given in the nomenclature. The fluid properties are calculated by the Peng-Robinson Equation of State. To solve the equations simultaneously, a velocity profile is first generated in equation (3.3) by specifying the flowrate of each segment and initial estimate of velocity, pressure and temperature profiles. Then, the pressure profile is solved based on velocity profiles. After that, the model calculates temperature based on the results of the velocity and pressure profiles. The solving procedure for these three equations is repeated until the temperature reaches convergence.

3.2 Two-Phase Flow

3.2.1 Homogeneous Model

For two-phase flow, we implement two models (homogeneous and drift-flux) in our results. The difference between these two models is the procedure to calculate phase holdup and velocity profiles. In the homogeneous model, take oil-gas flow as an example, oil holdup is obtained as:

$$y_{Oj} = \frac{q_{Oj}}{q_{Oj} + q_{Gj}} \tag{3.9}$$

The mixture velocity is calculated as:

$$u_{mj} = u_{SOj} + u_{SGj} = \frac{q_{Oj} + q_{Gj}}{A} \tag{3.10}$$

To solve pressure in the two-phase flow system, the solution procedure is the same as for the single-phase flow, except that fluid properties are replaced by mixture properties. Finite difference form of pressure equation is:

$$\frac{p_{j+1} - p_j}{\Delta x_j} = -\left(\frac{\rho_{m\,j+1}\, u_{m\,j+1}^2 - \rho_{m\,j}\, u_{m\,j}^2}{\Delta x_j g_c J_0}\right) + \frac{F_{w\,j}}{J_0} + \frac{F_{g\,j}}{J_0} \tag{3.11}$$

Following expression can be used to solve for pressure in each segment:

$$p_j = p_{j+1} + C_j \tag{3.12}$$

where,

$$C_j = \Delta x_j \left[-\frac{F_{w\,j}}{J_0} - \frac{F_{g\,j}}{J_0}\right] + \left[\frac{\left(\rho_{m\,j+1}\, u_{m\,j+1}^2\right) - \left(\rho_{m\,j}\, u_{m\,j}^2\right)}{g_c J_0}\right]$$

The finite difference form of the temperature equation in each phase can be written as:

$$\frac{T_{j+1} - T_j}{\Delta x_j} = \frac{\sum_i \Gamma_{ij}\left[\left(h^*_{j} - h_j\right) + \frac{\left(u_{m\,j}^2 + u^{*2}_{j}\right)}{2 g_c J_1}\right]_i}{u_{m\,j}\, \sum_i \left(y_j \rho_j C_{p\,j}\right)_i} + \frac{2(1-\gamma)}{r u_{m\,j}\, \sum_i \left(y_j \rho_j C_{p\,j}\right)_i} U_j(T^*_{j} - T_j)$$

$$-\frac{1}{\sum_i \left(y_j \rho_j C_{p\,j}\right)_i}\frac{F_{w\,j}}{J_2 J_0} + \frac{\sum_i \left(y_j \rho_j C_{p\,j}\frac{\alpha_j T_j}{\rho_j C_{p\,j} J_2}\right)_i}{\sum_i \left(y_j \rho_j C_{p\,j}\right)_i}\frac{p_{j+1} - p_j}{\Delta x_j} \tag{3.13}$$

Similarly to the single-phase solution procedure, one can solve the equation (3.13) using the expression below:

$$T_j = \frac{T_{j+1} + \Delta x_j\left(-D_j - E_j T^* + F_j\right)}{1 + \Delta x_j\left(-E_j + G_j\right)} \tag{3.14}$$

$$D_j = \frac{\sum_i \Gamma_{ij} \left[(h^*_j - h_j) + \frac{\left(u_{m}{}^2{}_j + u^{*2}{}_j\right)}{2g_c J_1} \right]_i}{u_{m_j} \sum_i \left(y_j \rho_j C_{p_j} \right)_i}$$

$$E_j = \frac{2(1-\gamma)}{r u_{m_j} \sum_i \left(y_j \rho_j C_{p_j} \right)_i} U_j$$

$$F_j = \frac{1}{u_{m_j} \sum_i \left(y_j \rho_j C_{p_j} \right)_i} \frac{F_{w_j}}{J_2 J_0}$$

$$G_j = \frac{\sum_i \left(y_j \rho_j C_{p_j} \frac{\alpha_j T_j}{\rho_j C_{p_j} J_2} \right)_i}{\sum_i \left(y_j \rho_j C_{p_j} \right)_i} \frac{p_{j+1} - p_j}{\Delta x_j}$$

3.2.2 Drift-flux Model

For oil-water flow in drift-flux model, u_G and y_G is calculated simultaneously by solving equation (2.51). Substituting equations (2.52) and (2.53) into (2.51), we have:

$$u_{G_j} = C_{o_j} u_{m_j} + u_{D_j} \tag{3.12}$$

where,

$$C_{o_j} = \frac{2}{1 + (Re_{m_j}/1000)^2} + \frac{1.2 - 0.2\sqrt{\rho_{G_j}/\rho_{o_j}}\left(1 - \exp(-18 y_{G_j})\right)}{1 + (1000/Re_{m_j})^2}$$

$$u_{D_j} = A\cos\theta + B \left(\frac{g(\tau_{O-G})_j |\Delta\rho|_j}{\rho_{o_j}{}^2} \right)^{0.25} \sin\theta$$

The u_G and y_G are calculated iteratively. y_G is initialized as an input to get C_0. u_m is calculated by equation(3.9). After calculating u_D, u_G is evalutated in equation(3.12). Based on this, new y_G is updated in the loop until input and output y_G results are considered the same as each other.

After that, velocity and holdup of oil are calculated as:

$$y_{Oj} = \frac{u_{SOj}}{u_{Oj}} = 1 - y_{Gj} \qquad (3.13)$$

For oil-water flow, water velocity is calculated as:

$$u_{Wj} = C_{dj}u_{mj} + u_{Dj} \qquad (3.14)$$

where,

$$C_{dj} = X_{dj}\left[1 + \left(\frac{1}{X_{dj}} - 1\right)^{\left(\frac{\rho_{Wj}}{\rho_{Oj}}\right)^{0.1}}\right]$$

$$X_{dj} = \frac{q_{Wj}}{q_{Wj} + q_{Oj}}$$

$$u_{Dj} = 2.9\left(\frac{g(\tau_{O-W})_j|\Delta\rho_j|}{{\rho_{Oj}}^2}\right)^{0.25}$$

Water holdup is decided as:

$$y_{Wj} = \frac{u_{SWj}}{u_{Wj}} \qquad (3.15)$$

Velocity and holdup of oil phase is calculated as:

$$y_{Oj} = \frac{u_{SOj}}{u_{Oj}} = 1 - y_{Wj} \qquad (3.16)$$

$$\frac{p_{j+1} - p_j}{\Delta x_j} = -\left(\frac{\Sigma_i(y_{j+1}\rho_{j+1}u_{j+1}{}^2)_i - \Sigma_i(y_j\rho_j u_j{}^2)_i}{\Delta x_j g_c J_0}\right) + \frac{\Sigma_i\left(y_j F_{w\,j}\right)_i}{J_0} + \frac{\Sigma_i\left(y_j F_{g\,j}\right)_i}{J_0}$$

$$(3.17)$$

The following expression can be used to solve for pressure in each segment:

$$p_j = p_{j+1} + C_j$$

$$(3.18)$$

where,

$$C_j = \Delta x_j\left[-\frac{\Sigma_i\left(y_j F_{w\,j}\right)_i}{J_o} - \frac{\Sigma_i\left(y_j F_{g\,j}\right)_i}{J_o}\right] + \left[\frac{\Sigma_i(y_{j+1}\rho_{j+1}u_{j+1}{}^2)_i - \Sigma_i(y_j\rho_j u_j{}^2)_i}{g_c J_0}\right]$$

$$(3.19)$$

Finally, finite difference form of temperature equation is expressed as:

$$\frac{T_{j+1} - T_j}{\Delta x_j} = \frac{\Sigma_i \Gamma_{ij}\left[(h^*{}_j - h_j) + \frac{(u^2{}_j + u^{*2}{}_j)}{2g_c J_1}\right]_i}{\Sigma_i\left(y_j\rho_j u_j C_{p\,j}\right)_i} + \frac{2(1-\gamma)}{r\,\Sigma_i\left(y_j\rho_j u_j C_{p\,j}\right)_i}U_j(T^*{}_j - T_j)$$

$$-\frac{\Sigma_i\left(y_j u_j F_{w\,j}\right)_i}{\Sigma_i\left(y_j\rho_j u_j C_{p\,j}\right)_i J_2 J_0} + \frac{\Sigma_i\left(y_j\rho_j u_j C_{p\,j}\frac{\alpha_j T_j}{\rho_j C_{p\,j}J_2}\right)_i}{\Sigma_i\left(y_j\rho_j u_j C_{p\,j}\right)_i}\frac{p_{j+1} - p_j}{\Delta x_j}$$

$$(3.20)$$

Similarly to the homogeneous model solution procedure, one can solve the equation (3.20) using the expression below:

$$T_j = \frac{T_{j+1} + \Delta x_j\left(-D_j - E_j T^* + F_j\right)}{1 + \Delta x_j\left(-E_j + G_j\right)}$$

$$(3.21)$$

$$D_j = \frac{\sum_i \Gamma_{ij}\left[(h^*_j - h_j) + \frac{(u^2_j + u^{*2}_j)}{2g_cJ_1}\right]_i}{\sum_i \left(y_j\rho_j u_j C_{p_j}\right)_i}$$

$$E_j = \frac{2(1-\gamma)}{r\sum_i \left(y_j\rho_j u_j C_{p_j}\right)_i}U_j$$

$$F_j = \frac{\sum_i \left(y_j u_j F_{w_j}\right)_i}{\sum_i \left(y_j\rho_j u_j C_{p_j}\right)_i J_2 J_0}$$

$$G_j = \frac{\sum_i \left(y_j\rho_j u_j C_{p_j}\frac{\alpha_j T_j}{\rho_j C_{p_j}J_2}\right)_i}{\sum_i \left(y_j\rho_j u_j C_{p_j}\right)_i}\frac{p_{j+1} - p_j}{\Delta x_j}$$

The solution procedure flow chart is in Figure 3.2:
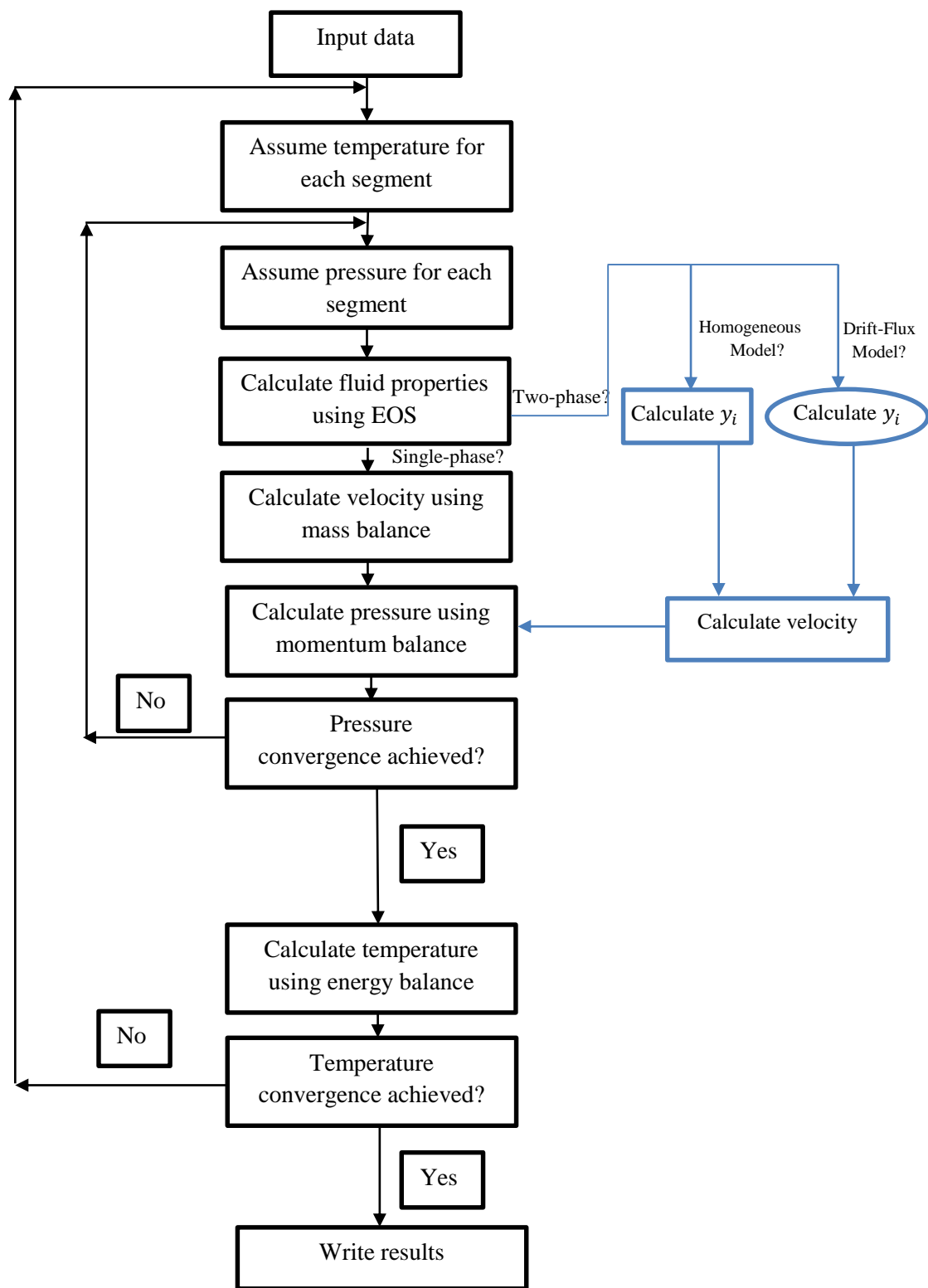
Fig. 3.2 Solution Flow Chart

CHAPTER 4

SINGLE-PHASE FLOW RESULTS AND DISCUSSIONS

In this chapter, we first generate velocity, pressure and temperature profiles by proposed model of single-phase oil, water and gas. Comparison between our model (η_s-driven model) and η_h-driven model is implemented to show the temperature difference caused by different assumptions. Then, sensitivity study is conducted to discuss wellbore fluids' sensitivity to the change of wellbore inclination, flowrate, wellbore roughness, radius and completion type.

4.1 Openhole Wellbore Single-phase Flow Problem

To illustrate the applicability of the η_s-driven wellbore thermal model, we present the thermal responses of the most relevant single-phase flow cases—oil, water, and natural gas flows—and interpret how they behave differently when compared against each other. We consider a horizontal wellbore section fully open to flow, having a length of 4000 ft. divided into 50 equal segments for the numerical methodology. The horizontal wellbore also has standard values for its relative roughness and diameter which are shown in Table 4.1.

<div align="center">

Table 4.1 Openhole Wellbore Description

Inner diameter(in)	2.5
Wellbore length(ft)	4000
Inclination(degree)	0
Relative roughness	0.027

</div>

For consistency purposes, reservoir pressure and temperature for all the cases were taken with the values of 3900 psia and 190 ºF, respectively. Compositions of the oil and natural gas fluids are presented in Table 4.2.

Table 4.2 Fluid Composition

Oil		Gas	
Component	mol %	Component	mol %
C1	0.6	C1	0.886
C3	0.1	C2	0.049
C6	0.1	C3	0.025
C10	0.1	nC4	0.01
C15	0.05	nC5	0.01
C20	0.05	N2	0.02

The phase envelopes are shown in Figures 4.1 and 4.2, and their initial single-phase condition is highlighted. The reservoir condition guaranteed that fluids are in their single-phase condition.
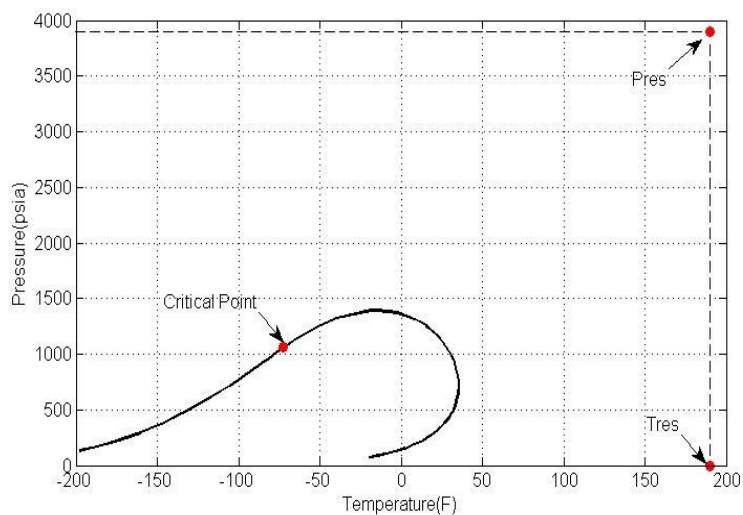
Fig. 4.1 Phase Envelope for Gas
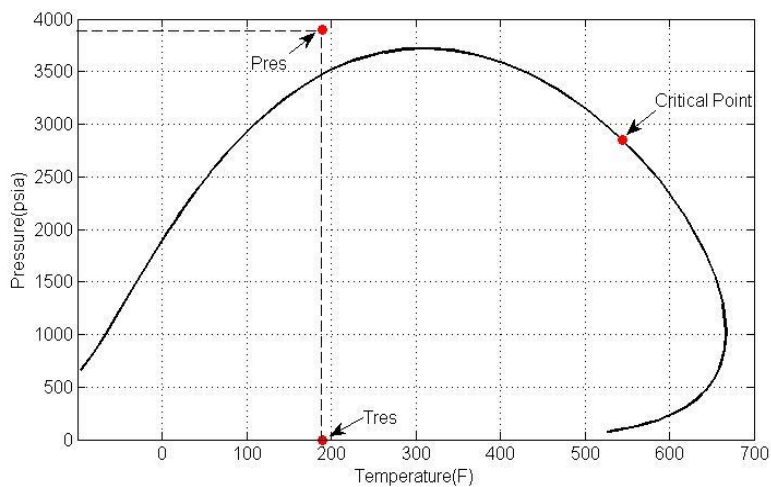
Fig. 4.2 Phase Envelope for Oil

Water, gas, and oil cumulative flow rates along the wellbore are specified in Figure 4.3.

Production of oil and water are specified at the same rate for better comparison of their thermal

response.
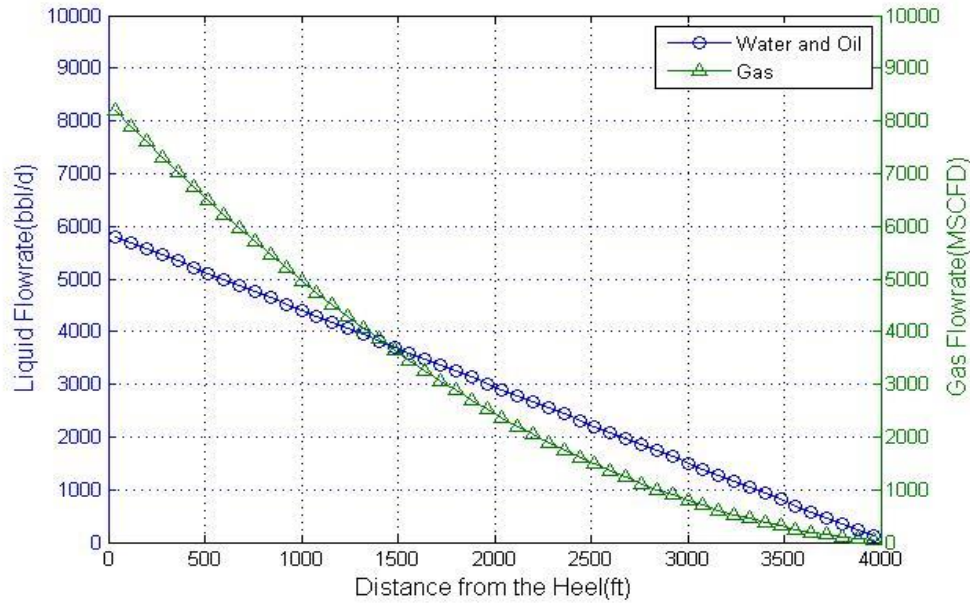
Fig. 4.3 Cumulative Flow Rates of Water, Oil and Gas along Wellbore

Figure 4.4 and Figure 4.5 show the velocity and pressure response in water, oil and gas cases. With

the same flowrate, velocity profiles of oil and water solved by the mass balance equation are almost

overlapping each other. Since water has the highest density among three fluid, it experiences the

largest friction force (F_w), therefore results in the highest pressure drop among three fluids.
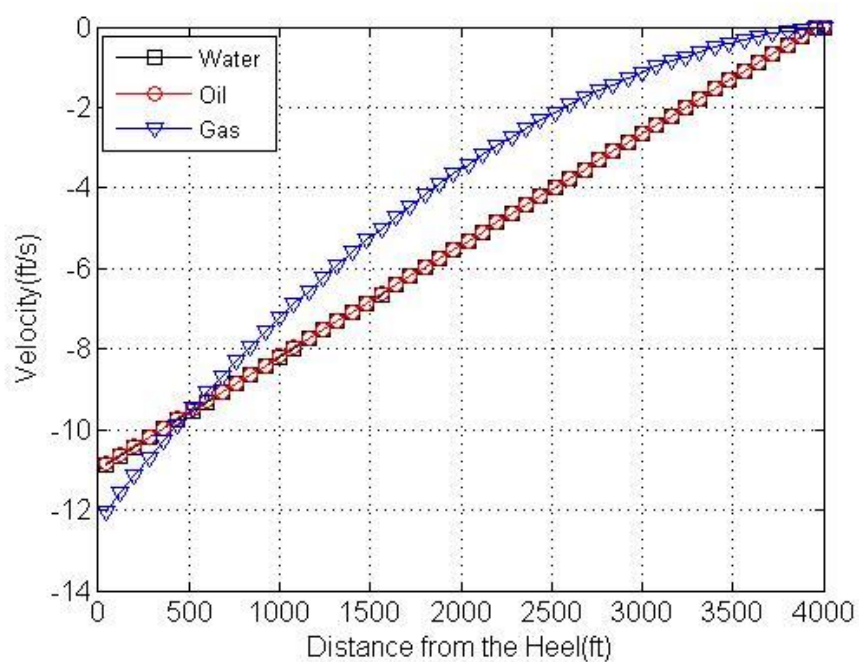
Fig. 4.4 η_S-driven Model Velocity Profiles for Oil, Water and Gas Single-Phase Flow-Horizontal Wellbore
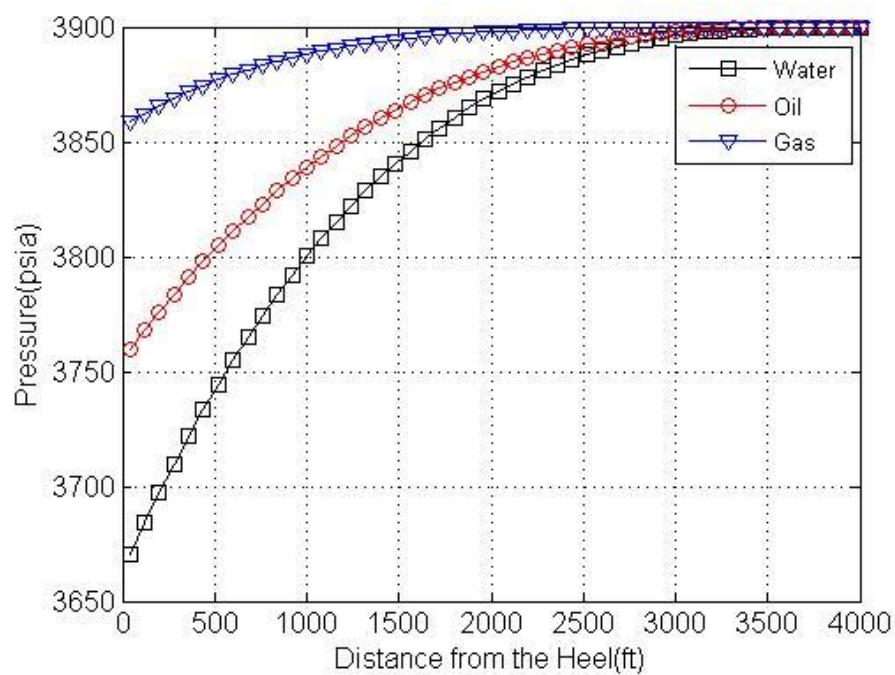
Fig. 4.5 η_S-driven Model Pressure Profiles for Oil, Water and Gas Single-Phase Flow-Horizontal Wellbore

Figure 4.6 displays the associated temperature response for each fluid. In this case, we can see that oil and water have been heated along the wellbore from toe to heel, while gas has been cooled. In order to explain this phenomenon, we plot the contribution of each factor that has an effect on wellbore temperature change based on equation (2.33a). Figure 4.7 shows how each factor in equation (2.33b) contributes to temperature change along this horizontal wellbore. In Figure 4.7, the value of the total temperature change $(\Delta T/L)_t$ (toe versus heel) for oil and water cases is negative (indicating heating), while the value of $(\Delta T/L)_t$ for the gas case is positive (i.e., experiencing cooling from toe to heel). Each bar in this figure represents the contribution of each factor from heel to toe. Because, for openhole wellbore, only heat convection happened between the reservoir and the wellbore fluid, the energy exchange effect is being eliminated to mass exchange which is denoted as 'me'.
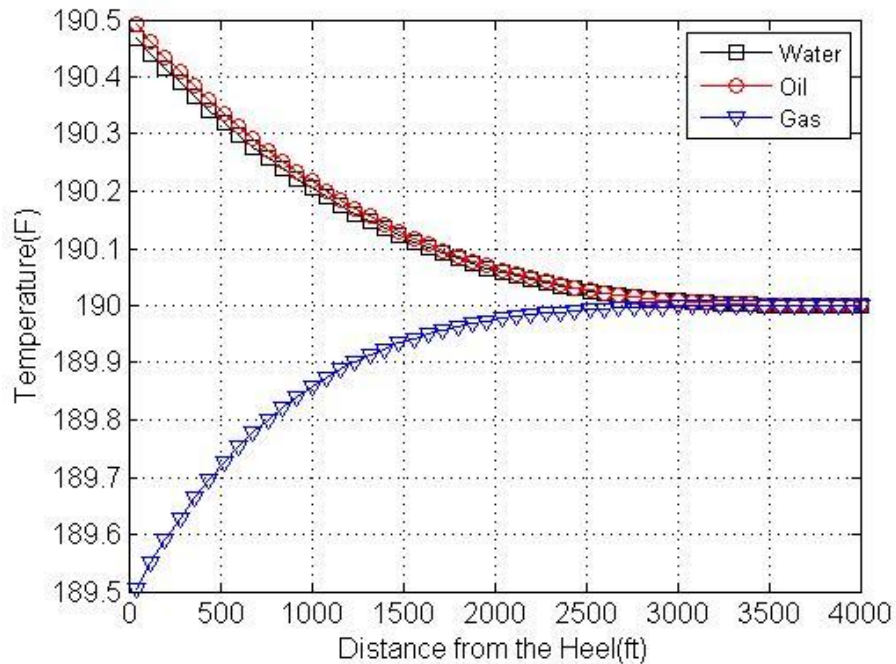
Fig. 4.6 η_S-driven Model Temperature Profiles for Oil, Water and Gas Single-Phase Flow in Horizontal Wellbore

As illustrated, the contribution of mass exchange is comparatively small; and it is hardly recognizable on the plot for the gas phase. In all cases, two factors dominate the temperature response: isentropic and friction effects. Friction heats the wellbore while the isentropic effect cools the wellbore. For the oil and water cases, frictional heating overwhelmed any manifestation of isentropic cooling. However, for gases, isentropic cooling overwhelmed the much reduced frictional heating effect. As a result, the wellbore was cooled. Gases typically have the largest isentropic thermal coefficients, while liquids exhibit much smaller values. In the limit, for truly incompressible fluids, $\eta_s \rightarrow 0$—given that in this limit, $C_p \rightarrow C_v$ and $\alpha \rightarrow 0$, $k \rightarrow 1$ in (see Equation 2.31). In this example, the average calculated values of isentropic thermal coefficients for gas, oil and water were 0.034, 0.005, and 0.001 F/psi, respectively.
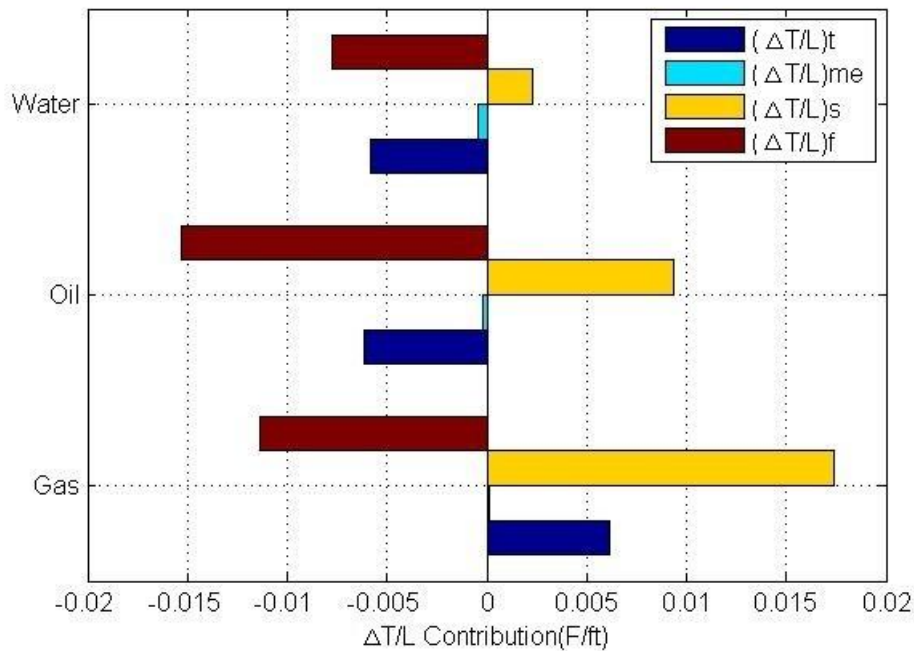
Fig. 4.7 η_S-driven Model Overall Contributions to Temperature Gradient for Oil, Water and Gas Flow in Horizontal Wellbore

4.2 Comparison with the η_h-driven Model

In the η_h-driven model, wellbore thermal behavior is expressed in terms of energy exchange, kinetic, elevation, and JTC effects. To demonstrate the interchangeability of the η_s- and JTC-models (Equations 2.33 and 2.36), Figure 4.8 presents the resulting contribution of each of these effects to the same water, oil, and gas single-phase flow scenarios for the horizontal wellbore case using the JTC model (Equation 2.36). For this horizontal wellbore with no inclination, the contribution of $(\Delta T/L)_{pe}$ is zero. While the contribution of mass exchange and acceleration is comparatively small, $(\Delta T/L)_t$ is largely controlled by the JTC effect, which is negative for liquids and positive for gas. In this example, average calculated JTC values for gas, oil and water were 0.018, -0.004, and -0.002 F/psi, respectively.
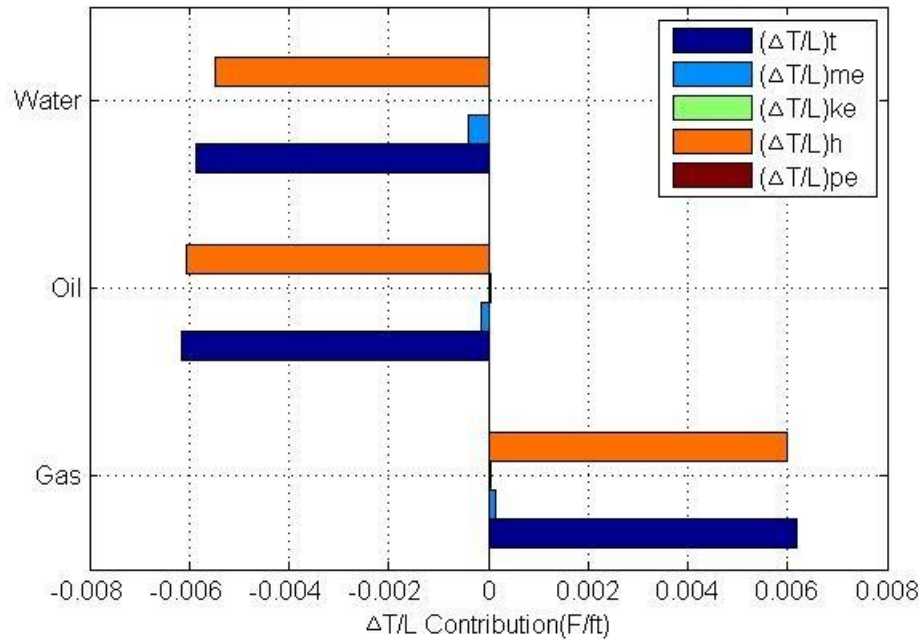
Fig. 4.8 η_h-driven Model Overall Contributions to Temperature Gradient for Oil, Water and Gas in Horizontal Wellbore.

Figures 4.9 to 4.11 present comparisons between the predictions of the thermal models discussed in this study and in Yoshioka's (2005a) model for the horizontal wellbore case of interest. Each

figure displays three temperature profiles. Two of these profiles display the seemingly different predictions from Yoshioka's (2005a) model and our proposed models. The difference in predictions stems from assumption (2) above, since Figure 4.11 shows that kinetic energy effects have very little effect on temperature response in this case. This is corroborated by the third temperature profile on these figures, which matches Yoshioka's trends. In those additional profiles, our model is implemented with the assumption $dh = C_p dT$ in order to obtain successful matches. As shown, models that neglect the enthalpy dependency on pressure may slightly under predict or over predict wellbore temperature responses. The difference in prediction is a direct function of mass influx, fluid momentum, pressure difference, and the fluid's JTC, as shown in Figures 4.9-4.11:
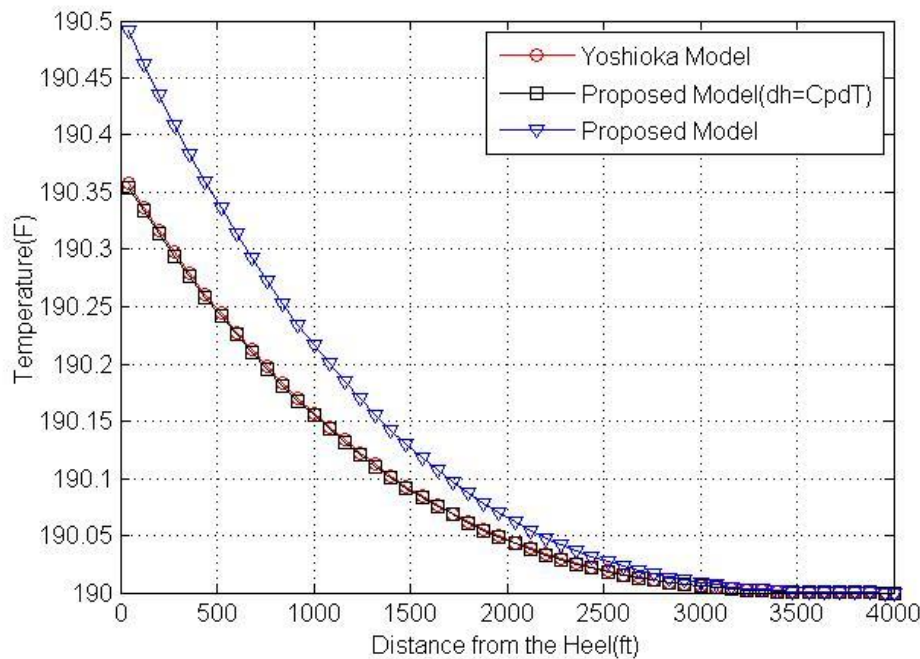
Fig. 4.9 Comparison of Proposed and Yoshioka's Model – Single-Phase Oil
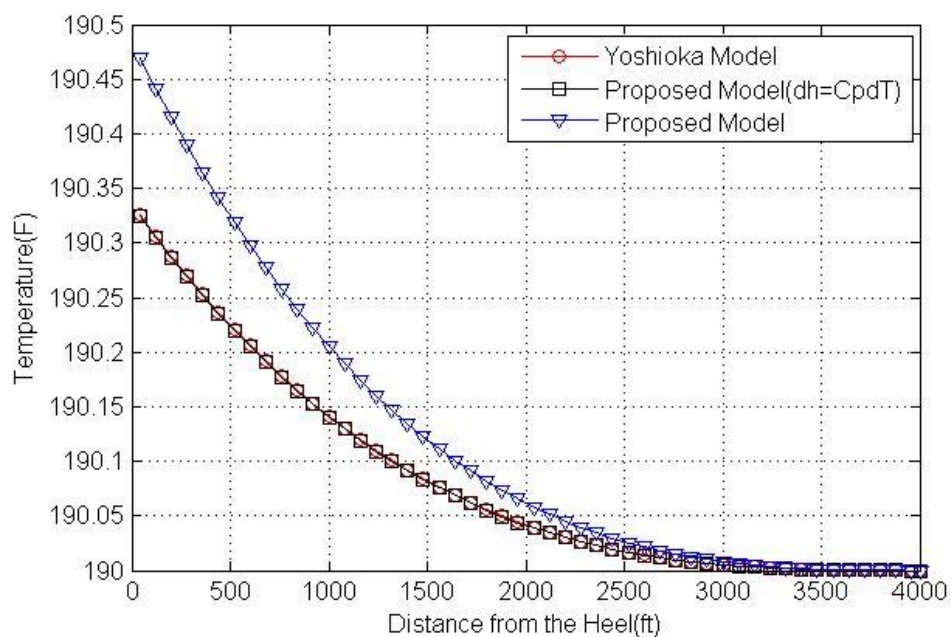
Fig. 4.10 Comparison of Proposed and Yoshioka's Model – Single-Phase Water
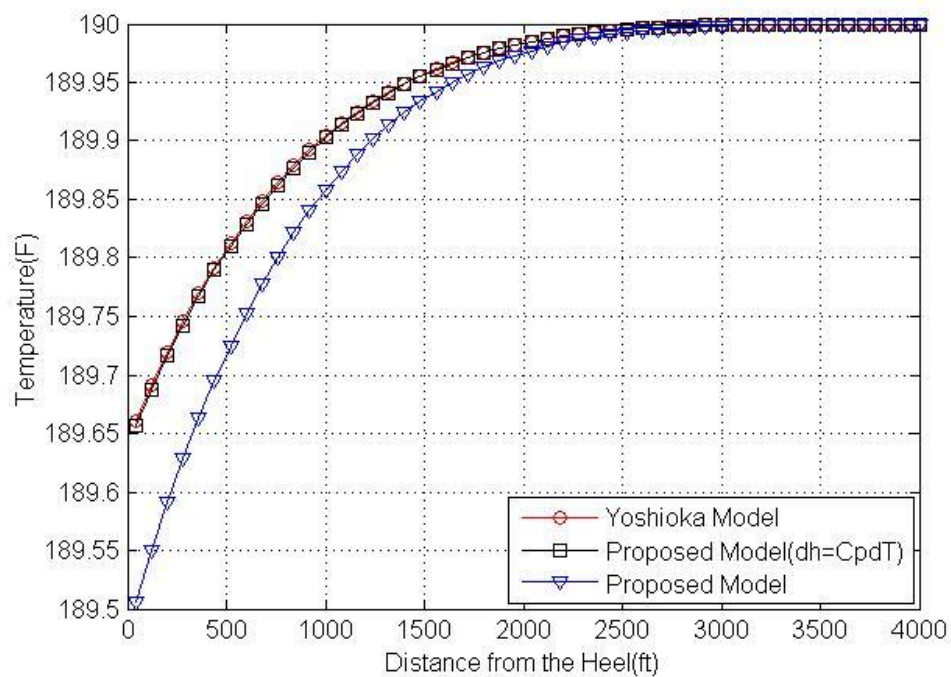
Fig. 4.11 Comparison of Proposed and Yoshioka's Model – Single-Phase Gas

4.3 Inclination Effect

Our proposed model can be applied to the inclined wellbore case. In this case, single-phase gas flows in four different inclined wellbore situations are considered (i.e., 2 degree/4 degree upward, 2 degree/4 degree downward and horizontal). Compared with the horizontal wellbore case, the reservoir pressure and temperature also change along the wellbore in the inclined case. Expressions to calculate reservoir pressure and temperature can be written as follows:

$$T_{formation} = T_{ref} + G_T Z \tag{4.1}$$

$$p_{formation} = p_{ref} + G_P Z \tag{4.2}$$

G_T, G_P is geothermal and geopressure gradient, respectively; Z is vertical distance from the reference. In our case, G_T is given as 0.01(F/ft) and G_P is 0.442(psi/ft). Besides, fluid will experience gravity force (F_g) in the inclined wellbore. The gravity force will influence pressure drop, subsequently affects temperature change.
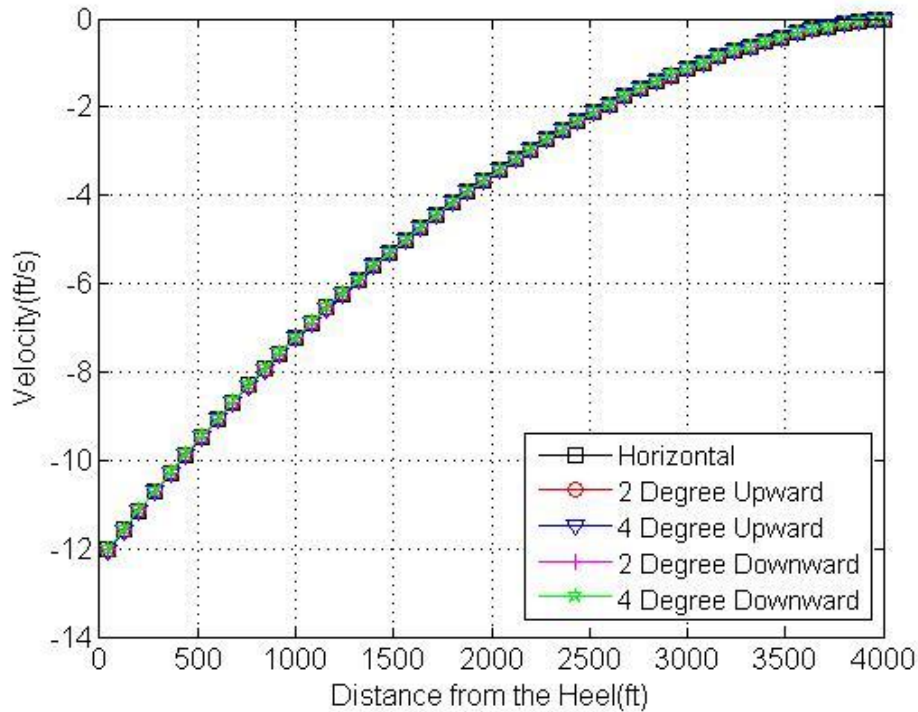
Fig.4.12 Velocity Profiles due to Wellbore Inclination-Gas Phase

Figures 4.12, 4.13 and 4.14 show the model's velocity, pressure and temperature sensitivity to different inclinations. The difference of velocity response between different inclinations is not able to be detected. That is because velocity in our model is solved by the mass balance equation, in which the inclination effect is not applied. For pressure and temperature profiles, however, the difference is significant enough to be observed. Because of the formation pressure gradient, for upward inclination wellbores, formation pressure decreases from toe to heel; for downward inclination wellbores, formation pressure increases from toe to heel. In the horizontal wellbore case, because θ is zero, gravity force has no effect on the pressure profiles. While in this case, for upward wellbores, gravity force increases the pressure drop; but for downward wellbores, gravity force decreases the pressure drop. Therefore, as we can see in Figure 4.13, the 4-degree upward case has the largest pressure drop, while the 4-degree downward case has the smallest pressure drop.
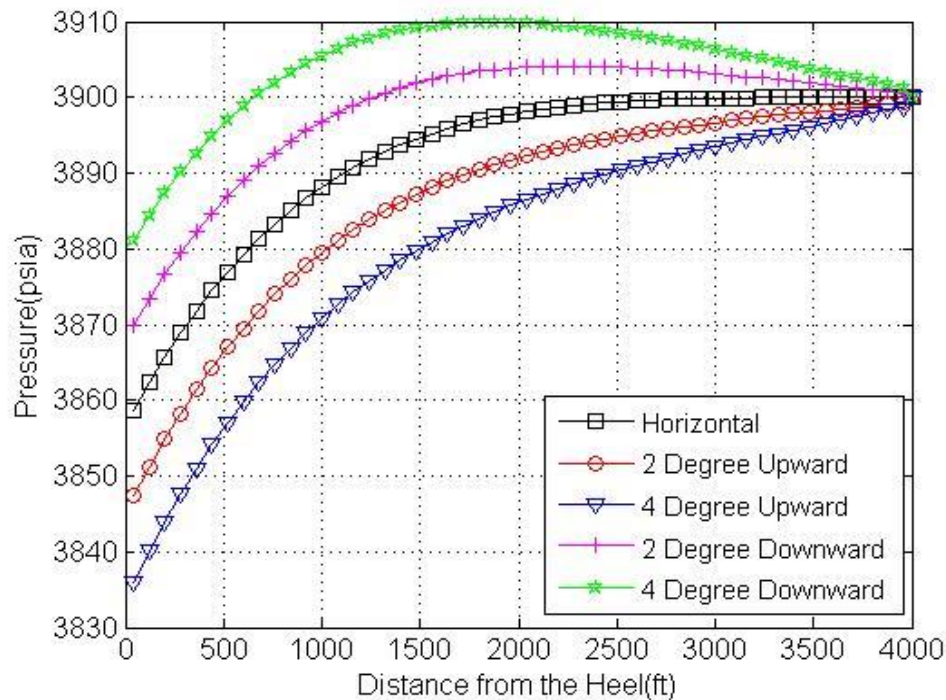
Fig.4.13 Pressure Profiles due to Wellbore Inclination-Gas Phase
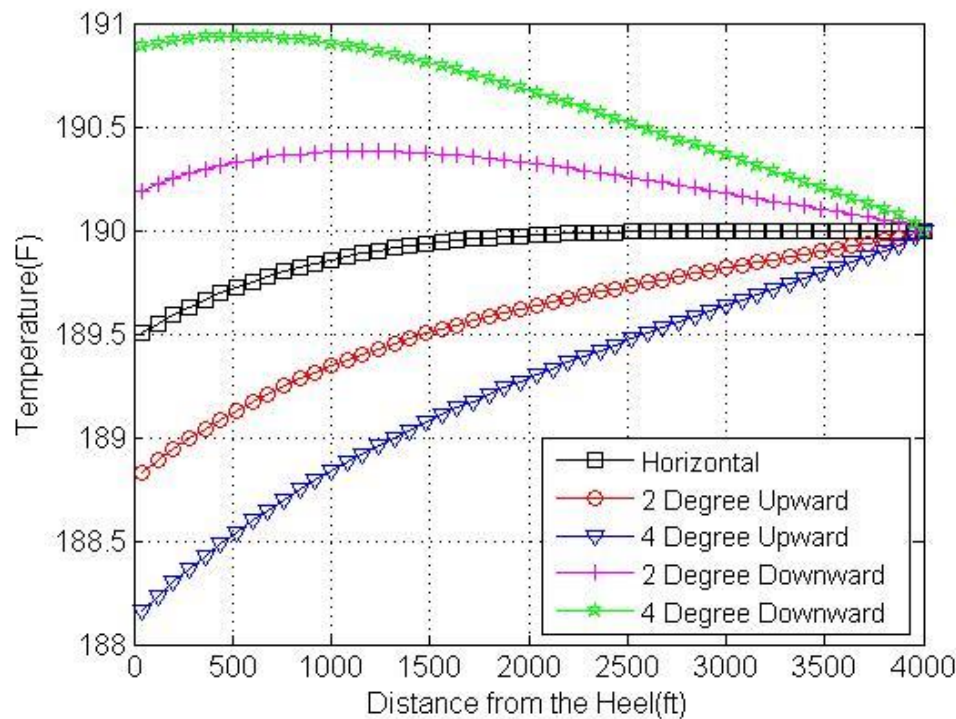
Fig.4.14 Temperature Profiles due to Wellbore Inclination-Gas Phase

In temperature response, the geothermal gradient makes formation temperature in the upward wellbore decrease from toe to heel and makes it increase in downward wellbores. Because h^* is a strong function of formation temperature, the mass exchange contribution in the temperature model is highly dependent on wellbore inclinations. Figure 4.15 shows the overall contribution of temperature gradient for each factor. The cooling effect of the mass exchange in the 4-degree upward wellbore becomes more significant than that in the horizontal wellbore due to geothermal gradient. Also, the larger pressure drop in 4-degree upward case causes larger isentropic coefficient cooling effect. The combination of this two factors result in higher temperature drop in the 4-degree upward wellbore.
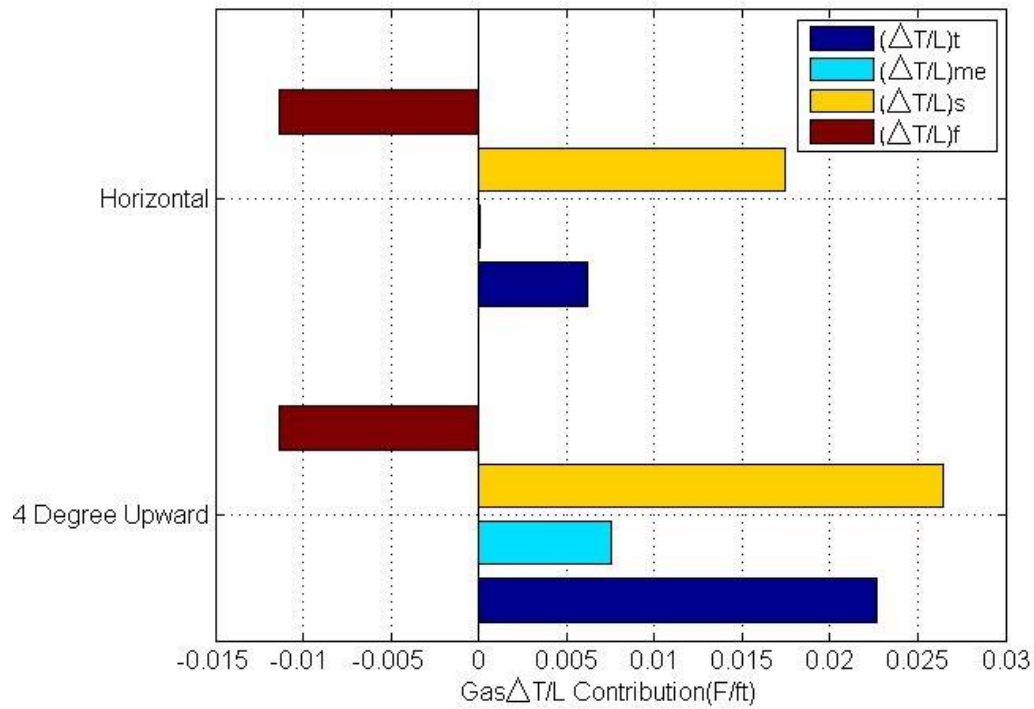
Fig.4.15 Comparison of Overall Contribution in Temperature Gradient in Inclination Study-Gas Phase

4.4 Flowrate Effect

In this case, our proposed model's sensitivity to different flowrate is discussed. The study applies different total gas flowrates including the baseline case, while maintaining other parameters as constant. Figure 4.16 is the accumulated flowrate for each case.
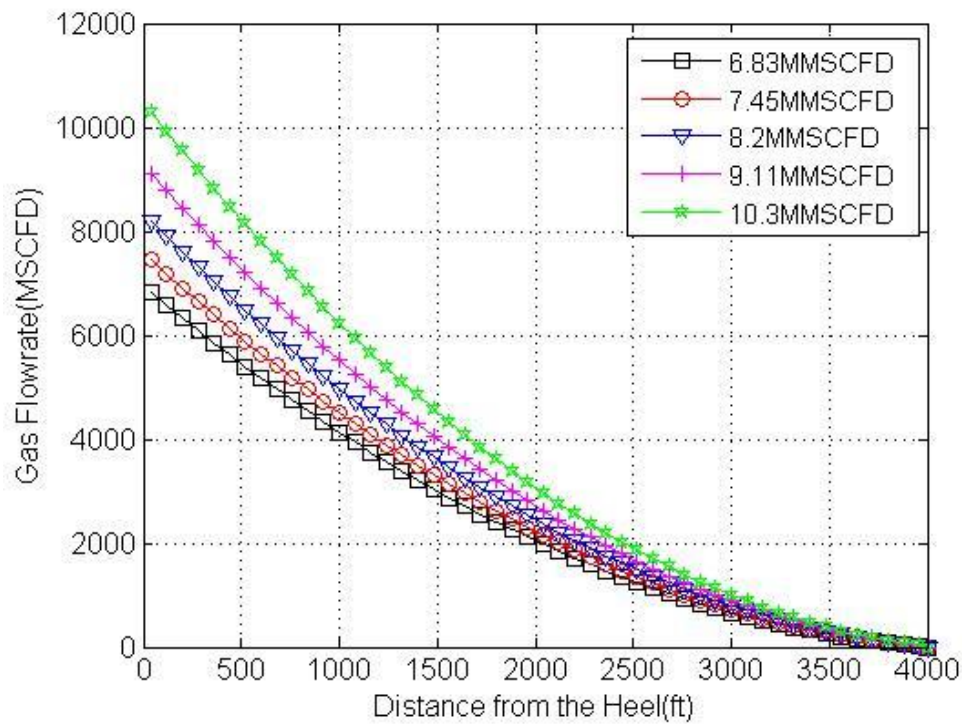
Fig.4.16 Accumulated Gas Flowrate

Figures 4.17-4.19 show velocity, pressure and temperature response, respectively. Larger mass influx in the larger flowrate case leads to higher fluid velocity. Pressure drop and temperature drop tend to increase with the increase of flowrate. The increase of velocity leads to a larger friction force to the system, thus causing a larger pressure drop. In addition, temperature drop increases because the larger pressure drop causes larger isentropic coefficient cooling effect. In summary, a larger flowrate in the wellbore results in a more significant temperature response.
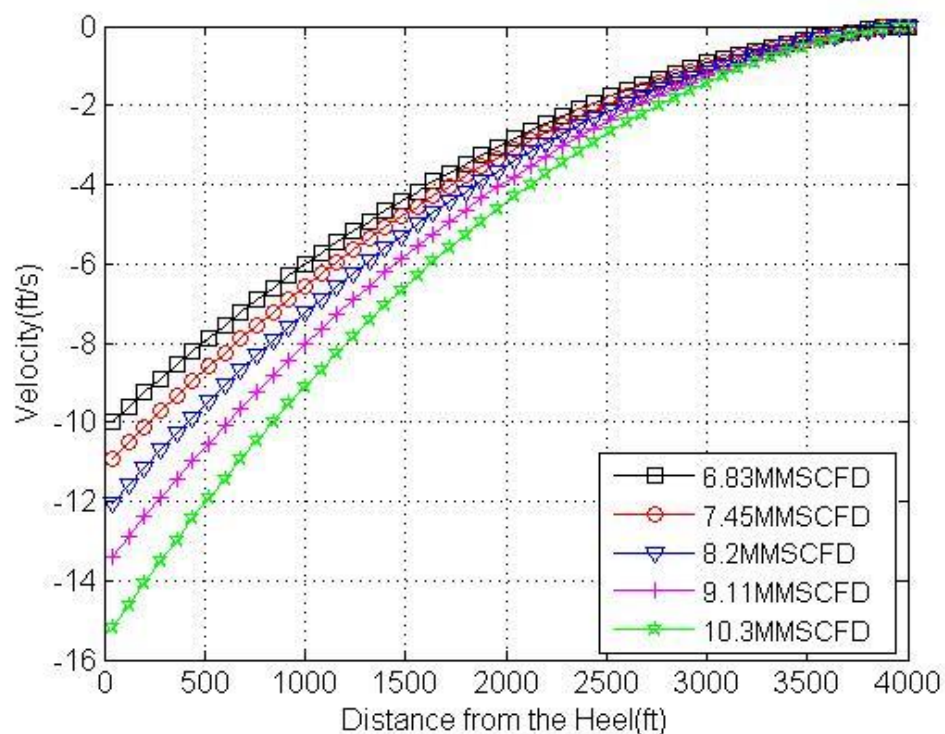
Fig. 4.17 Velocity Profiles for Flowrate Study-Gas Phase
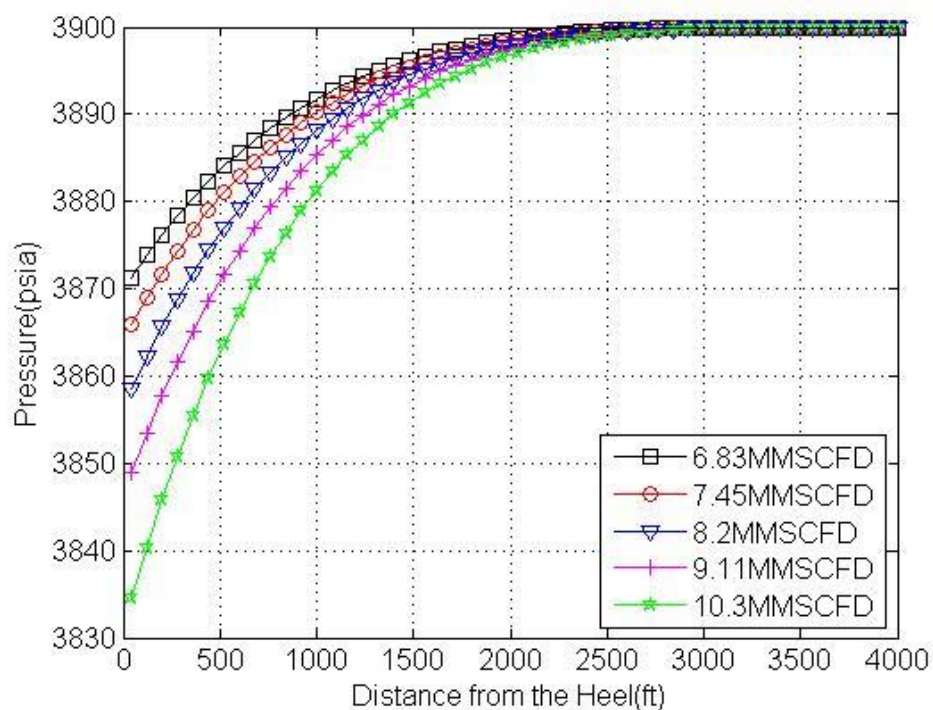
Fig. 4.18 Pressure Profiles for Flowrate Study-Gas Phase
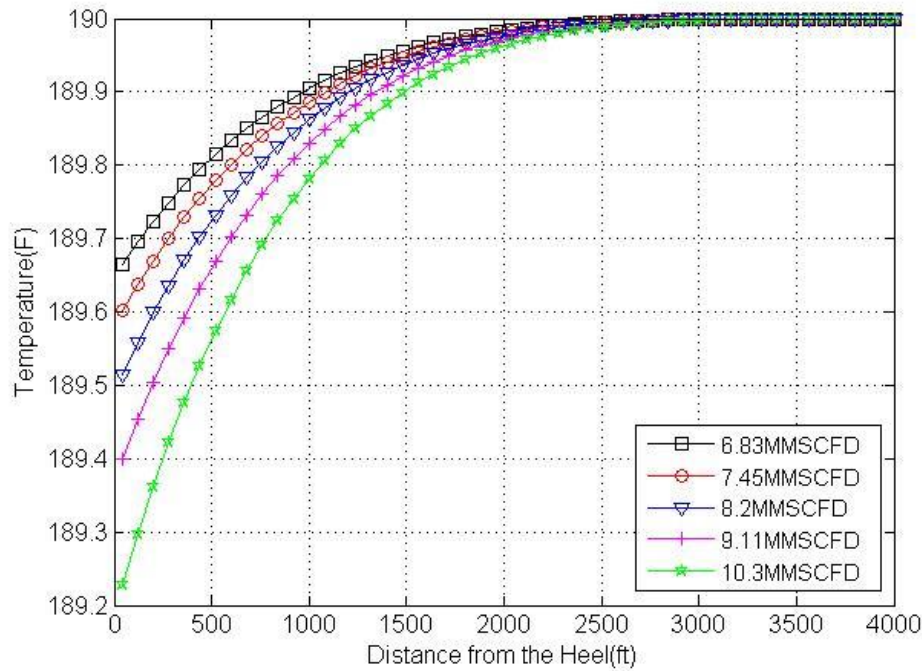
Fig.4.19 Temperature Profiles for Flowrate Study-Gas Phase

4.5 Wellbore Roughness Effect

In this section, pressure and thermal responses of flowing fluid due to changing wellbore roughness is discussed. Figures 4.20-4.22 show velocity, pressure and temperature profiles due to the wellbore roughness change. Since wellbore roughness only has an effect on friction calculation, the mass balance equation remains the same, having no influence on velocity profiles, as shown in Figure 4.20. Figure 4.21 gives each pressure response for the wellbore with different relative roughness. In the momentum equation, fluid will experience a larger friction force with larger roughness. Therefore, larger wellbore roughness results in a higher pressure drop. The increased pressure drop consequently increases the temperature drop due to the isentropic coefficient effect in the temperature equation. It can, therefore, be concluded that higher wellbore roughness results in a larger temperature change.
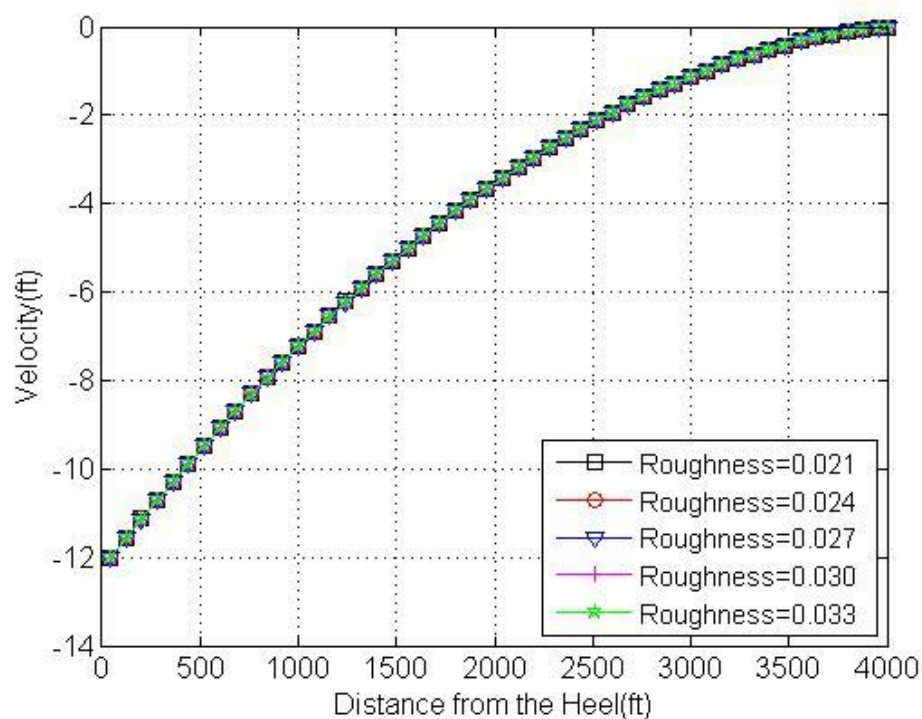
Fig.4.20 Velocity Profiles for Roughness Study-Gas Phase
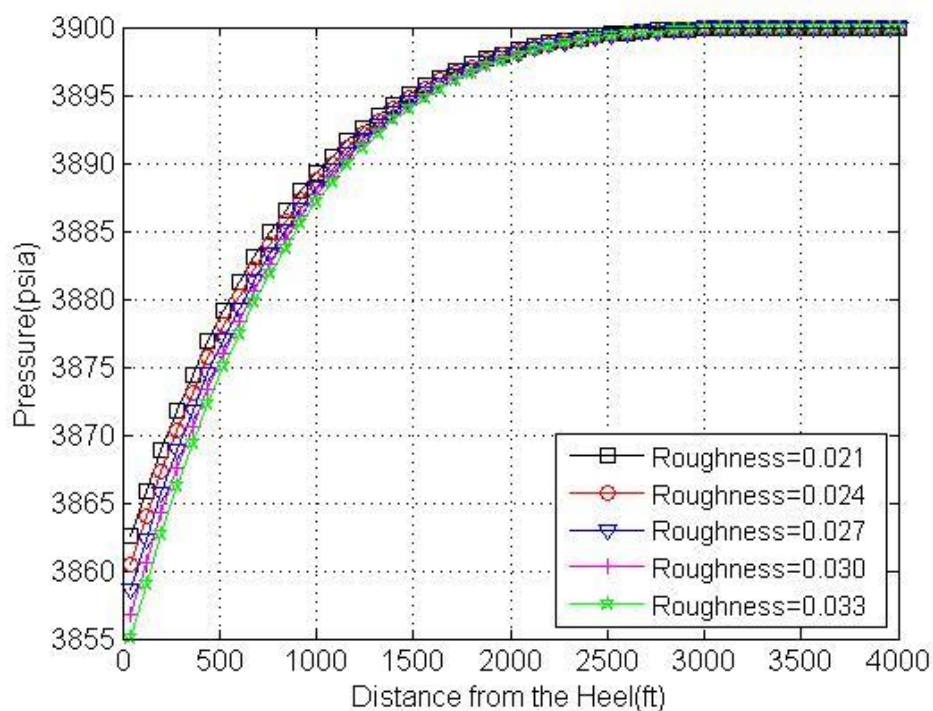
Fig.4.21 Pressure Profiles for Roughness Study-Gas Phase
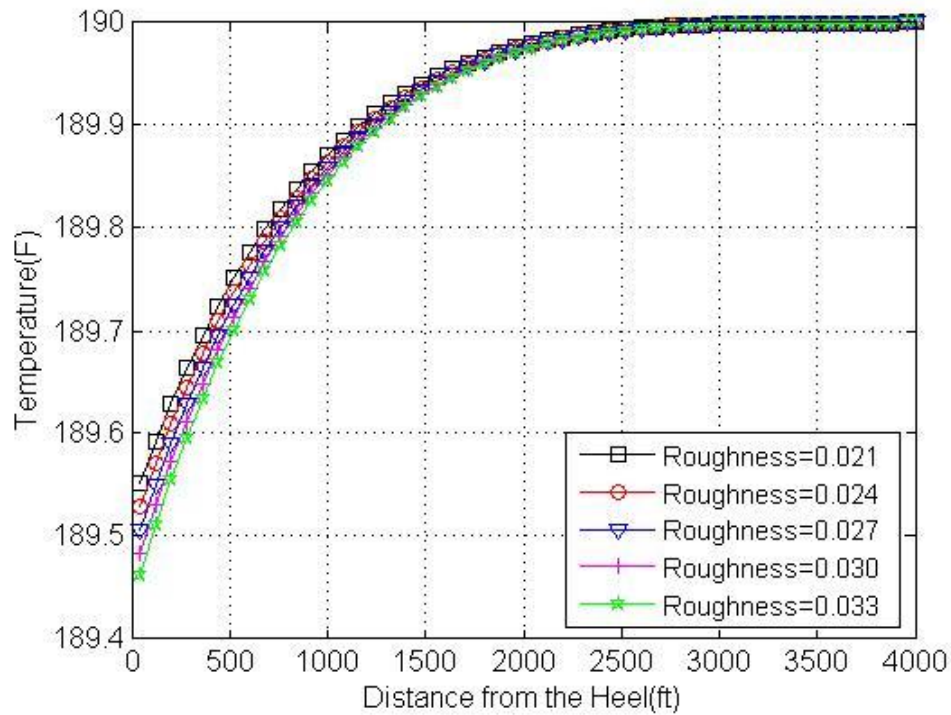
Fig. 4.22 Temperature Profiles for Roughness Study-Gas Phase

4.6 Wellbore Radius Effect

In this section, the dependence of our proposed model on the wellbore radius is investigated. We fix the wellbore inflow rate so that the wellbore radius effect can be observed. Figure 4.23 represents velocity response at different wellbore radii. It is observed that smaller wellbore radius fluid results in larger velocity because of its larger radial mass influx. Higher velocity fluid will experience higher friction force, thus having a larger pressure drop, as shown in Figure 4.24. Again, due to larger isentropic coefficient cooling effect because of larger pressure change, the temperature change increase with the decrease of wellbore radius. From this study we can conclude that the smaller the wellbore radius, the larger the pressure and temperature drops the wellbore fluid has.
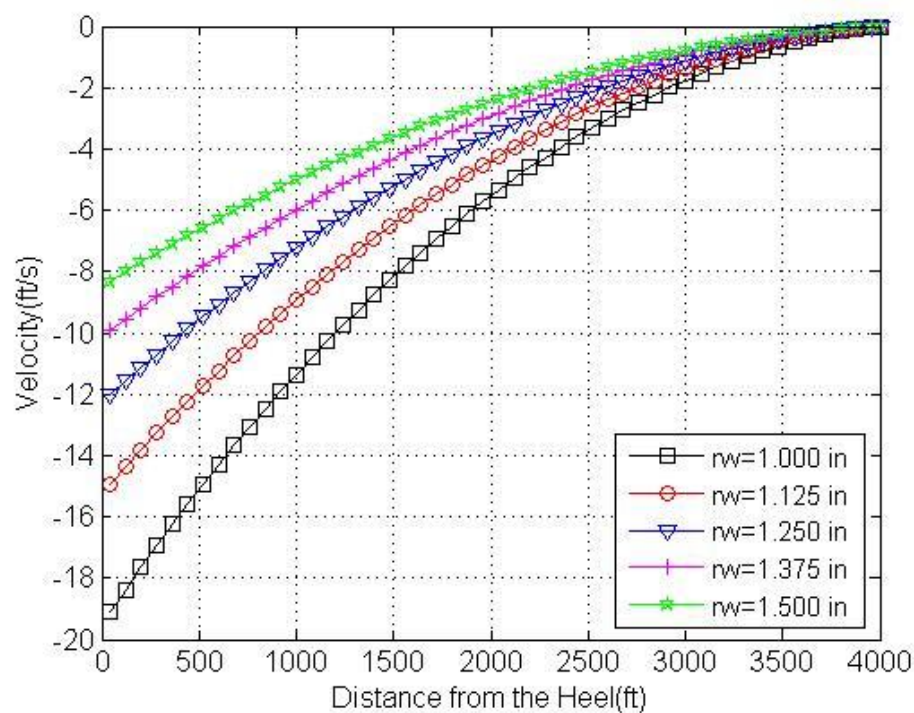
Fig. 4.23 Velocity Profiles for Radius Study-Gas Phase
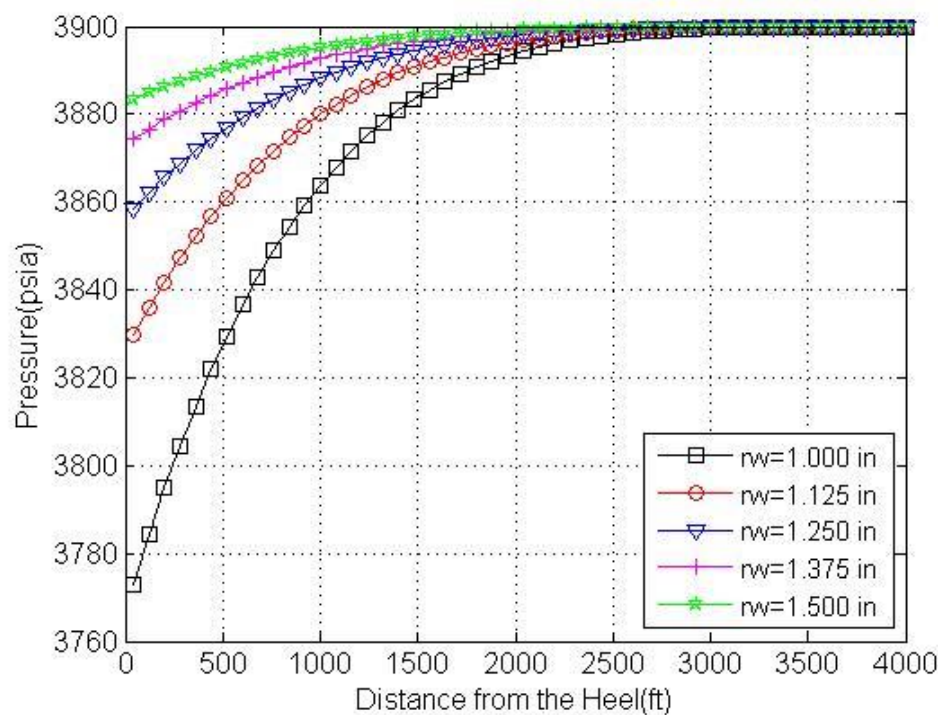
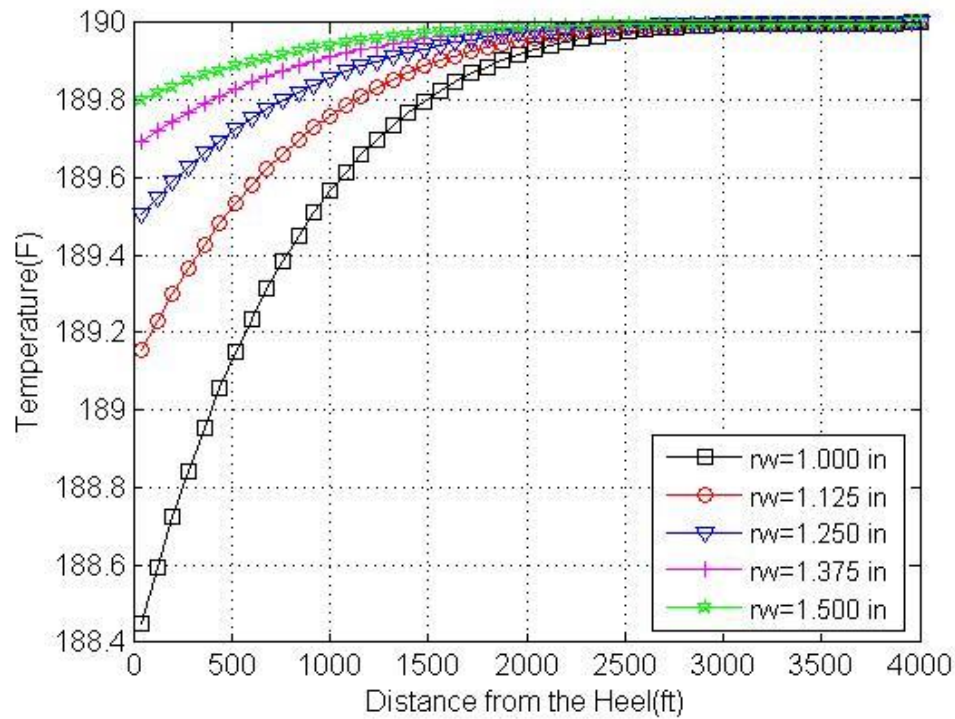**Fig.4.24 Pressure Profiles for Radius Study-Gas Phase**

Fig.4.25 Temperature Profiles for Radius Study-Gas Phase

4.7 Well Completion Effect

So far, the wellbore type that we applied in this case study is openhole. For thermal model in an openhole wellbore, the pipe's open ratio γ is 1, so that energy exchange only appears in the mass exchange part. In this case, we introduce heat conduction into our model for a perforated wellbore type and compare the result with the openhole wellbores. Fluid and perforated wellbore properties are given in Table 4.3 (Yoshioka et al., 2005a). The length and inner diameter of the wellbore are the same as in the openhole wellbore case. With the same gas mass influx in the two wellbore types, Figures 4.26-4.28 show the results of a thermal response comparison between openhole and perforated wellbore types.

Table 4.3 Perforated Wellbore Description and Fluid Properties (Yoshioka, et al, 2005a)

Pipe Open Ratio	0.02
Oil Conductivity (BTU/hr·ft·F)	0.797
Gas Conductivity (BTU/hr·ft·F)	0.0116
Water Conductivity (BTU/hr·ft·F)	0.3886
Cement Conductivity (BTU/hr·ft·F)	4.021
Casing Conductivity (BTU/hr·ft·F)	6.933
Oil-gas Interfacial Tension(dyne/cm)	10
Cement Diameter (in)	5
Casing Diameter (in)	3.5
Relative Roughness	0.01
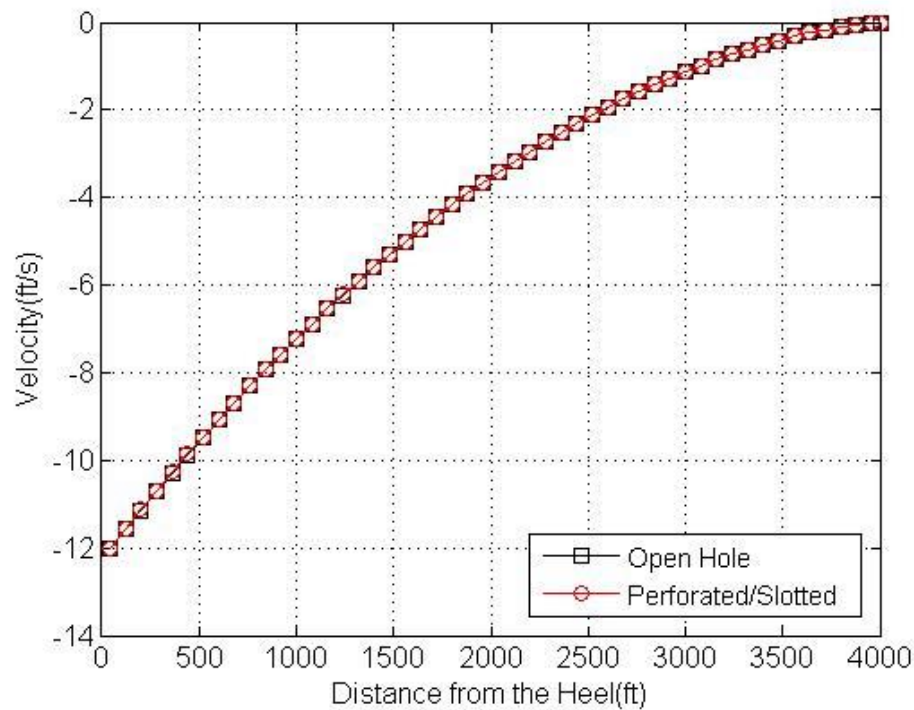
Fig.4.26 Velocity Profiles for Completion Study-Gas Phase

With the assumption that both wellbores have the same mass influx, wellbore fluid in the two wellbores have the same velocities, as is shown in Figure 4.26. Due to smaller roughness compared to the openhole wellbore case, the pressure drop of the perforated wellbore fluid is less than that of the openhole wellbore fluid seen in Figure 4.27.
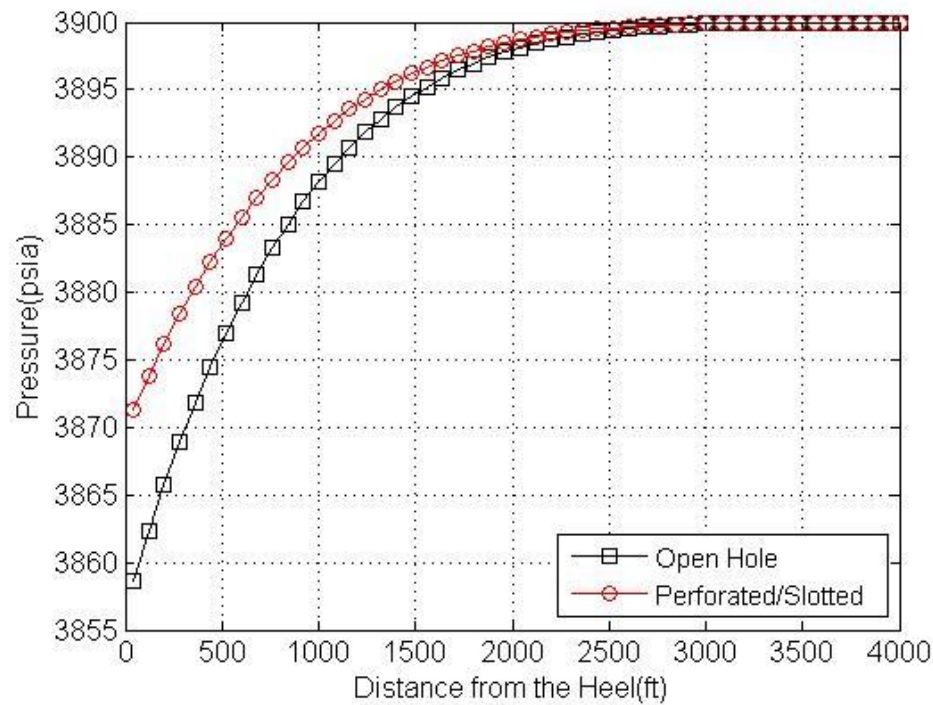
Fig.4.27 Pressure Profiles for Completion Study-Gas Phase

Figure 4.28 shows the comparison of a temperature profile in both the openhole and perforated cases. Compared to the openhole case, perforated wellbore fluid has a smaller temperature change. In order to analyze different thermal responses of the two wellbore types, Figure 4.29 is presented to show the factors' contributions to the overall temperature gradient. In the perforated wellbore, heat conduction heated the wellbore due to a temperature difference between fluids in the reservoir and wellbore. It also can be seen that the friction force in the perforated wellbore case performs less heating effect compared with the openhole wellbore case, and the cooling effect of mass exchange also becomes more obvious. In addition, due to the smaller pressure change in the perforated case, the isentropic coefficient cooling effect is also smaller compared to the openhole case.
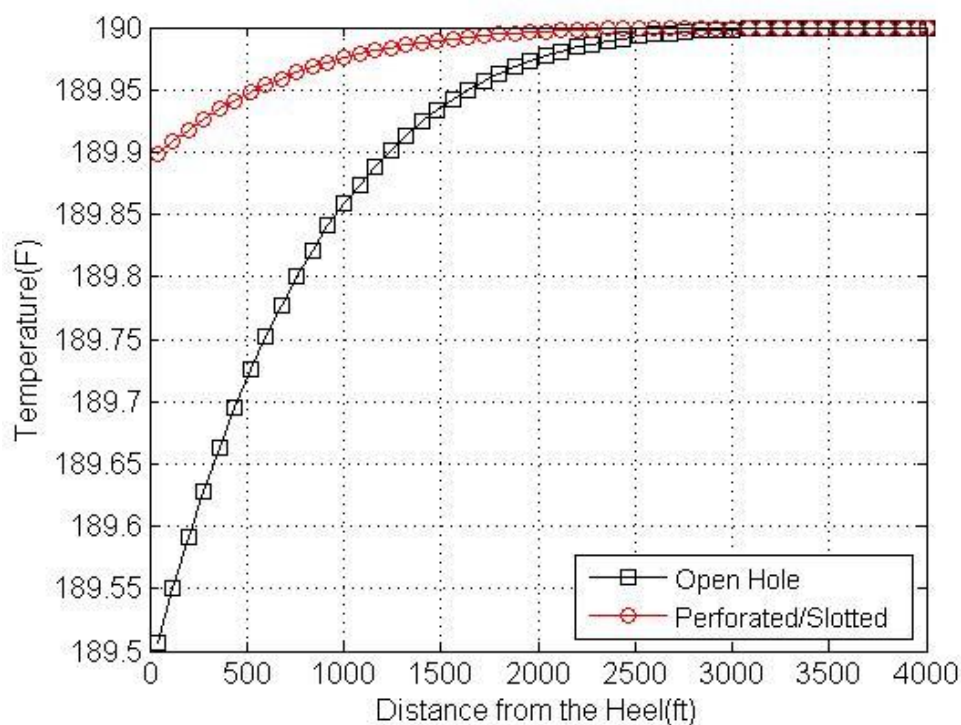
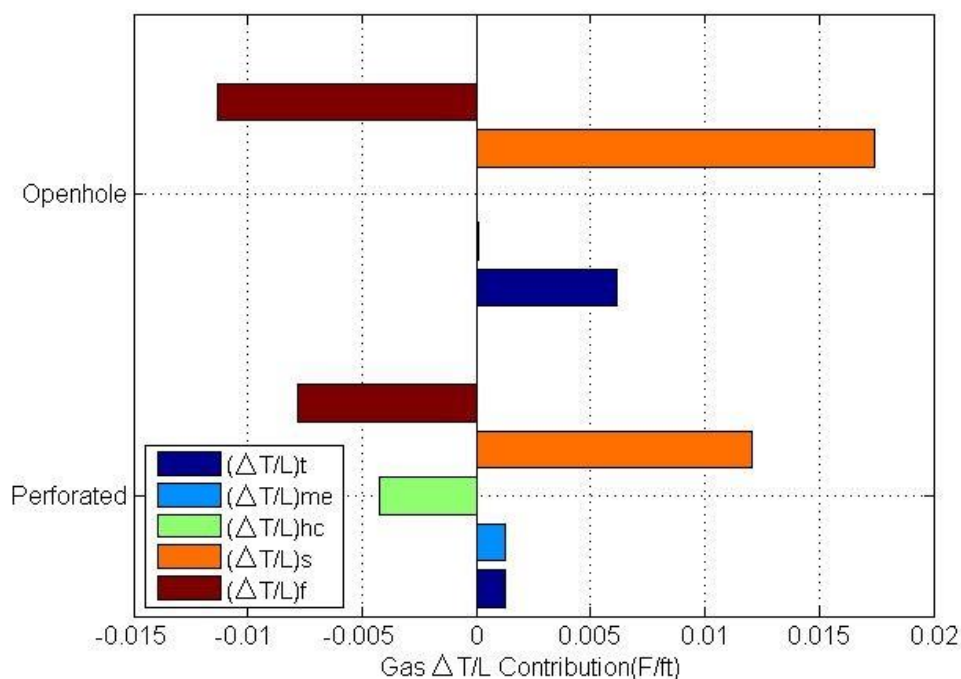**Fig.4.28 Temperature Profiles for Completion Study-Gas Phase**

Fig. 4.29 Comparison of Overall Contributions in Temperature Gradient in Completion Study-Gas Phase

CHAPTER 5

TWO-PHASE FLOW RESULTS AND DISCUSSIONS

In this section, a sensitivity study of the proposed two-phase flow model in several scenarios is conducted. Both homogeneous and drift-flux models have been applied in either oil-water or oil-gas flows. In an oil-water two-phase flow, water entry effect is discussed; while in the oil-gas two-phase flow, effect of an oil-gas mixture production at different gas flowrates is analyzed.

5.1 Oil-Water Two-phase Flow Problem

In an oil-water flow system, we specify oil and water production along the wellbore. Water entered the wellbore, respectively, at different locations including toe, middle and heel of wellbores. The inflow fluid in this case is either oil or water. Oil and water flowrate specifications are shown in Figures 5.1-5.3.
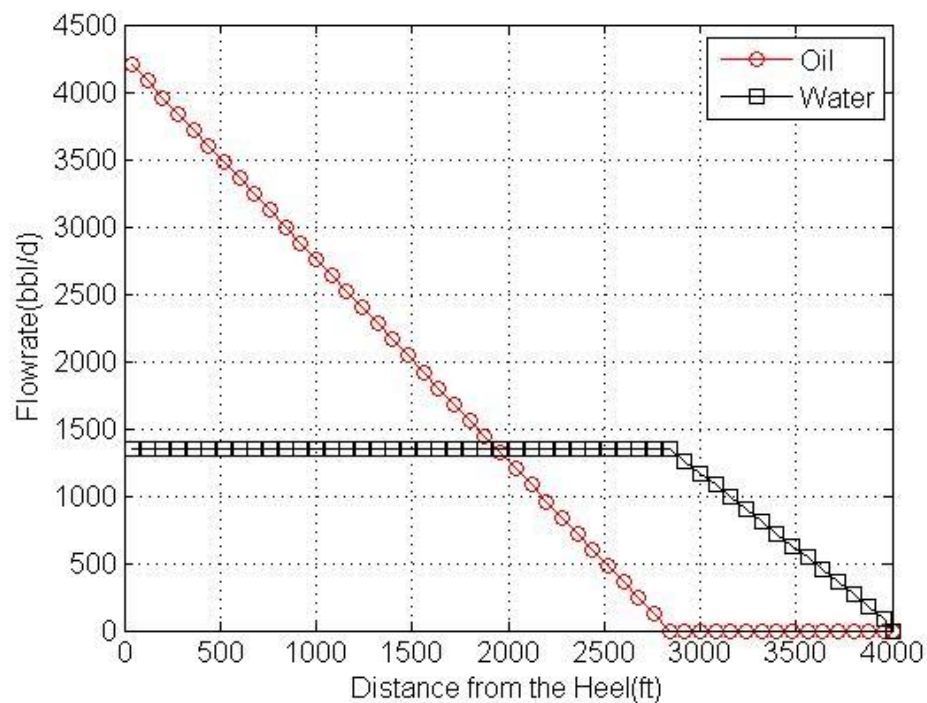
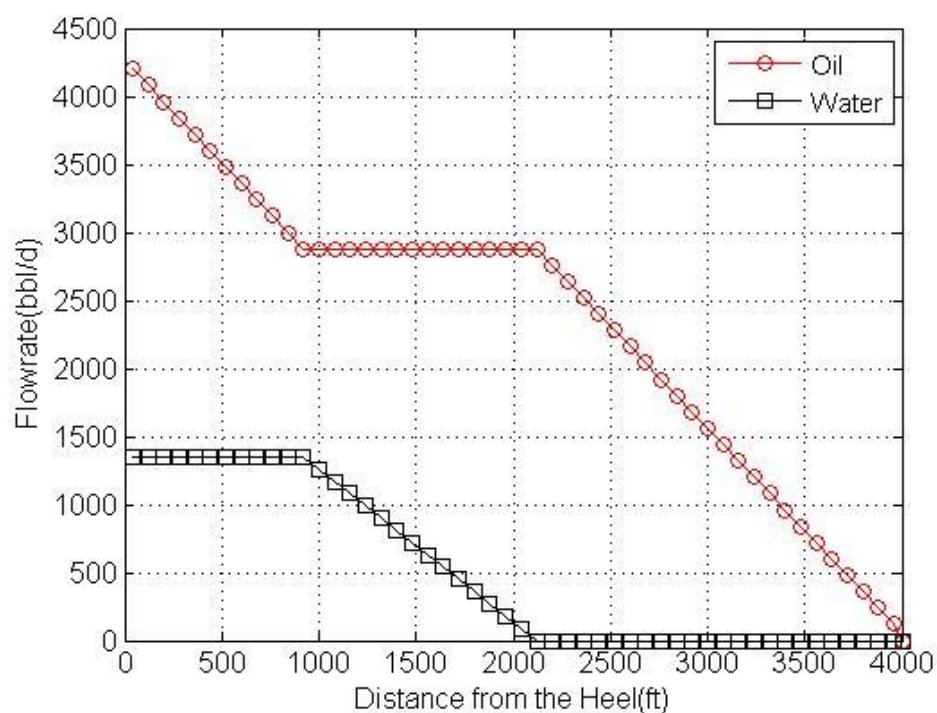**Fig. 5.1 Oil and Water Production along Wellbore-Water Entered at Toe**

Fig. 5.2 Oil and Water Production along Wellbore-Water Entered at Middle
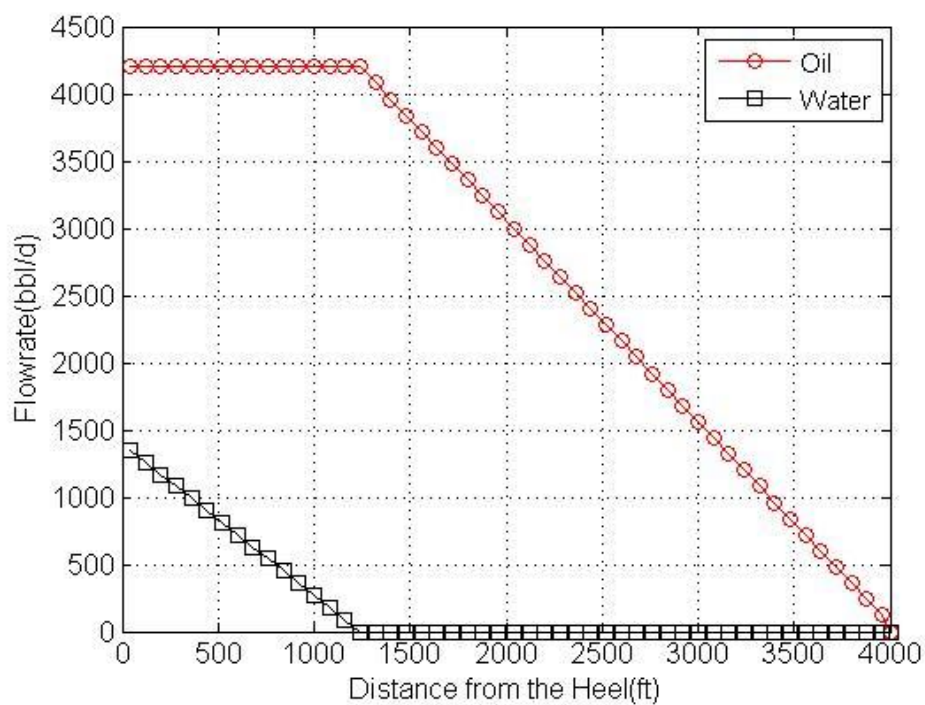

Fig. 5.3 Oil and Water Production along Wellbore-Water Entered at Heel

5.1.1 Homogeneous Model Results

The homogeneous oil-water flow model is initially applied in the openhole wellbore condition. Figure 5.4 gives the water holdup profiles in three cases. When water enters at the toe of the wellbore, because there is no oil production during that time, its holdup is first kept at 1. As oil begins to produce, water's cumulative production is fixed and its holdup begins to decrease. When water enters wellbore at the middle and heel of wellbore, its holdup is kept at zero until it begins to produce. When fluid reaches the heel of the wellbore, the water holdup is the same in all three cases, i.e., about 0.24.
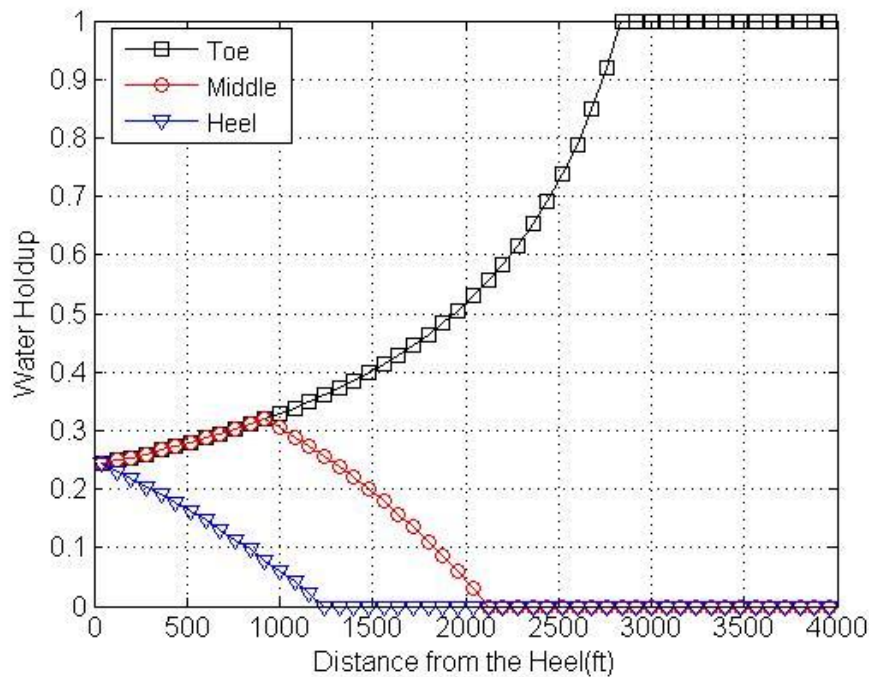

Fig. 5.4 Water Holdup-Homogeneous Model

Figure 5.5 shows the pressure response in all three cases and their comparison with the single-phase case. Compared to single-phase oil flow, the pressure drop in each case is continuous and close to each other. Therefore, one could not recognize the entry of water from the pressure profiles.
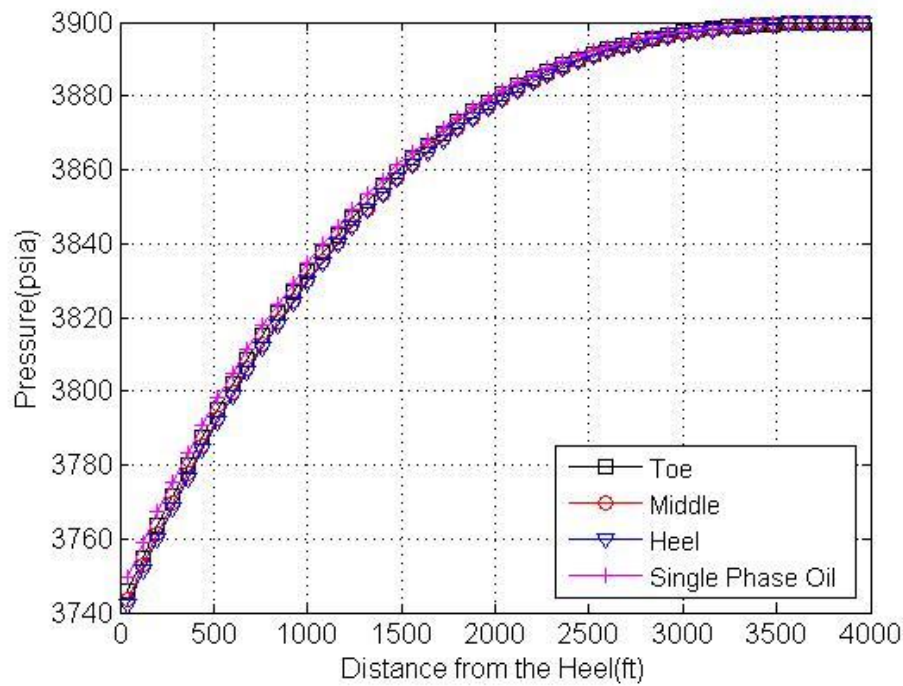
Fig. 5.5 Pressure Profiles at Different Water Entry Locations-Homogeneous Model

Figures 5.6-5.8 present temperature responses in all three cases with their comparison of the single-phase case. When water enters the wellbore at different locations, different temperature responses are observed from Figure 5.6 to Figure 5.8. The temperature profile begins to deviate from the single-phase fluid case at the location where water enters the wellbore. In the single-phase case, it is already observed that water is less heated than oil along the wellbore. Besides, water produces at a smaller flowrate compared to oil. When these two factors come together in the two-phase flow, different temperature behaviors happen, and water entry can be detected. Therefore, it is concluded that the temperature profile of wellbore fluid can be utilized to interpret water entry phenomenon during production.
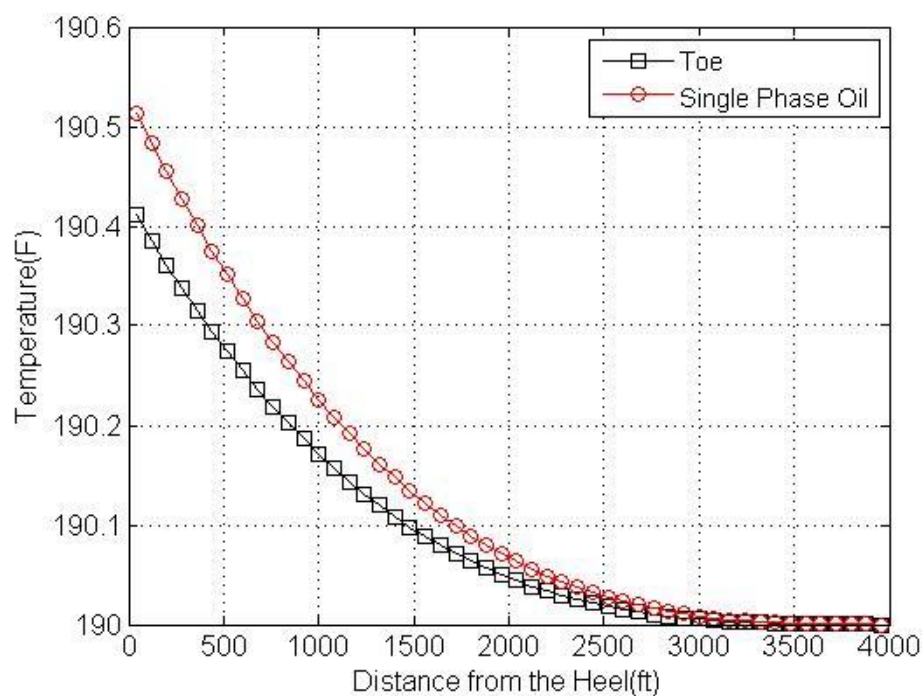
Fig. 5.6 Temperature Profiles Comparison for Water Entered at Toe-Homogeneous Model
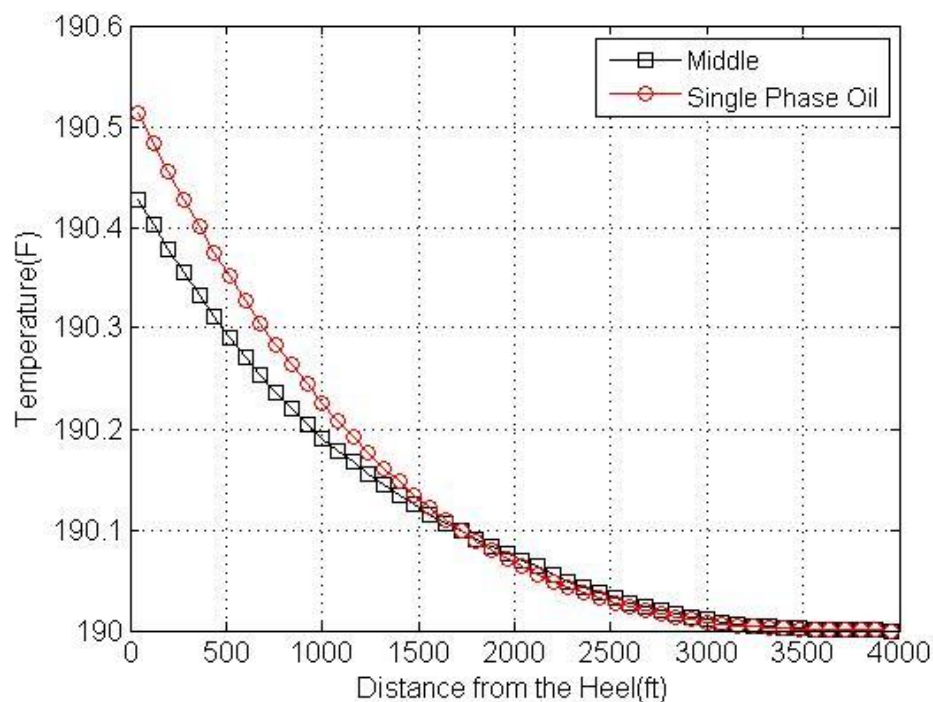

Fig. 5.7 Temperature Response Comparison for Water Entered at Middle-Homogeneous Model
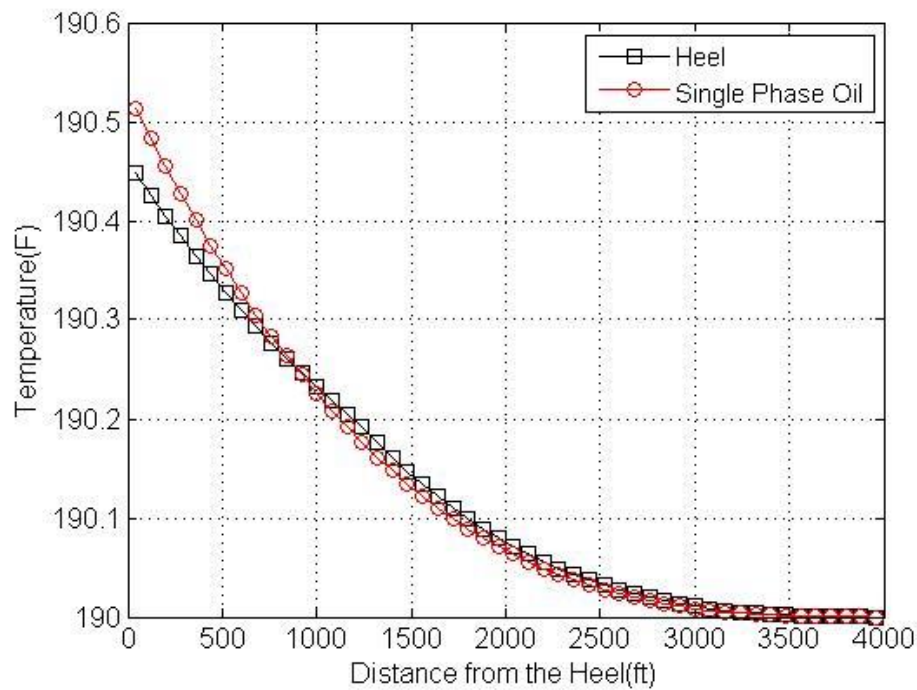
Fig. 5.8 Temperature Response Comparison for Water Entered at Heel-Homogeneous Model

5.1.2 Drift-flux Model Result

The main difference between the drift-flux model and homogeneous model is that the drift-flux

model considers slip in evaluating phase holdup and velocity. In an oil-water flow, to make each

thermal profile in continuous format, we assume that the flow pattern in the flow system is W/O,

which means that water is dispersed in continuous oil. Water holdup profiles are given in Figure

5.9. Compared to the water holdup calculated by the homogeneous model in Figure 5.4, Figure 5.9

has a similar trend of water holdup. Figure 5.10 is generated to show the difference between these
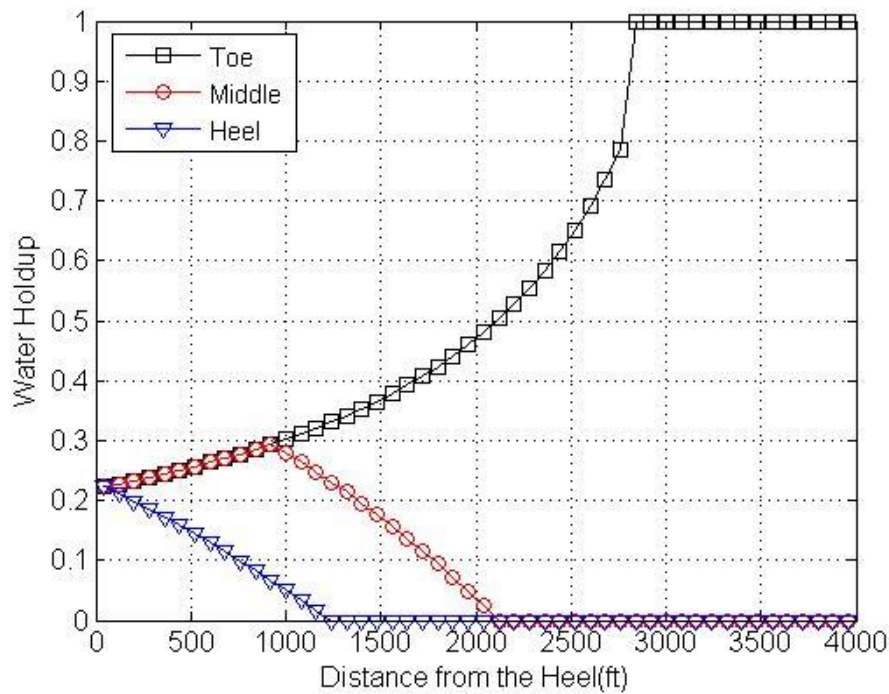
two results.

Fig. 5.9 Water Holdup-Oil-water Drift-flux Model

Take water entered at the middle as an example in Figure 5.10. It is shown that the homogeneous model over predicts the water holdup along the wellbore, compared to the drift-flux model. That is because the two models utilize different algorithms in calculating phase holdup. In the homogeneous model, phase holdup is calculated directly by cumulative production of each phase. While in the drift-flux model, phase holdup is calculated by drift-flux correlations. The result of the velocity profile for the middle location case is in Figure 5.11. V_o and V_w in the figure gives the velocity profiles of oil and water phase respectively. V_m is the mixture velocity of the two-phase flow calculated in homogeneous model.
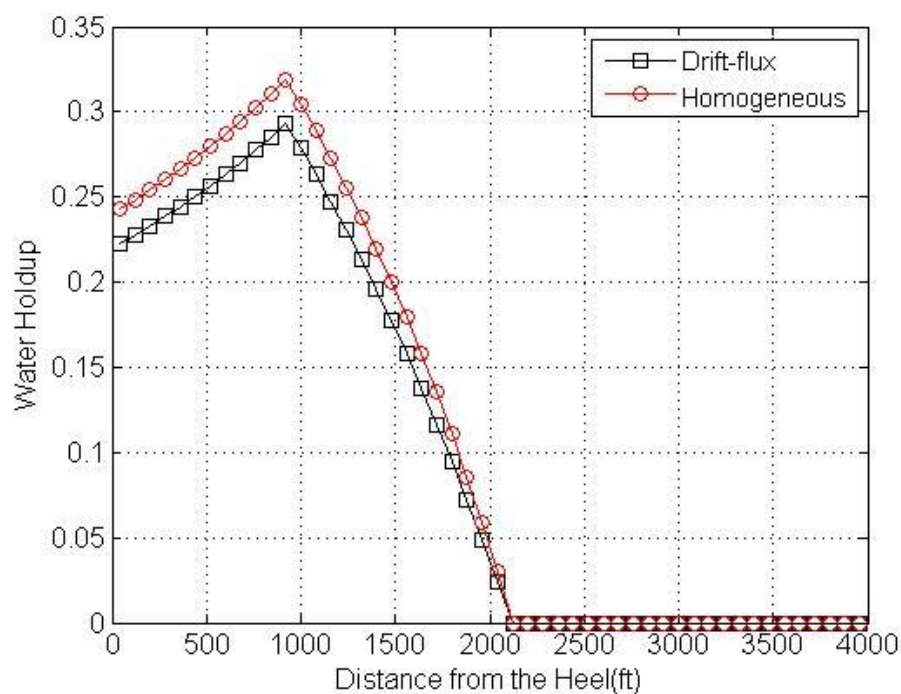
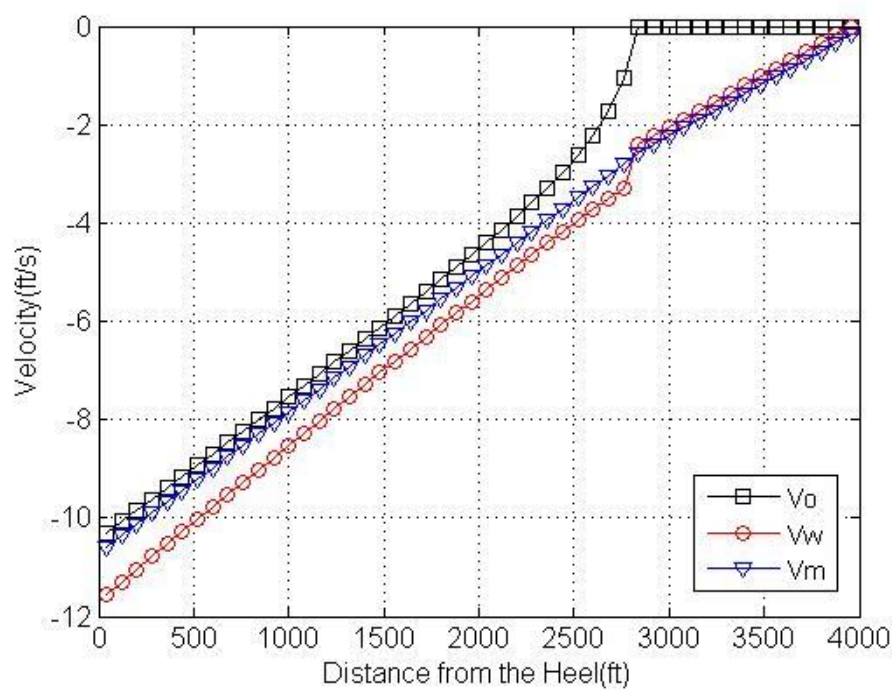**Fig. 5.10 Comparison of Water Holdup in Two Model**

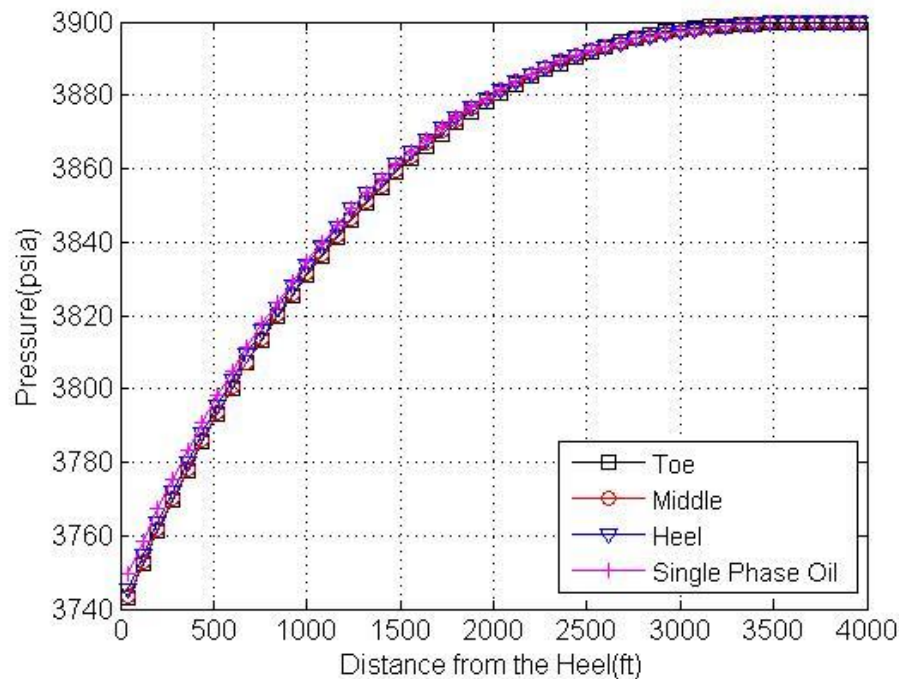**Fig. 5.11 Velocity Profile for Water in Toe Location-Oil-water**

Fig. 5.12 Pressure Profiles at Different Water Entry Locations –Oil-water Drift-flux Model

Figure 5.11 shows that the dispersed water phase travels at a higher velocity than the oil phase along the wellbore, while mixture velocity has a value between the oil and water velocities. The velocity profiles obey one basic assumption—that in the drift-flux model, one phase is transported at a higher speed than another phase. Pressure profiles in each case are generated by the drift-flux model as shown in Figure 5.12. Similar to the pressure profiles in homogeneous model, pressure profiles are almost overlapped each other, and one could not detect the water entry effect and water location from pressure profiles. Figures 5.13-5.15 give the temperature profiles of each case relative to the single-phase oil case. There are similar phenomena in temperature profiles generated by drift-flux model compared to homogeneous model. Temperature of two-phase flow deviates from single-phase flow at the location where water begins to enter.
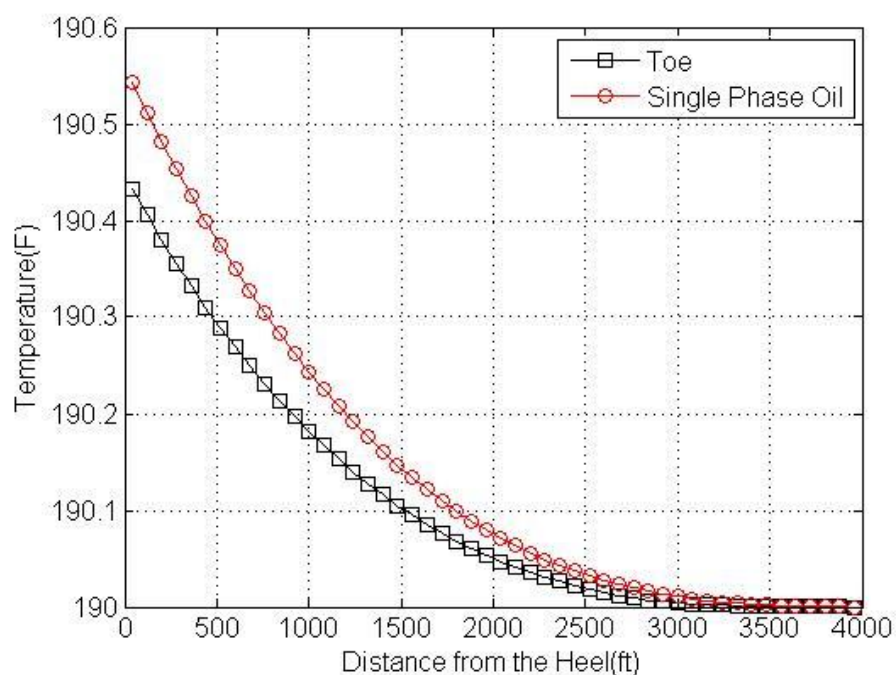
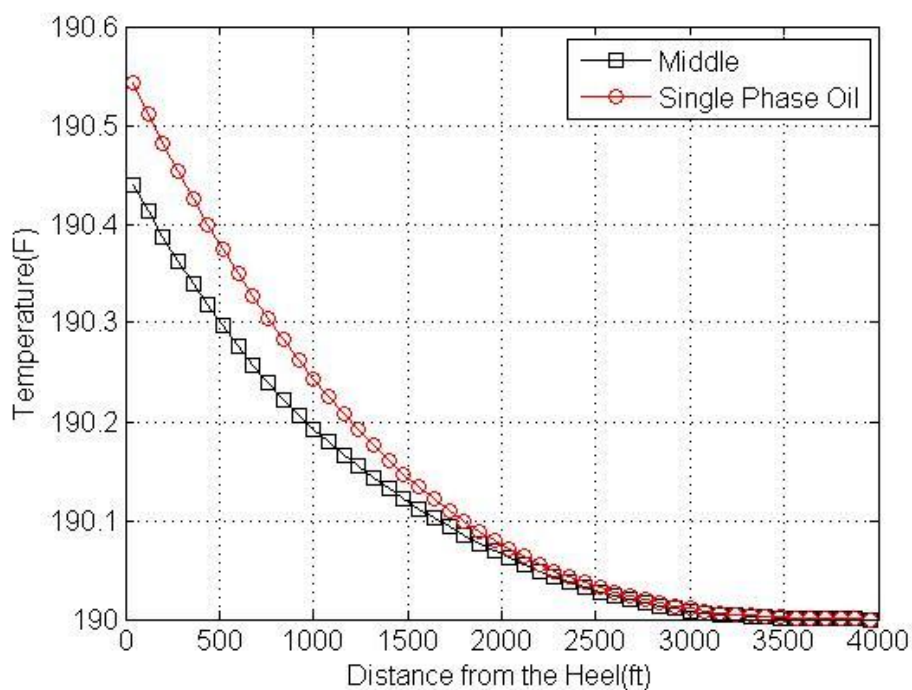**Fig. 5.13 Temperature Profiles Comparison for Water Entered at Toe-Drift-flux Model**

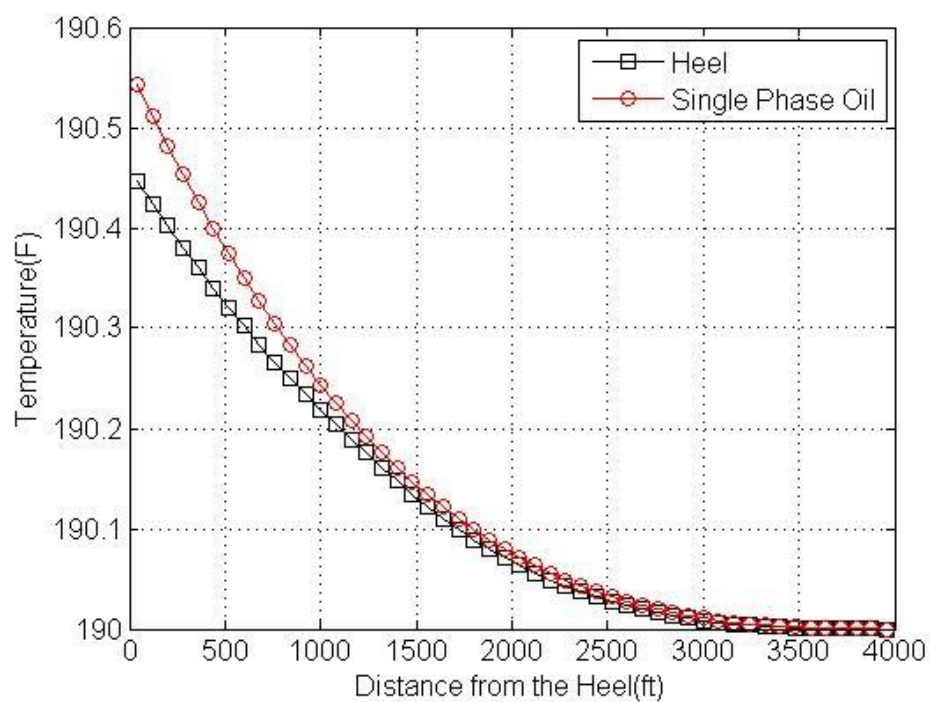**Fig. 5.14 Temperature Profiles Comparison for Water Entered at Middle-Drift-flux Model**

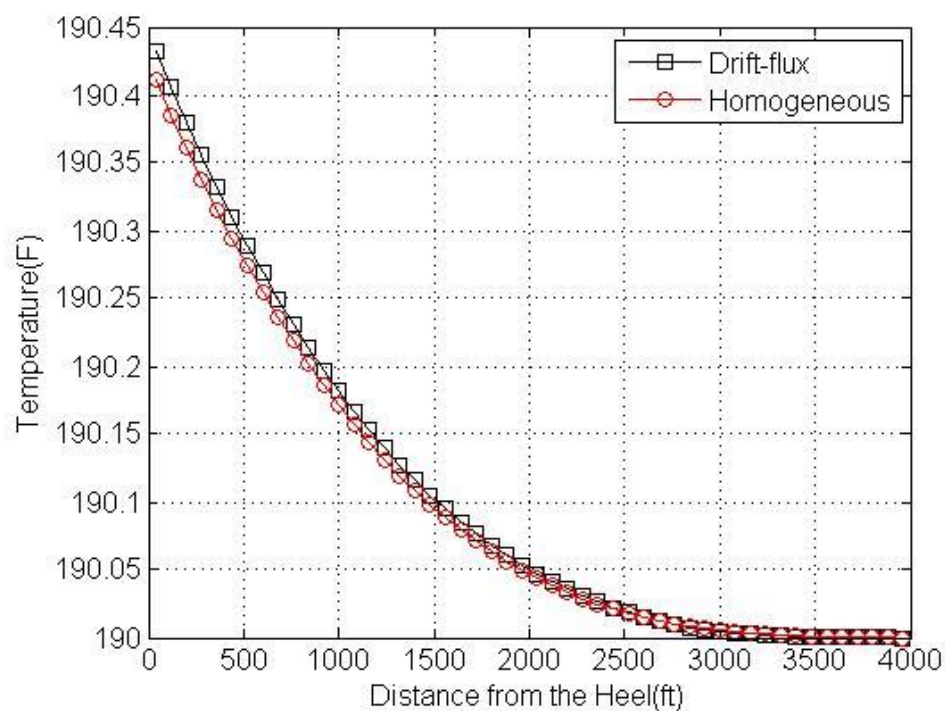**Fig. 5.15 Temperature Profiles Comparison for Water Entered at Heel-Drift-flux Model**

Fig. 5.16 Temperature Comparison of Two Models with Water Entering at Toe-Oil-water Drift-flux Model

Figure 5.16 gives the comparison of temperature profiles of two models with water entering wellbore at the toe. It is shown that temperature change in drift-flux model is larger that of homogeneous model. Therefore, homogeneous model tends to under predict wellbore thermal behavior compared to drift-flux model.

5.2 Oil-Gas Two-phase Flow Problem

In the oil-gas two-phase flow problem, the thermal effect of gas appearance during oil production is discussed. We assume that gas enters the oil production zone at each segment of the wellbore and is mixed with oil during production. Gas enters the wellbore at different flowrates in three cases. The cumulative productions of oil and gas phase are shown in Figure 5.17. With the same oil production, gas flowrates are specified in three types—high, medium and low.
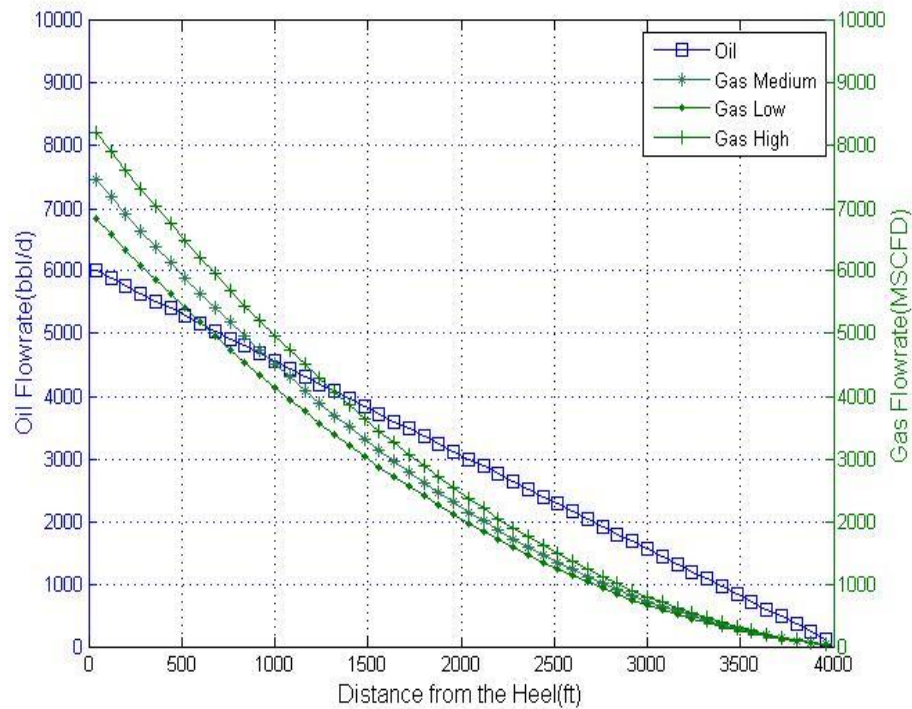

Fig. 5.17 Oil and Gas Phases Production

5.2.1 Homogeneous Model Results

Similarly, we first show the result of the homogeneous model in an openhole wellbore type. Gas

holdup is given in Figure 5.18. Since gas enters the wellbore simultaneously at each segment,

cumulative production of gas makes its holdup increase from toe to heel. The larger the gas

flowrate, the higher the holdup gas phase will be. Figure 5.19 shows pressure profiles in three

cases. With the same oil flowrate, the largest gas flowrate case results in the largest pressure drop,
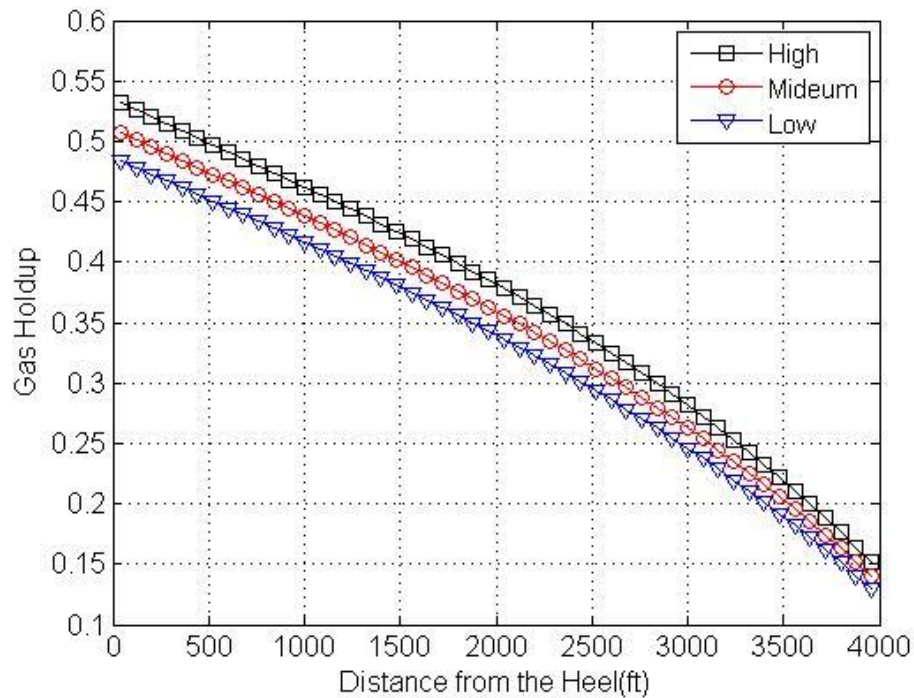
then the medium and low gas flowrates.
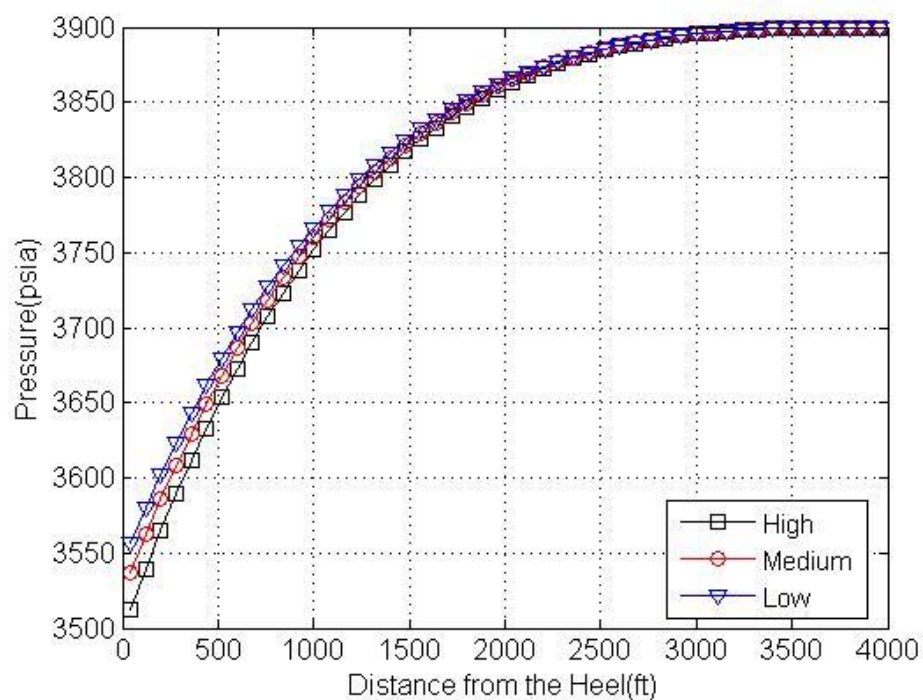

Fig. 5.18 Gas Holdup-Homogeneous Model

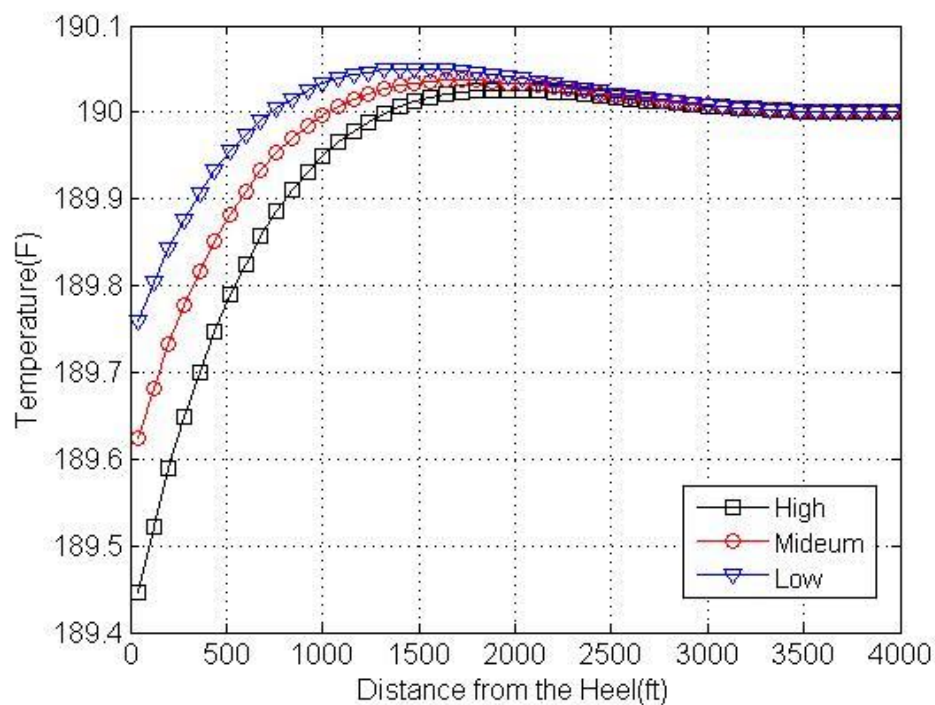**Fig. 5.19 Pressure Profiles in Different Gas Flowrate-Homogeneous Model**

Fig. 5.20 Temperature Profiles in Different Gas Flowrate-Homogeneous Model

Figure 5.20 shows the temperature profiles in three cases. It is interesting to find that in three cases, from toe to heel, temperature first increases then decreases due to the effect of gas entry. As demonstrated in the single-phase case study, oil is heated while gas is cooled along the wellbore. When the two-phase flows come together, the fluid mixture at the first half of the wellbore experiences heating like the oil phase; then it's being cooled like the gas phase. Since higher gas flowrate leads to larger pressure drop, the oil-gas mixture in the largest gas production has the largest range of temperature change. Due to the cooling effect in the gas phase, it is easy to diagnose entry of the gas during oil production from its temperature profile.

5.2.2 Drift-flux Model Results

In the drift-flux model, gas holdup is evaluated with drift-flux techniques in Figure 5.21. The trend of the profiles is similar with holdup results in the homogeneous model in Figure 5.18.
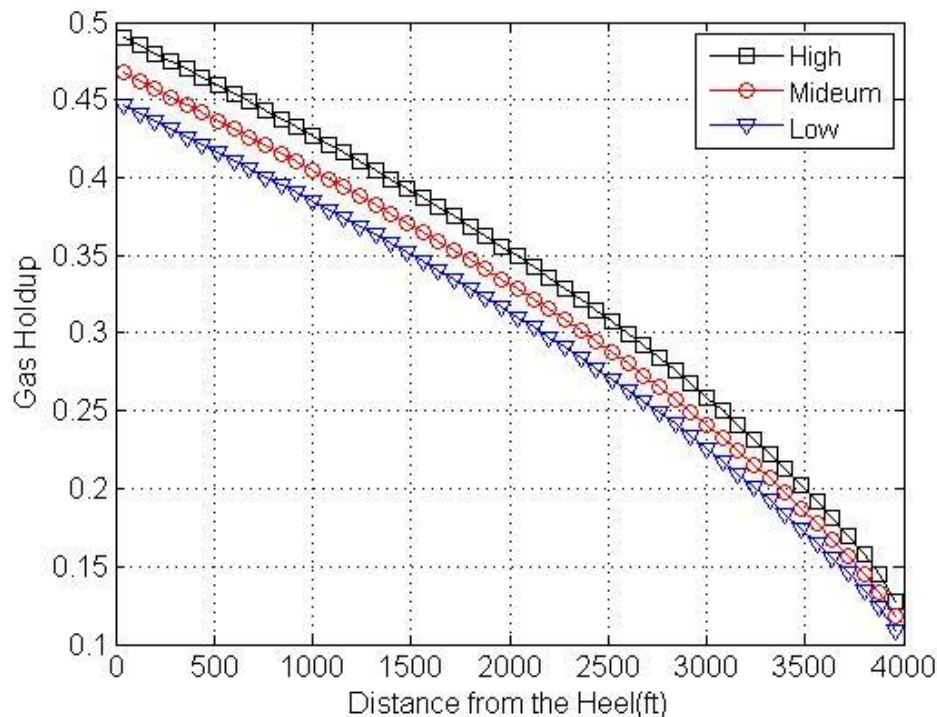

Fig. 5.21 Gas Holdup-Oil-gas Drift-flux Model

Figure 5.22 is given in order to compare the difference of holdup results in the two models. As illustrated in Figure 5.22, when slip is considered in the drift-flux model, the gas holdup becomes smaller compared to the homogeneous case. Again, this is caused by different algorithms in evaluating phase holdup; and the homogeneous model tends to over predict gas holdup. The velocity profile in the high gas flowrate case is given in Figure 5.23.
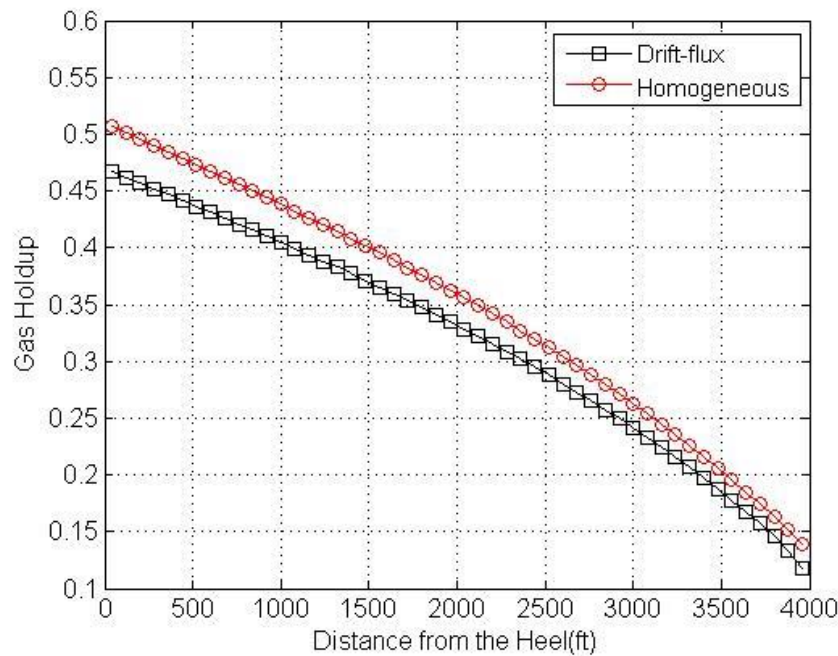
Fig. 5.22 Comparison of Gas Holdup in Two Model

As expected, due to slip between the two phases, the gas phase has a higher velocity than that of the oil phase, and the mixture velocity in homogeneous model is also between the two velocity profiles. Figures 5.24 and 5.25 present pressure and temperature profiles in the drift-flux model. The pressure and temperature profiles have similar trends compared to those in the homogeneous model in Figures 5.19 and 5.20.

Fig. 5.23 Velocity Profile in High Gas Flowrate Case- Oil-gas Drift-Flux Model

Fig. 5.24 Velocity Profile in High Gas Flowrate Case- Oil-gas Drift Flux Model

Fig. 5.25 Temperature Profiles in Different Gas Flowrate-Oil-gas Drift-flux Model

Fig. 5.26 Temperature Comparison of Two Models with High Gas Flowrate
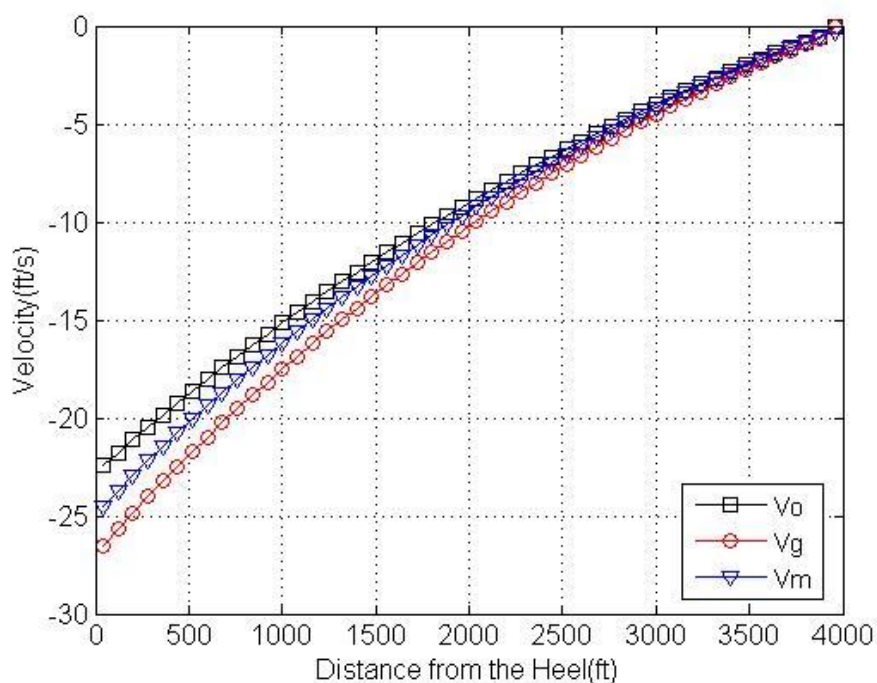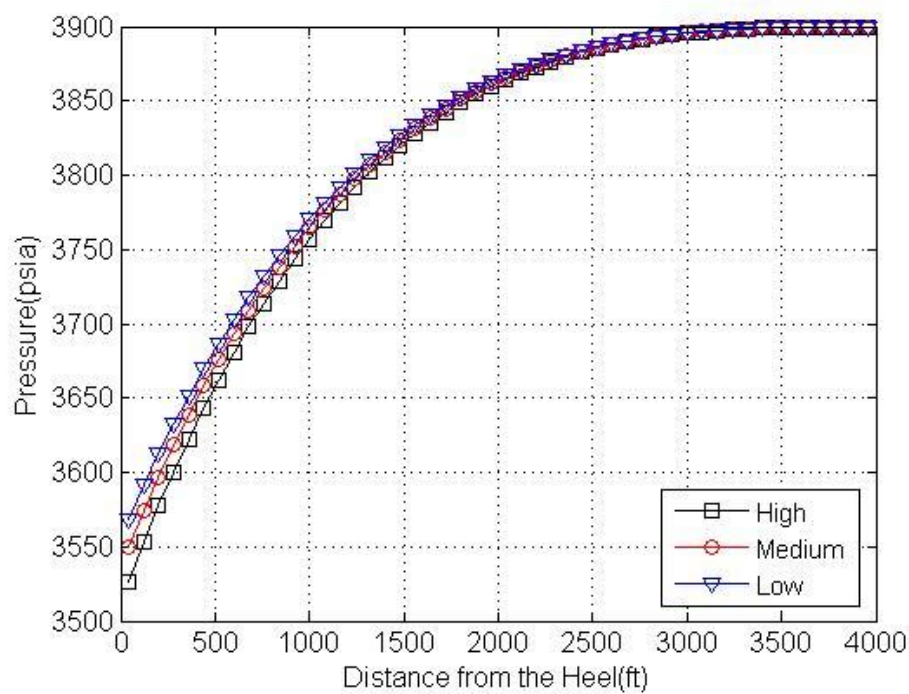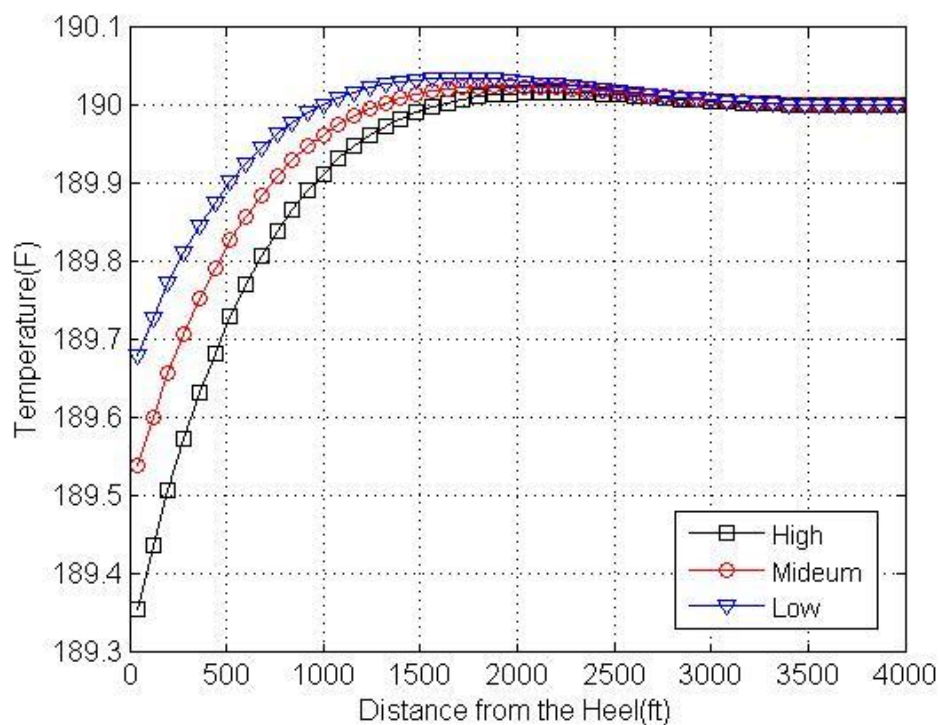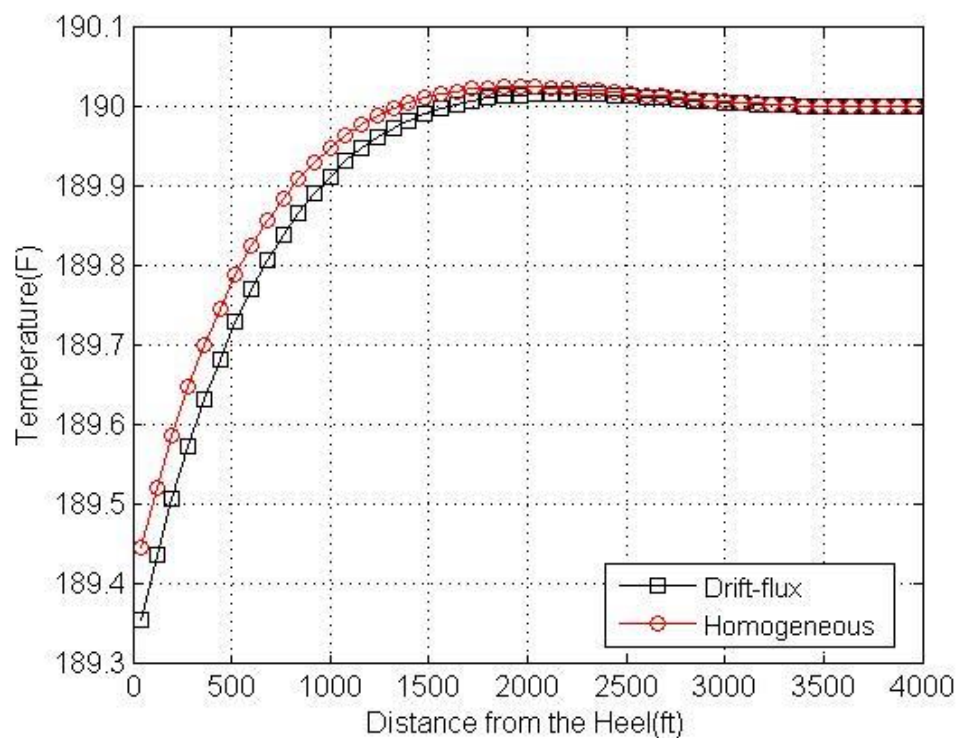
Figure 5.26 gives the temperature profile comparison between two models in the high flowrate case. As is shown, the temperature change of drift-flux model is larger than that of homogeneous model. Using different protocols to solve thermal response between two models, homogeneous model tends to under predict temperature change compared to drift-flux model.

5.3 Well Completion Effect

The results discussed so far for the two-phase flow are in openhole wellbore types. In this section, a perforated wellbore type has been applied in the same oil-gas flow case. Pressure and temperature results are generated by the drift-flux model. Figure 5.27 shows pressure profiles in three oil-gas cases. A similar profile can be found compared to the openhole case in Figure 5.24. However, due to smaller roughness of the wellbore, the pressure drop of perforated wellbore fluid in the figure is relatively smaller than that of the openhole wellbore fluid. Figure 5.28 gives temperature profiles in this case. Temperature change in a perforated wellbore is not as significant as that in an openhole wellbore. Two reasons can be considered for this fact. First, the smaller pressure drop weakens the effect of the isentropic thermal coefficient, leading to the wellbore fluid being less cooled. Second, heat conduction from reservoir to wellbore always has an opposite effect in determining the overall trend of temperature change. For example, in this case, the first half of the wellbore from toe to the middle is being heated, while heat conduction cools the wellbore fluid because the reservoir temperature is lower; the remaining half of the wellbore from middle to heel is being cooled while heat conduction heats the wellbore because the reservoir temperature is higher. Combination of these two factors results in the non-sensitive thermal response of a perforated wellbore fluid.
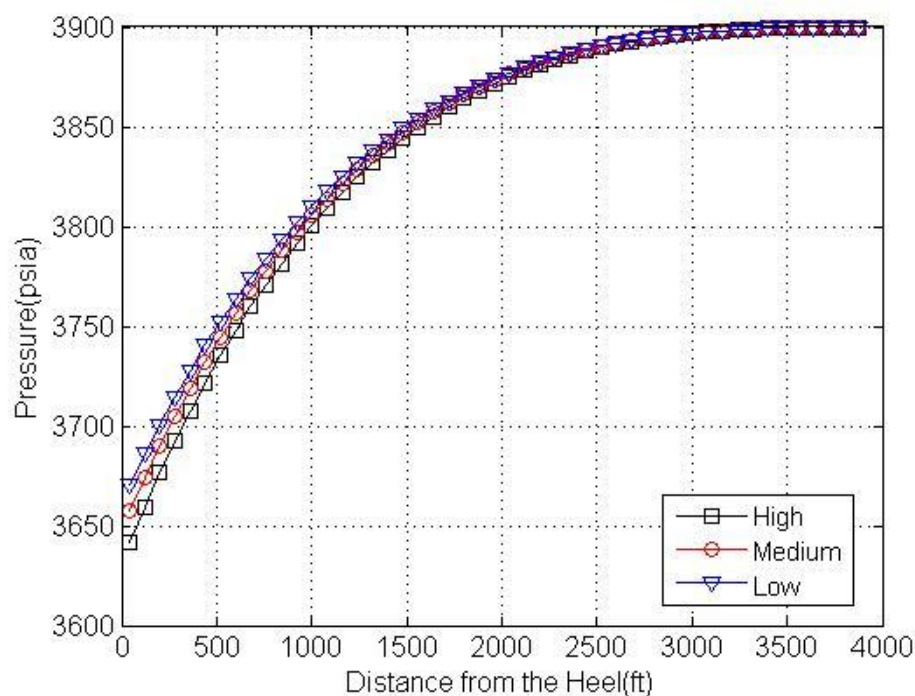
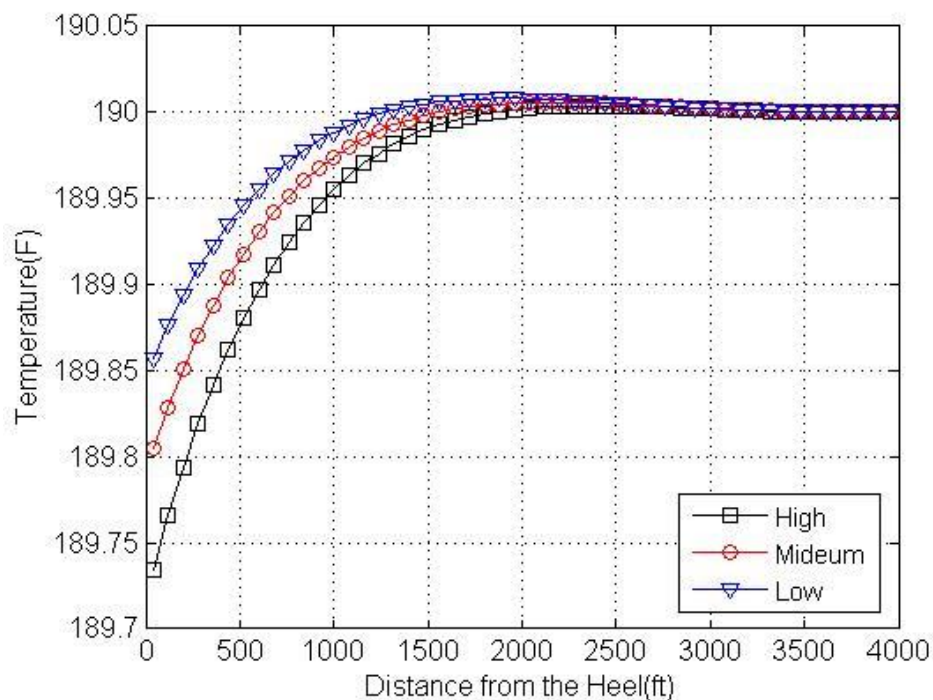**Fig. 5.27 Pressure Profiles in Perforated Wellbores-Oil-gas Drift-flux Model**

Fig. 5.28 Temperature Profiles in Perforated Wellbores-Oil-gas Drift-flux Model

CHAPTER 6

CONCLUSIONS AND SUGGESTIONS

Based on the study of thermal response for single-phase and two-phase flow in one-dimensional steady-state flow conditions, the following conclusions can be drawn:

1. The η_s-driven model (proposed model) presents a new way to interpret wellbore fluid thermal behavior. Isentropic thermal coefficient in the thermal response model makes a cooling contribution in temperature change. The thermal behavior of the wellbore fluid is decided by the combination effects of energy exchange, friction and the isentropic thermal coefficient.

2. For a single-phase fluid in a horizontal wellbore, water and oil are heated while gas is cooled along the wellbore. For fluid-like oil and water that display heating behaviors along the wellbore, their heating contributions of friction are larger than that of thermal coefficient cooling. For fluid that has cooling behavior along the wellbore like gas, its cooling effect of thermal coefficient is larger than that of frictional heating.

3. Wellbore inclination has effect on fluid thermal response. First of all, gravity in an inclined wellbore is not zero, which influences fluid pressure drop. Second, because of formation pressure and temperature gradient, reservoir pressure and temperature changes along the wellbore; therefore results in larger mass exchange effects on temperature profiles.

4. Wellbore thermal response is also driven by flowrate, wellbore radius and roughness. Larger flowrate, larger wellbore roughness and smaller radius cause larger pressure and temperature changes in each case study.

5. In a perforated wellbore, thermal response is not as sensitive as in the openhole case. Due to smaller wellbore roughness and heat conduction between the reservoir and the wellbore

fluid (in the single-phase case), oil- and water-phase fluid tends to be less heated while gas is less cooled.

6. During the production of oil, the entry of the second phase including water and gas can be detected via the temperature profile.

The model can be further developed into transient flow form to analyze the flow in early time regime. In addition, in order to match field data, the reservoir model is necessary to be coupled with the wellbore model to generate more realistic flowrate, reservoir pressure and temperature as inputs before calculating the wellbore temperature profile. Also, flash calculation can be applied in every block of the wellbore in an oil-gas two-phase flow system to have a more accurate evaluation of gas entry effect and a better estimation of oil and gas production on the surface.

REFERENCES

Ayala, H, Luis, F. (2001). *A Unified Two-fluid Model for Multiphase Flow in Natural Gas Pipeline.* M.S. Thesis, The Pennsylvania State University.

Alves, I.N, Alhanati, F.J.S, Shoham, O. (1992). *A Unified Model for Predicting Flowing Temperature Distribution in Wellbores and Pipelines.* SPE Paper 20632, *SPE production Engineering, 7*(4), 363-367.

Bird, R.B., Stewart, W.E., and Lightfoot, E.N. (2006): *Transport Phenomena*, Revised 2nd edition, John Wiley & Sons, New York.

Chen, N. H. (1979): *An Explicit Equation for Friction Factor in Pipe*, Industrial & Engineering Chemistry Fundamentals, v. 18, n. 3, p.296-297.

Choi, J, Pereyra, E, Sarica, C, Park, C, Kang, J. M. (2012). *An Efficient Drift-Flux Closure Relationship to Estimate Liquid Holdups of Gas-Liquid Two-Phase Flow in Pipes. Energies, 5*(12), 5294-5306.

Dix, G.E. (1971). *Vapor Void Fractions for Forced Convection with Subcooled Boiling at Low Flow Rates.* Ph.D Thesis, University of California, Berkeley.

Firoozabadi, A, Ramey Jr, H. J. (1988). *Surface Tension of Water-hydrocarbon Systems at Reservoir Conditions. Journal of Canadian Petroleum Technology, 27*(03).

França, F, and Lahey Jr, R.T. (1992). *The Use of Drift-flux Techniques for the Analysis of Horizontal Two-phase Flows. International Journal of Multiphase Flow, 18*(6), 787-801.

Govier, G.W, Aziz, K. (2008). *The Flow of Complex Mixtures in Pipes*: Richardson, TX: Society of Petroleum Engineers; 2nd ed.

Hapanowicz, J. (2008). *Slip Between the Phases in Two-phase Water–oil Flow in a Horizontal Pipe. International Journal of Multiphase Flow, 34*(6), 559-566.

Hasan, A.R, and Kabir, C.S. (1988a). *Predicting Multiphase Flow Behavior in a Deviated Well*. *SPE production engineering, 3*(04), 474-482.

Hasan, A.R, and Kabir, C.S. (1988b). *A Study of Multiphase Flow Behavior in Vertical Wells*. *SPE production engineering, 3*(02), 263-272.

Hasan, A.R and Kabir, C.S, (2002). *Fluid Flow and Heat Transfer in Wellbores*: Society of Petroleum Engineers Richardson, TX.

Hasan, A.R, and Kabir, C.S. (1994). *Aspects of Wellbore Heat Transfer During Two-phase*. *SPE Production & Facilities, 9*(03), 211-216.

Hasan, A.R, and Kabir, C.S. (1999). *A Simplified Model for Oil/water Flow in Vertical and Deviated Wellbores. SPE production & facilities, 14*(01), 56-62. `

Yoshida,N, Zhu,D, Hill, A.D. (2013). *Temperature Prediction Model For A Horizontal Well with Multiple Fractures In A Shale Reservoir.* Paper presented at the SPE Annual Technical Conference and Exhibition.

Kim, J, and Ghajar, A. J. (2006). *A General Heat Transfer Correlation for Non-boiling Gas–liquid Flow with Different Flow Patterns in Horizontal pipes. International Journal of Multiphase Flow, 32*(4), 447-465.

Li, Z, Zhu, D. (2009). *Predicting Flow Profile of Horizontal Wells by Downhole Pressure and DTS Data for Infinite Waterdrive Reservoir.* Paper presented at the SPE Annual Technical Conference and Exhibition.

Ouyang, L, and Aziz, K. (2000). *A Homogeneous Model for Gas–liquid Flow in Horizontal Wells*. *Journal of Petroleum Science and Engineering, 27*(3), 119-128.

Petalas, N, and Aziz, K. (1998). *A Mechanistic Model for Multiphase Flow in Pipes.* Paper presented at the Annual Technical Meeting.

Pourashary, P., Varavei, A., Sepehrnoori, K. and Podio, A.L: *A Compositional Wellbore/Reservoir Simulator to Model Multiphase Flow and Temperature Distribution*, SPE Paper 12115 presented at the International Petroleum Technology Conference, 3-5 December, 2008, Kuala Lumpur, Malaysia.

Radespiel, E. (2010). *A Comprehensive Model Describing Temperature Behavior in Horizontal Wells*. *The Pennsylvania State University*.

Ramey Jr, H.J. (1962). *Wellbore Heat Transmission*. *Journal of Petroleum Technology, 14*(04), 427-435.

Semenova, A, Livescu, S, Durlofsky, L. J, Aziz, K. (2010). *Modeling of Multisegmented Thermal Wells in Reservoir Simulation.* Paper presented at the SPE EUROPEC/EAGE Annual Conference and Exhibition.

Shi, H, Holmes, J. A, Durlofsky, L. J, Aziz, K, Diaz, L.R, Alkaya, B, Oddie, G. (2005). *Drift-flux Modeling of Two-phase Flow in Wellbores*. *SPE Journal, 10*(01), 24-33.

Shoham, O. (2006). *Mechanistic Modelling of Gas-liquid Two-phase Flow in Pipes*: Society of Petroleum Engineers.

Sieder, E.N and Tate, G. E. (1936). *Heat Transfer and Pressure Drop of Liquids in Tubes*. *Industrial & Engineering Chemistry, 28*(12), 1429-1435.

Wilkes, J. O. (2006). *Fluid Mechanics for Chemical Engineers with Microfluidics and CFD*: Pearson Education.

Yoshioka, K, Zhu, D, Hill, A. D, Lake, L W. (2005). *Interpretation of Temperature and Pressure Profiles Measured in Multilateral Wells Equipped with Intelligent Completions (SPE94097).* Paper presented at the 67th EAGE Conference & Exhibition.

Yoshioka, K, Zhu, D, Hill, A.D, Dawkrajai, P, and Lake, L. W. (2005). *A Comprehensive Model of Temperature Behavior in a Horizontal Well.* Paper presented at the SPE Annual Technical Conference and Exhibition.

Zakaria, M.H. (2012). *Analytical Modeling and Thermodynamic Analysis of Thermal Responses in Horizontal Wellbores.* M.S. Thesis, The Pennsylvania State University.

Zuber, N and Findlay, J.A. (1965). *Average Volumetric Concentration in Two-phase Flow Systems. Journal of Heat Transfer, 87*(4), 453-468.

APPENDIX A

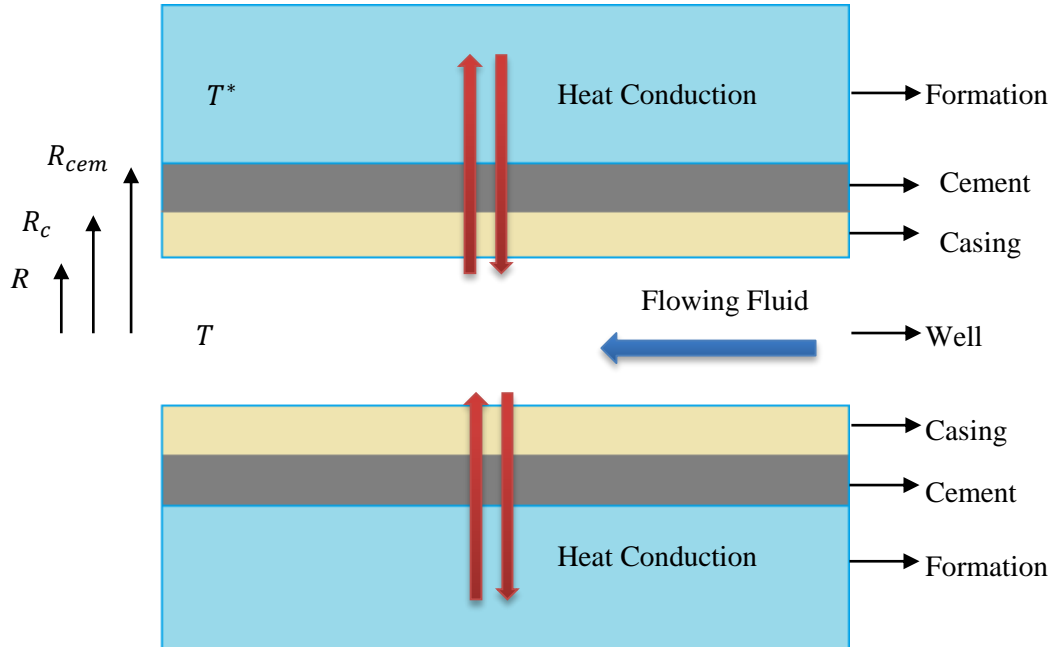# EQUATIONS OF OVERALL HEAT TRANFER COEFFICIENT

Fig. A-1 Wellbore Profile

As illustrated from Figure A-1, heat conduction happened between the reservoir fluid and the wellbore flow through cement and casing. Derived by Yoshioka et al. (2005), the relationship between wellbore fluid temperature and reservoir fluid temperature can be written as:

$$T - T^* = \frac{\dot{Q}}{2\pi(1-\gamma)}\left[\frac{ln\left(\frac{r_c}{r}\right)}{K_c} + \frac{ln\left(\frac{r_{cem}}{r_c}\right)}{K_{cem}} + \frac{1}{rC_h}\right] \tag{A.1}$$

C_h is heat transfer coefficient of fluid, $\dot{Q}$ (BTU/ft hr) is heat transfer rate, K is thermal conductivity, subscript c and cem denote casing and cement, respectively. Based on the equation above, the overall heat transfer coefficient can be expressed as:

$$U = \frac{Q}{(T^*-T)2\pi r(1-\gamma)} = \left[\frac{rln\left(\frac{r_c}{r}\right)}{K_c} + \frac{rln\left(\frac{r_{cem}}{r_c}\right)}{K_{cem}} + \frac{1}{C_h}\right]^{-1} \tag{A.2}$$

According to Yoshioka et al. (2005), for laminar flow, heat transfer coefficient is:

$$C_h = 3.656 \frac{K_{fl}}{2r} \tag{A.3}$$

While for turbulent single-phase or oil-water two-phase flow, Gnielinski's (2008) formula is used:

$$C_h = \frac{\left(\frac{f}{2}\right)(Re - 1000)Pr}{1 + 12.7 \left(\frac{f}{2}\right)^{0.5} (Pr^{2/3} - 1)} \frac{K_{fl}}{2r} \tag{A.4}$$

Pr is fluid Prandtl number, given as:

$$Pr = \frac{C_p \mu}{K} \tag{A.5}$$

In terms of two-phase flow, Re, Pr and K_{fl} is determined by mixture properties.

For oil-gas two-phase flow, correlation from Kim and Tang (2006) is applied. A flow pattern factor (F_P) is introduced in order to reflect the real shape of oil-gas interface:

$$F_P = (1 - y_G) + y_G F_s^{\,2} \tag{A.6}$$

F_S refers to shape factor defined in equation (A.7) :

$$F_s = \frac{2}{\pi} tan^{-1} \left(\sqrt{\frac{\rho_G (u_G - u_O)^2}{gd(\rho_O - \rho_G)}} \right) \tag{A.7}$$

The heat transfer coefficient of oil-gas two-phase flow is introduced in equation (A.8)

$$C_h = F_P C_L \left\{ 1 + c \left(\left[\frac{x}{1 - x}\right]^k \left[\frac{1 - F_P}{F_P}\right]^l \left[\frac{Pr_G}{Pr_O}\right]^m \left[\frac{\mu_G}{\mu_O}\right]^n \right) \right\} \tag{A.8}$$

where c, m, n, p, q are constant which are determined experimentally as:

c	k	l	m	n
0.7	0.08	0.06	0.03	-0.14

C_L is the liquid heat transfer coefficient that comes from Sieder and Tate (1936), for turbulent

flow:

$$C_L = 0.027 Re_L{}^{4/5} Pr_L{}^{1/3} \left(\frac{K_L}{d}\right) \left(\frac{\mu_B}{\mu_W}\right)_L^{0.14} \tag{A.9}$$

x is quality which defined as:

$$x = \frac{M_G}{M_G + M_O} \tag{A.10}$$

where M (lbm/s) is the mass flow rate of each phase.

APPENDIX B

SENSITIVITY OF THERMAL RESPONSE ON WELLBORE GRIDS

In this section, a sensitivity study of the wellbore thermal response on wellbore grids number is conducted. Single-phase gas is applied with the same cumulative flowrate (8200MSCF/D) as we discussed in Chapter 3. In this case, reservoir fluid goes into wellbore at uniform rate in each block. Besides the grids number (50) that is selected in our case study, we also select the grids numbers of 2, 5, 10, 25, 75, and 100 in this study. Figures B-1 to B-3 show the velocity, pressure and temperature profiles in each case. Legend in the figures represent grids number in each case.
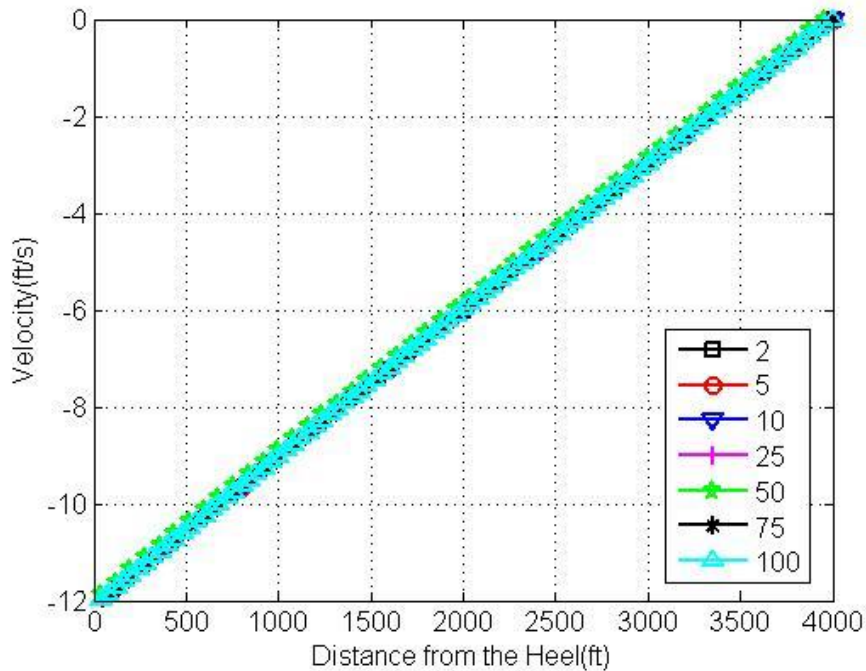

Fig. B-1 Velocity Profiles in Different Grids Numbers

Figure B-1 shows that the velocity profiles in each case has smaller difference so that the velocity profiles are not sensitive to number of blocks.
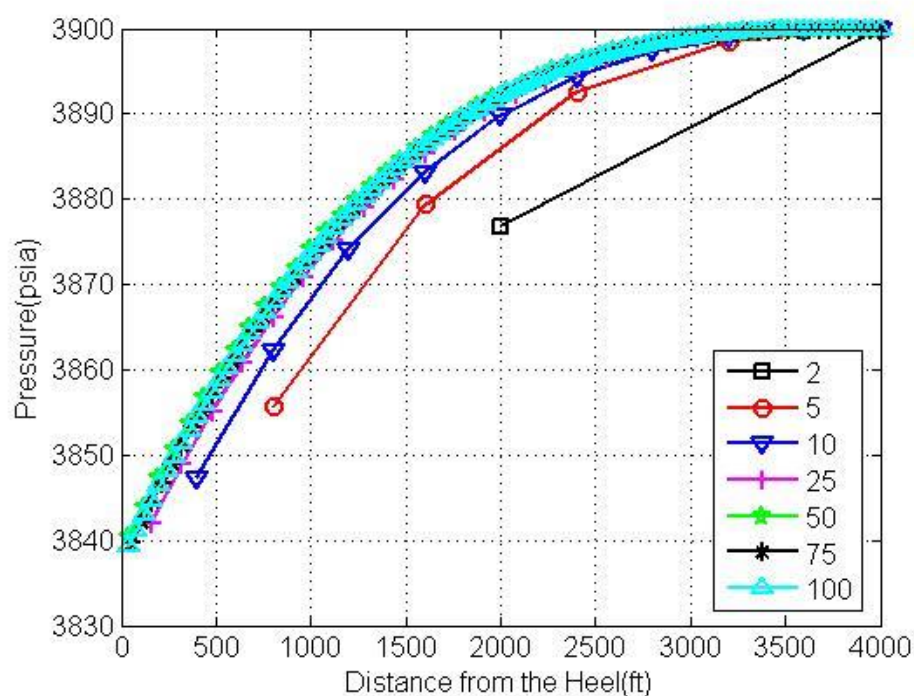
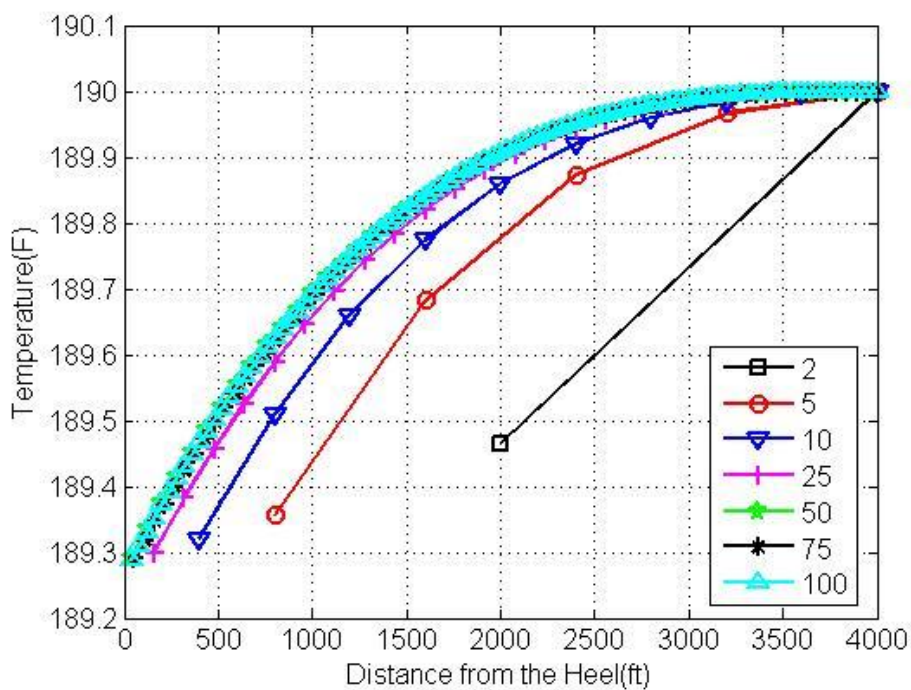**Fig. B-2 Pressure Profiles in Different Grids Numbers**

Fig. B-3 Temperature Profiles in Different Grids Numbers

However, clear differences can be observed from pressure and temperature profiles in Figure B-2 and Figure B-3. With the increase of grids numbers from 2 to 25, pressure and temperature profiles changes sharply, and larger grids number wellbore leads to larger total pressure and temperature changes. But, when grids number increases from 50 to 100, the increments of pressure and temperature changes are much smaller (less than 0.61psia and 0.0024F), and their profiles are about to overlap each other. Therefore, it is concluded that a sufficient number of grids is needed to have an accurate estimation thermal response of wellbore fluid. On the other hand, when the number of grids specified on wellbore is already able to predict sensitive thermal response (i.e. 50 blocks), there is no need to enlarge the number of grids since more time is consumed on calculation without significant different results.